8-1-2019

GEOCHEMISTRY AND ORGANIC PETROGRAPHY OF THE ANNA SHALE (PENNSYLVANIAN) AND THE OCCURENCE OF PYRITE "SUNS" IN SOUTHWESTERN ILLINOIS

Jacob Dyson
Southern Illinois University Carbondale, xjacques94@gmail.com

GEOCHEMISTRY AND ORGANIC PETROGRAPHY OF THE ANNA SHALE (PENNSYLVANIAN) AND THE OCCURRENCE OF PYRITE "SUNS" IN SOUTHWESTERN ILLINOIS

by

Jacob R. Dyson

B.S., Southern Illinois University, 2016

A Thesis
Submitted in Partial Fulfillment of the Requirements for the
Master of Science Degree

Department of Geology
in the Graduate School
Southern Illinois University Carbondale
August 2019

THESIS APPROVAL

GEOCHEMISTRY AND ORGANIC PETROGRAPHY OF THE ANNA SHALE (PENNSYLVANIAN) AND THE OCCURRENCE OF PYRITE "SUNS" IN SOUTHWESTERN ILLINOIS

by

Jacob R. Dyson

A Thesis Submitted in Partial

Fulfillment of the Requirements

for the Degree of

Master of Science

in the field of Geology

Approved by:

Dr. Susan Rimmer, Chair

Dr. Liliana Lefticariu

Dr. Daniel Hummer

Graduate School
Southern Illinois University Carbondale
May 24, 2019

AN ABSTRACT OF THE THESIS OF

Jacob Dyson, for the Master of Science degree in Geology, presented on May 24, 2019, at Southern Illinois University Carbondale.

TITLE: GEOCHEMISTRY AND ORGANIC PETROLOGY OF THE ANNA SHALE (PENNSYLVANIAN) AND THE OCCURRENCE OF PYRITE "SUNS" IN SOUTHWESTERN ILLINOIS

MAJOR PROFESSOR: Dr. Susan Rimmer

The Anna Shale (Pennsylvanian) is an organic-rich, marine black shale that commonly overlies the Herrin (No. 6) Coal of the Carbondale Formation, Illinois Basin. Disk-shaped iron sulfide concretions, called pyrite suns, which are commonly up to 10 cm or more across are found in the lowest few centimeters of the Anna Shale in coal mines near Sparta in southwestern Illinois. This area is the only known location where pyrite suns of this size have been found, suggesting that unusual geochemical and/or depositional conditions led to their formation. The primary objective of this study was to evaluate the geochemical conditions at the time of Anna Shale deposition in the area where the pyrite suns formed.

Four cores of the Anna Shale from Washington County, IL, along with several in-mine samples of the Anna roof shale and pyrite suns were collected from the Prairie Eagle underground coal mine (Pinckneyville, IL) for this study. Redox sensitive trace elements (TE), C-S-Fe relationships, and TE – total organic carbon (TOC) relationships were used to evaluate paleo-redox conditions at the time of Anna Shale deposition. Paleo-redox conditions were cyclic and fluctuated between dysoxic and anoxic throughout deposition of the Anna Shale. Large amounts of organic matter were preserved during anoxic intervals with a maximum TOC of 37.0%, whereas relatively low amounts were preserved during dysoxic intervals, with a minimum of 2.2% TOC. Organic matter in the Anna Shale is composed primarily of micrinite,

bituminite, and solid bitumen. The Anna Shale is a Type II kerogen with an average hydrogen index (HI) of 225 mg HC/g TOC and has excellent oil potential (typical S2 values ~10-150 mg HC/g). The shale has excellent source rock potential but is immature in southwestern Illinois with an average Tmax of 422°C.

Pyrite suns were analyzed for mineralogy and TE concentration to provide insight into their formation. X-ray diffraction demonstrated that the concretions are composed entirely of pyrite. Concentrations of TE in pyrite suns are below the detection limits of electron probe microanalysis (EPMA). Methods with lower detection limits should be explored, such as laser ablation inductively coupled mass spectrometry (LA-ICP-MS), to determine whether there is any zoning of TEs as this may provide insight into processes that formed pyrite suns.

ACKNOWLEDGMENTS

This research would not have been possible without the benevolent offering of time and effort by numerous people along the way. A sincerest thank you to my advisor Dr. Sue Rimmer, not only for the crucial direction and instruction she provided throughout building this thesis, but also for being an inspirational professor that I greatly enjoyed learning from over the years. I would like to thank Scott Elrick for his assistance in obtaining samples, for providing guidance at various stages of the project, and for being a source of positivity. I would also like to thank Dr. David Moecher for conducting the electron probe microanalysis (EPMA) at the University of Kentucky at Lexington. I would like to express deep gratitude to Prairie State Generating Company as a whole and specifically John Schmale, Chris Landoll, and Bill Duff for enabling me to make my own observations and collect samples at the Lively Grove Mine. I also would like to thank Zain Abdi for his instruction and assistance in conducting the X-Ray Fluorescence and plotting data. Thanks also to Joe Devera for lending his insight on various samples and providing assistance in core observations. Additional thanks to Barry Sargeant for taking me out to one of Knight Hawk's mines to collect Anna Shale samples. A final thank you to my family and friends for the unending support they showed me throughout the process of completing this thesis, I truly could not have done it without them.

TABLE OF CONTENTS

CHAPTER PAGE

ABSTRACT i

ACKNOWLEDGMENTS iii

LIST OF FIGURES vi

CHAPTERS

CHAPTER 1 – Introduction 1

CHAPTER 2 – Methods 14

CHAPTER 3 – Results 22

CHAPTER 4 – Discussion 30

CHAPTER 5 – Conclusions 41

REFERENCES 79

APPENDICES

APPENDIX A – Limit of Determination of a Method for Trace and Major Elements 90

APPENDIX B – Rock-Eval Data 91

APPENDIX C – Petrographic Data 95

APPENDIX D – C-S-Fe Data 97

APPENDIX E – X-Ray Fluorescence Data for Trace Elements 100

APPENDIX F – Duplicate X-Ray Fluorescence Data for Trace Elements 118

APPENDIX G – X-Ray Fluorescence Data for Major Elements 120

APPENDIX H – Duplicate X-Ray Fluorescence Data for Major Elements 138

VITA 140

LIST OF FIGURES

FIGURE PAGE

Figure 1 – Stratigraphic column of members of the Carbondale Formation 43

Figure 2 – Stratigraphic relationships of the interval between the Herrin (No. 6) Coal and the Piasa Limestone 44

Figure 3 – Distribution of the Herrin (No. 6) Coal, Walshville Channel, and Energy Shale 45

Figure 4 – Distribution of roof lithologies of the Herrin (No. 6) Coal 46

Figure 5 – Regional paleogeography of the Late Pennsylvanian 47

Figure 6 – Idealized carbon-sulfur plot 48

Figure 7 – Map of sample locations 49

Figure 8 – Photograph of core samples with sampling intervals 50

Figure 9 – Diagram of pyrite sun sample preparation 51

Figure 10 – Profile of redox sensitive trace element concentrations and TOC for core C6848 52

Figure 11 – Profile of redox sensitive trace element concentrations and TOC for core C7003 53

Figure 12 – Profile of redox sensitive trace element concentrations and TOC for core C7005 54

Figure 13 – Profile of redox sensitive trace element concentrations and TOC for core C7009 55

Figure 14 – Pseudo van Krevelen diagram 56

Figure 15 – Profiles of petrographic data for all cores 57

Figure 16 – Photomicrographs of micrinite 58

Figure 17 – Photomicrographs of bituminite 59

Figure 18 – Photomicrographs of solid bitumen 60

Figure 19 – Carbon-sulfur plot 61

Figure 20 – C-S-Fe ternary diagram 62

Figure 21 – Profile of trace element paleo-redox proxies and TOC for core C6848.....63

Figure 22 – Profile of trace element paleo-redox proxies and TOC for core C7003.....64

Figure 23 – Profile of trace element paleo-redox proxies and TOC for core C7005.....65

Figure 24 – Profile of trace element paleo-redox proxies and TOC for core C7009.....66

Figure 25 – Graphs of trace element paleo-redox proxies and clastic proxies versus TOC.....67

Figure 26 – Graphs of trace element paleo-redox proxies for roof shale samples.....68

Figure 27 – Profile of clastic sedimentation proxies and TOC for core C6848.....69

Figure 28 – Profile of clastic sedimentation proxies and TOC for core C7003.....70

Figure 29 – Profile of clastic sedimentation proxies and TOC for core C7005.....71

Figure 30 – Profile of clastic sedimentation proxies and TOC for core C7009.....72

Figure 31 – X-ray diffraction pattern for pyrite sun 1C.....73

Figure 32 – X-ray diffraction pattern for pyrite sun 2B.....74

Figure 33 – Plots of aluminum normalized trace elements with strong euxinic affinity versus TOC.....75

Figure 34 – Plots of aluminum normalized trace elements with weak euxinic affinity versus TOC.....76

Figure 35 – Pictures of burrows in the Anna Shale.....77

Figure 36 – Pictures of cross-sections and faces of pyrite suns.....78

CHAPTER 1

INTRODUCTION

The Anna Shale is an organic-rich, marine black shale that commonly overlies the Herrin (No. 6) Coal of the Carbondale Formation, Illinois Basin. Disk-shaped iron sulfide concretions called pyrite suns, commonly up to 10 cm or more across, are found in mines in the Sparta, IL region. This area is the only known location where pyrite suns of this size have been found, suggesting that unusual geochemical and/or depositional conditions led to their formation. The primary objective of this study was to elucidate the geochemical conditions at the time of Anna Shale deposition in the area where the pyrite suns formed.

The Middle Pennsylvanian Anna Shale Member of the Carbondale Formation in the Illinois Basin has been included in studies of stratigraphic relationships and interpretations of the depositional environment have been made based on sequence stratigraphy, paleoecology, and geochemical analysis (Wetendorf, 1967; Johnson, 1972; Palmer et al., 1979; Eble and Greb, 2018). Some investigation of the source rock potential and organic matter content of the Anna Shale has also been conducted in the Illinois and western Kentucky portions of the Illinois Basin (Chou et al., 1991, Eble and Greb, 2018). Studies of depositional environment have been conducted on various Pennsylvanian black shales across the midcontinent of North America. The paleo-redox conditions of similar Pennsylvanian black shales in Missouri, Kansas, Oklahoma, and Illinois have been determined using trace element (TE) analysis and TE/organic carbon relationships (Wenger and Baker, 1986; Algeo et al., 2004; Algeo and Maynard, 2004). Trace element enrichments in black shale pyrite have also been used to interpret depositional environment conditions and paleo-redox conditions (Berner et al., 2013). These methods of

analyses have been applied to the Anna Shale to provide a high-resolution timeline of the evolving paleo-redox conditions that contributed to organic matter preservation.

Pyrite suns, also known as pyrite dollars or miner's dollars, are enigmatic pyrite concretions that form near the contact between the Anna Shale and the underlying Herrin (No. 6) Coal seam over a limited spatial extent in southwestern Illinois (Wetendorf, 1967). These disk-shaped, radial pyrite concretions have gained popularity among mineral collectors due to their unique structure and appearance. Concretions of this size are currently only known to exist at this locality, indicating that some unique chemical conditions and mechanisms were likely present for their formation.

The occurrence of pyrite suns in the lower Anna Shale near the contact with the Herrin (No. 6) Coal causes them to fall into loosened coal at the time of mining contributing additional sulfur to an already high sulfur coal, thus increasing the demand on coal cleaning processes. The Herrin (No. 6) Coal seam is one of the most extensively mined coal seams in the Illinois Basin, and has high average sulfur contents ranging from 3-5% (Krausse et al., 1979; Treworgy and Jacobson, 1979).

1.1 Hypothesis and objectives

The hypothesis to be tested in this thesis is that the Anna Shale was deposited under an anoxic water column; under such oxygen-restricted conditions organic matter could accumulate and ultimately be preserved.

The specific objectives of this study were:

1) To use redox-sensitive trace elements and C-S-Fe relationships to evaluate the geochemical conditions at the time of Anna Shale deposition in the area where the pyrite suns formed;

2) to investigate trace element enrichments of pyrite suns to provide insight into geochemical conditions related to concretion formation;

3) to determine the sources of organic matter in the Anna Shale using organic petrography; and

4) to assess the source-rock quality of the Anna Shale using TOC/Rock-Eval pyrolysis.

1.2 Geologic background and setting

Sedimentary packages of Pennsylvanian strata in the Illinois Basin make up cyclic sequences of coals, shales, siltstones, limestones, and sandstones called cyclothems that were produced by repeated transgression-regression cycles of glacio-eustatic origin (Heckel, 1977, 1994; Wenger and Baker 1986; Greb et al., 2003; Algeo et al., 2004; Algeo and Heckel, 2008). Illinois Basin cyclothems are generally characterized by an underclay overlain by coal and fluvial sandstones, followed by transgressive marine gray and black shales, highstand limestones, and lowstand sandstones and shales (Palmer et al., 1979; Cecil et al., 2003). The Illinois Basin cyclothems differ from those of the Western Interior Basin in that they often lack transgressive limestones due to the presence of a reducing peat swamp environment that inhibited carbonate production (Heckel, 1994).

The basin was relatively stable tectonically during deposition of the Middle Pennsylvanian Desmoinesian series although several structures including the Du Quoin Monocline, Salem and Louden Anticlines, and the Las Salle Anticlinorium were still active as indicated by thinning of

strata over their axes (Wanless, 1955; Palmer, 1979). In the study area for this project, the package of rock strata associated with the Anna Shale was deposited on a stable shelf to the west of the DuQuoin Monocline (Palmer et al., 1979). A stratigraphic column of the Middle Pennsylvanian Desmoinesian series is shown in Figure 1. The Anna Shale commonly directly overlies the Herrin (No. 6) Coal. Normal marine fauna increase in abundance vertically in the Anna Shale, while brackish fauna decrease in abundance (Givens, 1968). This shift in fauna suggests the shallow, marine-shelf environment transitioned from at least partially brackish conditions to normal marine salinity during deposition of the Anna Shale (Wetendorf, 1967; Givens, 1968; Palmer et al., 1979, Kravits and Crelling, 1981). Bioturbation has been observed in the normal marine facies at the top of the shale (Palmer et al., 1979).

In some areas where the Anna Shale is absent, the Brereton Limestone Member directly overlies the Herrin (No. 6) Coal (Palmer et al., 1979). Differential compaction of the fluvial complex underlying the Herrin (No. 6) Coal could have resulted in the non-deposition of the Anna Shale and the Brereton Limestone in certain localities where younger units overly the coal (Palmer et al., 1979). The variability in stratigraphic relationships and continuity is represented in Figure 2. Deposition of the Brereton Limestone has been associated with several models of deposition: a moderate increase in water depth with a transition to more open marine conditions (Palmer et al., 1979), deposition on topographic highs in the peat swamp where the limestone directly overlies the Herrin (No. 6) Coal (Givens, 1968), and a climate controlled increase in wind-driven water circulation oxygenating the epeiric sea (Cecil et al., 2003). Marine fauna of the Brereton indicate deposition in a warm, shallow carbonate shelf environment (Palmer et al., 1979).

The medium-gray Energy Shale is made up of tidal rhythmite deposits that occur in association with the Walshville Channel (Archer et al., 2016). The Walshville Channel is a sandstone complex deposited by fluvial processes that were contemporaneous with the peat swamps of the Herrin (No. 6) Coal (Johnson, 1972). The Anna Shale and Brereton Limestone thin over Energy Shale lenses and where the Energy Shale exceeds 9.1 m (30 ft) in thickness they are often not present (Palmer et al., 1979). The thicker deposits of the Energy Shale form lobate wedges adjacent to the Walshville Channel that contain plant remains as well as marginal marine fauna (Palmer et al., 1979). The lobes of the Energy Shale are up to several miles wide and thicken towards the Walshville Channel (Nelson, 1979). Lenses of Energy Shale up to 6.1 m (20 ft) thick, ranging from several tens of meters to hundreds of meters (hundreds to thousands of feet) across, occur beyond the channel associated lobes (Nelson, 1979). The distribution of the Energy Shale is shown in Figures 3 and 4.

1.3 Depositional Models for the Anna Shale

The Anna Shale has been interpreted as shallow anoxic estuary and lagoon deposits (Zangerl et al., 1963; Wetendorf, 1967; Givens, 1968), which likely formed as a result of a transgression from the melting of Gondwanan glaciers (Heckel, 1977, 1994; Wenger and Baker 1986; Algeo et al., 2004; Algeo and Heckel, 2008). The water depths during deposition of the Anna Shale may have been shallower than 3 m (10 ft) (Givens, 1968; Johnson, 1972). Deposition of the Anna Shale required calm waters to deposit very fine, evenly bedded, organic-rich muds (Givens, 1968). Zangerl et al. (1963) suggested the older Mecca Quarry and Logan Quarry Shales were deposited in shallow lagoons and estuaries where a floating mat of vegetation prevented vertical mixing while also supplying a source of organic matter; this interpretation was initially applied to

other black shales of the cyclothems (Wetendorf, 1967; Givens, 1968; Johnson, 1972; Palmer et al., 1979; Utgaard, 1979).

Numerous studies of other Pennsylvanian black shales have interpreted them as deep-water deposits (James, 1970; Heckel, 1977, 1994; Algeo and Heckel, 2008). The Excello Shale is a similar cyclothemic black shale that overlies the Summum (No. 4) Coal and is overlain by the Hanover Limestone (James, 1970), representing the same interval in a cyclothem as the Herrin (No. 6) Coal, Anna Shale, and Brereton Limestone sequence. The Excello Shale has been interpreted as being deposited in anoxic deep waters during maximum transgression rather than shallow, nearshore deposition during transgression due to its vast extent across the Illinois and Western Interior Basins (James, 1970; Heckel, 1977, 1994; Algeo and Heckel, 2008). The Anna Shale of the Illinois Basin has been correlated with the Anna Shale Member of the Pawnee Formation in the Western Interior Basin, although, the same level of lithologic consistency is not observed (Jewett, 1941; Eble and Greb, 2018).

Water depths during deposition of the Western Interior Basin black shales have been interpreted to be the order of ~100 m (Heckel, 1977, 1994; Algeo and Heckel, 2008). The presence of nonskeletal phosphorite in black shales suggests deposition at water depths greater than 50 m (164 ft) (Heckel, 1977). Correlation of the Mecca Quarry Shale by Zangerl et al. (1963) over a wider lateral extent led to the discovery of phosphorite lenses and deep-water conodonts suggesting deep-water deposition in those parts of the basin (Heckel, 1977).

Some models for deposition of Pennsylvanian black shales include a strong proximal halocline, sustained by freshwater input from highlands and easterly tradewinds, and a weaker distal thermocline sustained by weak upwelling from the oxygen-minimum zone of the open

ocean across thousands of kilometers of the Midcontinent Sea (Algeo et al., 2004; Algeo and Heckel, 2008). The paleogeography of the midcontinent during the Late Pennsylvanian is shown in Figure 5. These models also suggest minimum water depths of approximately 50 m (164 ft) to allow for development of density stratification (Heckel, 1977, 1994; Algeo and Heckel, 2008). These studies have noted that black shale deposition may have occurred at shallower depths in the Illinois and Appalachian Basin regions of the Midcontinent Sea as freshwater influence increases with proximity to the Appalachian front forming a stronger, halocline (Heckel, 1994).

A climate controlled deposition model has also been proposed for cyclothemic black shale deposition. In this model, during lowstands a permanent low-pressure belt was confined to low latitudes by high pressure zones that formed at the poles during glacial intervals (Cecil et al., 2003). This low-pressure belt sustained an ever-wet climate that maintained peat swamps (Cecil et al., 2003). Black shale deposition began in the early stages of transgression due to low wind speeds and lack of wind-driven circulation in the epeiric sea as the low-pressure belt began to deteriorate with the high-pressure zones at the poles at the end of glacial periods (Cecil et al., 2003). Black shale deposition commenced once peritidal depths were exceeded and water depths may have never exceeded more than a few meters during deposition (Cecil et al., 2003). Marine limestones that overly the black shales were deposited as a result of increased water circulation due to higher wind speeds from north-south swings in the intertropical convergence zone during highstands (Cecil et al., 2003).

1.4 Formation of pyrite in shales

Pyrite is the most abundant, widespread sulfide and commonly occurs in association with organic matter in marine shales (Berner, 1970; Anthony et al., 1990). Sulfur for sedimentary

pyrite is sourced through bacterial reduction of marine sulfate which produces hydrogen sulfide (Berner, 1970). Hydrogen sulfide reacts with detrital iron minerals to form iron monosulfides that react with elemental sulfur to form pyrite (Berner, 1970). The limiting factors in pyrite formation in shales are the availability of organic matter for sulfate-reducing bacteria, the supply of marine sulfate, and the amount of reactive iron (Berner, 1970).

Pyrite formation in normal marine (oxic) sediments is limited by the amount of organic matter available to sulfate-reducing bacteria (Berner, 1970; Berner and Raiswell, 1983). Bacterial sulfate reduction only takes place below the sediment-water interface in normal marine sediments, therefore only the amount of organic matter buried during deposition is available for bacterial sulfate reduction (Raiswell and Berner, 1985). Organic matter may serve as the limiting factor for both initial iron monosulfide formation in the sediments and subsequent transformation of iron monosulfide to pyrite (Berner, 1970). This transformation requires excess hydrogen sulfide to be present, and the amount of hydrogen sulfide is limited by the availability of organic matter to sulfate-reducing bacteria (Berner, 1970). Organic matter acting as the limiting factor in normal marine sediments has been suggested by carbon-sulfur plots where the amount of pyritic sulfur and organic carbon show a positive correlation with a trend line intercepting the sulfur axis at zero (Figure 6) (Berner and Raiswell, 1983).

Pyrite formation in euxinic sediments is limited by the amount of reactive iron (Berner and Raiswell, 1983). Carbon-sulfur plots from euxinic sediments exhibit a trend line with a positive intercept on the sulfur axis (Figure 6) (Berner and Raiswell, 1983). The positive intercept results from formation of syngenetic pyrite in the water column and at the sediment-water interface due to dissolved hydrogen sulfide in the water column reacting with detrital iron minerals before

burial (Raiswell and Berner, 1985). Syngenetic pyrite formation is independent of the amount organic matter preserved in the sediments, producing a positive intercept on carbon-sulfur plots (Raiswell and Berner, 1985). Additional carbon-limited, diagenetic pyrite can form in the sediments below a euxinic water column producing a positive correlation on carbon-sulfur plots analogous to those in normal marine sediments (Figure 6) (Raiswell and Berner, 1985). The syngenetic pyrite component can be identified by the intercept on the sulfur axis and the diagenetic pyrite component as the difference between this value and the amount of sulfur for any amount of organic carbon (Raiswell and Berner, 1985).

1.5 Geochemical proxies

Proxies for clastic influx use element/Al ratios to assess qualitatively the contribution of various detrital elements from non-clay sources as aluminum only occurs in clay minerals (Caplan and Bustin, 1998). Ti/Al has been used as a proxy for siliclastic grainsize, sedimentation rate, and paleo-wind strength as Ti is partly derived from clays but is also found in sand- and silt-size grains of heavy mineral grains such as sphene, ilmenite, and rutile (Bertrand et al., 1996; Murphy et al. 2000; Rimmer et al., 2004). Si/Al has been used as a proxy for the amount of quartz relative to clay sedimentation (Caplan and Bustin, 1998; Rimmer et al., 2004).

Trace element paleo-redox proxies employ multiple redox sensitive elements including Mo, V, Cu, Ni, Cr, and Co (Algeo and Maynard, 2004). Trace element ratios including V/(V+Ni), V/Cr, and Ni/Co have been used to evaluate paleo-redox conditions (Hatch and Leventhal, 1992; Jones and Manning, 1994; Rimmer et al., 2004).

Observation of TOC-TE relationships of “strong euxinic affinity” (Mo, U, V, Zn) and “weak euxinic affinity” trace elements (Cu, Ni, Cr, Co) is another multiproxy approach to paleo-redox-

facies analysis of cyclothemic black shales (Algeo and Maynard, 2004). Mo, V, and Zn, where Zn is hosted in Fe-sulfides, have been shown to exhibit strong euxinic affinity in modern sediments and have been shown to also have this affinity in ancient sediments (Algeo and Maynard, 2004). This approach may be effective in distinguishing dysoxic, anoxic, and euxinic facies in cyclothemic black shales. These terms are used to define estimations of the concentration of dissolved oxygen in the water column at deposition. Oxic, dysoxic, and anoxic are characterized by concentrations of dissolved oxygen > 2.0, 2.0-0.2, and 0.2-0 mL O_2/L H_2O, respectively, and euxinic conditions are characterized by 0 mL O_2/L H_2O with the presence of free, dissolved H_2S (Edwards, 1985; Tyson and Pearson, 1991). Oxic conditions support macrofauna, while dysoxic conditions strongly limit the assemblage of macrofauna and extent of bioturbation in sediments (Tyson and Pearson, 1991). The transition from dysoxic conditions to anoxic conditions at 0.2 mL O_2/L H_2O marks the end of bioturbation because burrowing macrofauna cannot survive the low oxygen concentrations (Tyson and Pearson, 1991). Trace element – total organic carbon relationships have been shown to vary greatly between facies with <10% and >10% TOC in Western Interior Basin cyclothemic black shales (Algeo and Maynard, 2004). Trace elements in sediments deposited under dysoxic conditions may only show background enrichments that do not correlate with TOC, whereas sediments associated with anoxic facies may show a strong correlation between TOC and TE concentrations (Algeo and Maynard, 2004). In high-TOC intervals, strong TE enrichments of Mo, U, V, and Zn have been shown to occur with little correlation with TOC; the lack of correlation between strongly enriched TEs and TOC may be due to formation of authigenic TE-enriched sulfides or oxyhydroxides under euxinic conditions (Algeo and Maynard, 2004). Trace elements with strong

euxinic affinities (Mo, U, V, Zn) may show greater enrichments and weak correlation with TOC in euxinic facies, while TEs with weak euxinic affinities (Cu, Ni, Cr, and Co) may show moderate enrichments in euxinic facies in relation to anoxic facies and strong correlation with TOC (Algeo and Maynard, 2004).

Degree of pyritization (DOP) can be used to distinguish paleo-redox conditions at the time of deposition based on the process of bacterial sulfate reduction and pyrite formation; DOP is the ratio of pyritic Fe to total reactive Fe (Raiswell et al., 1988). DOP ratios below 0.42 suggest oxic conditions, those between 0.42 and 0.75 suggest dysoxic conditions, and values over 0.75 indicate anoxic or euxinic conditions (Raiswell et al., 1988). In sediments deposited under an oxygenated water column (normal marine conditions), pyrite formation is limited by the amount of organic matter and occurs beneath the sediment-water interface under anoxic conditions (Raiswell et al., 1988). Under normal marine conditions, bioturbation continually introduces oxygen into the sediments, disrupting bacterial sulfate reduction while also oxidizing hydrogen sulfide and organic matter; this slows pyrite formation and reduces the portion of pyritized iron (Raiswell et al., 1988). Additionally, higher influxes of organic matter under normal marine conditions are typically correlated with influxes of detrital sediment which contain iron minerals, increasing the amount of total reactive iron (Raiswell et al., 1988). The increase in bacterial sulfate reduction in the sediments from an influx of organic matter is matched by an increase in reactive iron (Raiswell et al., 1988). The decrease in pyritized iron by bioturbation and increase in detrital iron associated with influx of organic matter produces a low ratio of pyritic Fe to total reactive Fe (DOP) for normal marine sediments (Raiswell et al., 1988). Unlike under normal marine conditions, bacterial sulfate reduction, and, therefore pyrite formation continue

uninterrupted by bioturbation under anoxic and euxinic conditions (Raiswell et al., 1988). Euxinic conditions allow the formation of syngenetic pyrite in the water column, providing further opportunity for conversion of reactive iron to pyrite during deposition (Raiswell et al., 1988). These conditions result in a greater portion of reactive iron being converted to pyrite, producing a higher DOP.

C-S-Fe ternary diagrams allow recognition of consistent Fe/C, S/C, or S/Fe ratios and can be used to estimate DOP from TOC, total Fe, and total S (Dean and Arthur, 1989; Arthur and Sageman, 1994). Samples from iron-limited sediments plot along a line with a constant S/Fe ratio that depends on the amount of iron that was reactive (Dean and Arthur, 1989). If the assumption is made that all iron in the samples is reactive, an estimation of paleo-redox conditions can be made using total iron. Normal marine (oxic) samples are characterized by a S/C ratio of 0.4 that forms a line on the ternary diagram (Arthur and Sageman, 1994). A S/Fe ratio of 1.15 is corresponds to the stoichiometric ratio of sulfur and iron in pyrite; this ratio represents all reactive iron being taken up by pyrite (Dean and Arthur, 1989). Any data points that plot below 1.15 S/Fe would contain a form of sulfur other than pyrite (Dean and Arthur, 1989). For samples to plot along a S/Fe of 1.15, sufficient sulfate and metabolizable organic matter must be available, all iron must be reactive, and the sediments had to be deposited under anoxic/euxinic conditions (Dean and Arthur, 1989). Estimations of DOP can be made from data that plot along a consistent S/Fe ratio (Arthur and Sageman, 1994). Samples where all reactive iron is taken up in pyrite (1.15 S/Fe) would correspond to a DOP of 1.00. A trend-line of constant S/Fe ratio where only a fraction of the total reactive iron is taken up in pyrite can be plotted and used to estimate DOP. This method is only an estimation as samples from iron-limited sediments

also plot along a line with a constant S/Fe ratio that depends on the amount of total iron that was reactive (Dean and Arthur, 1989). If the assumption is made that total iron is equal to total reactive iron, a minimum DOP can be calculated from a C-S-Fe ternary diagram (Dean and Arthur, 1989; Arthur and Sageman, 1994).

CHAPTER 2

METHODS

2.1 Sampling locations

Samples of the Anna Shale and pyrite suns were collected from the roof of the Prairie Eagle underground mine near Pinckneyville, IL. Six Anna Shale samples were collected: four from areas of the mine where pyrite suns are found (roof sample 1, 2, 6, 7) and two from areas where they are not found (roof sample 4, 5). Roof sample 3 is Energy Shale and therefore is not included in this study. Four cores were selected at the Illinois State Geological Survey Samples Library and the interval containing the Anna Shale was sawn in half for sampling. One half of each core was brought back to Southern Illinois University Carbondale for sampling and analysis. The cores were drilled in northern Washington County (Figure 7).

The Anna Shale core samples are composed largely of hard, laminated black shale with some intervals of poorly laminated, poorly bedded, softer black shale. The bottom 61 cm (2 ft) of Anna Shale in core C7005 is composed of very fissile dark gray shale. Cores C6848, C7003, and C7009 contain shell fragments generally <3mm (<1/8 in) in the top few inches of the Anna Shale and the top 46 cm (1.5 ft) of core C7005. Cores C6848, C7003, and C7009 contain coaly stringers up to 3mm (1/8 in) thick. Cores C6848 and C7003 each contain a limestone nodule, 8.9 cm (3 ½ in) and 6.4 cm (2 ½ in) thick, respectively, at the bottom of the Anna Shale. Core C7005 contains a 12.1 cm (4 ¾ in) thick limestone nodule 61 cm (2 ft) above the base of the Anna Shale. These limestone nodules contain lime mud that supports the fabric of the rock and >10% grains, classifying them as wackestones (Dunham, 1962). The nodules also contain some clastic sediment.

2.2 Sample preparation

The sawn surfaces of the cores provided the necessary flat surface for XRF measurements. Roof samples were sawn perpendicular to bedding to provide a flat surface for XRF measurements. To remove surface contaminants, samples were wiped down and dried prior to XRF scanning. Shale samples were marked with chalk at 1 cm intervals for XRF analysis. Following XRF analysis (see below), sampling intervals for the cores were selected from intervals of high and low concentrations of redox sensitive elements. The intervals selected for sampling were 5 cm thick (Figure 8). Roof samples were prepared from the entire thickness of each sample.

Whole-rock core and roof samples were crushed and sieved to minus 20-mesh for petrographic analysis, and to minus 60-mesh for Rock-Eval pyrolysis. For petrographic analysis, representative splits of minus 20-mesh whole-rock samples were mixed with epoxy resin and hardener, and then allowed to harden in 1 inch-diameter molds. Four minus 60-mesh samples from each core were sent to National Petrographic Service, Inc. (Houston, TX) for kerogen concentration. Shale samples were treated sequentially with hydrochloric acid, hydrofluoric acid, and hydrochloric acid; kerogen concentrates were dried at ambient/low temperatures and the residues were returned in vials. For visual estimates and point counts of macerals, kerogen concentrates were mixed with epoxy resin and hardener, placed in 1-inch molds, allowed to cure, and then polished. Whole-rock and kerogen concentrate pellets were polished using a Buehler Automet 250. The pellets were ground using 320 grit, 400 grit, 600 grit, and polished using 1.0 µm (alpha alumina) and, lastly, 0.06 µm (colloidal silica) polishing compounds.

Samples of pyrite suns were analyzed using electron probe microanalysis (EPMA) at the University of Kentucky (Lexington, Kentucky). Pyrite sun samples were taken along the radius of the concretions. Samples from two pyrite suns were mounted in 1-inch pellets. They were prepared by first cutting a wedge of a pyrite sun and then cutting the wedge into three pieces that would fit into 1-inch molds. Sample 1 was cut from the center of the concretion, sample 3 from the outer rim, and sample 2 from between the other samples. The pieces were mounted in epoxy so that a cross-section of the pyrite sun could be analyzed (Figure 9).

2.3 TOC/Rock-Eval analyses and carbon and sulfur analysis

LECO total organic carbon/Rock-Eval pyrolysis was performed on Anna Shale samples at GeoMark Research, Ltd. (Houston, TX). Approximately 100 mg of minus 60-mesh whole-rock sample were analyzed with a TOC LECO C230 Carbon Analyzer and Rock-Eval II Analyzer. Samples for LECO TOC analysis were treated with concentrated HCl for 2 hours; the samples were then rinsed with water over a filter to remove the acid. The filter and washed sample was placed into a LECO crucible and dried at 110°C for 4 hours. Dried samples were placed in the LECO C230 instrument and heated to 1200°C in the presence of oxygen. Carbon dioxide and carbon monoxide are produced; any carbon monoxide is converted to carbon dioxide using a catalyst. An infrared cell is used to measure the amount of carbon dioxide. Standards are analyzed every 10 samples for calibration. Approximately 100 mg of minus 60-mesh whole-rock sample was washed, dried at ambient temperature, and analyzed in the Rock-Eval II instrument. The following operating parameters were used for the Rock-Eval Analyzer: 300°C initial temperature for 3 minutes, 300°C to 550°C at 25°C/minute temperature programming rate, 550°C final temperature for 1 minute.

TOC/Rock-Eval pyrolysis results provide volatile hydrocarbons (S1), thermogenic hydrocarbons (S2), CO_2 (S3), TOC, and thermal maturity (Tmax). These parameters were used to calculate hydrogen index (HI = S_2/TOC) and oxygen index (OI = S_3/TOC), which can be plotted in a pseudo van Krevelen diagram (Tissot and Welte, 1984).

Carbon and sulfur analysis was performed on Anna Shale samples at the Kentucky Geological Survey (Lexington, KY) using a LECO SC-144DR carbon-sulfur analyzer. Total carbon was determined according to ASTM method D5373-08 (ASTM, 2008). Total sulfur was determined according to ASTM method D4239-02 (ASTM, 2002).

2.4 Petrographic Analysis

Maceral content was evaluated using a Leica DM 2500 P oil immersion microscope equipped with both a white-light and a blue-light source. The percentage of each maceral was estimated to determine the contribution of each organic constituent to TOC. The portion each maceral makes up of all the organic matter in a field view was determined based on visual estimates (Terry and Chilingar, 1955). Visual estimates were made on 10 fields-of-view for each of the 16 kerogen concentrate pellets. Point counts were performed on 3 samples to confirm the accuracy of the visual estimates, collecting 300 points on each sample using a Swift point counter. Point counts were conducted after visual estimates to avoid bias.

Following exploratory observation of the pellets, maceral categories counted included micrinite, bituminite, solid bitumen, other inertinites, other liptinites, and vitrinite.

Micrinite is composed of < 2 μm, rounded grains that occur in granular aggregates and as isolated grains; it has a reflectance typically between accompanying vitrinite and other inertinite macerals (ICCP, 2001). Micrinite is hydrogen-rich compared to other inertinite macerals and may

have originated from liptinitic or hydrogen-rich vitrinitic material (Taylor and Liu, 1989; ICCP, 2001). Micrinite is often closely associated with bituminite, degraded alginite, and other liptinites, and it may form as a byproduct of hydrocarbon formation (Teichmüller, 1974; Teichmüller and Ottenjahn, 1977; Teichmüller and Wolf, 1977; Taylor and Liu, 1989).

Micrinite is thought to be the main residual product after maturation and hydrocarbon generation from bituminite in some shales (Pickel et al., 2017). Bituminite is suggested to be the degradation product of numerous possible source materials including algae, bacterial bodies, algal-fungal mats, and precipitated humic acids from underlying peat deposits (Pickel et al., 2017).

Bituminite can be dark brown to dark gray and sometimes almost black with a very low reflectance compared to vitrinite (Pickel et al., 2017). Under blue light, fluorescence colors are pale and range from yellow to red to brown depending on type and rank, with some varieties displaying no fluorescence in immature shales (Pickel et al., 2017).

The term bitumen is defined by geochemists as liquid or solid petroleum that is soluble in organic solvents, whereas kerogen is defined as the insoluble fraction of organic matter derived from original organic material (Tissot and Welte, 1984). In organic petrography, the term solid bitumen describes a secondary maceral that is derived from petroleum generation from kerogen and may be partially insoluble (Mastalerz et al., 2018). Solid bitumen is recognized in reflected-light microscopy based on its occurrence as fracture and pore space fillings (Mastalerz et al., 2018). Solid bitumen is divided into pre-oil and post-oil solid bitumen. Pre-oil solid bitumen is an early generation precursor of oil that is probably extruded from kerogen as a viscous fluid in immature to oil window maturity source rocks (Lewan, 1983; Curiale, 1986; Cardott et al.,

2015). Post-oil solid bitumen is an alteration product of previously liquid oil (Curiale, 1986; Cardott et al., 2015). These types of bitumen are further defined by the migration distance from source organic matter. Pre-oil solid bitumen has migrated a minimal distance **(**Curiale, 1986) or in some cases has undergone no migration and occupies the place of the source kerogen (Liu et al., 2017). Post-oil solid bitumen is the alteration product of formerly liquid hydrocarbon which can form extensive interconnected networks (Curiale, 1986; Cardott et al., 2015).

Vitrinite is a maceral group derived from the woody tissues made up of cellulose and lignin in plants (ICCP, 1998). The extent of cell structure preservation is dependent on the decomposition process, degree of gelification, and thermal maturity (ICCP, 1998). The vitrinite group maceral collotelinite appears as more-or-less homogeneous and may exhibit some poorly defined cell structure (ICCP, 1998). The reflectance of vitrinite is generally between the accompanying darker liptinites and lighter inertinites (ICCP, 1998). The reflectance of vitrinite increases with thermal maturation from dark gray in immature to light gray and white in mature and over mature coals and shales (ICCP, 1998). Collotelinite reflectance is widely used as a thermal maturity index (ICCP, 1998).

Vitrinite reflectance analysis was performed on the Herrin (No. 6) Coal sample from the Lively Grove Mine. Analysis was conducted by first using a three point calibration on a J&M Tidas CCD UV/NIR system, and then collecting 100 random reflectance measurements on collotelinite.

2.5 X-ray fluorescence analysis

Elemental analysis was conducted using a hand-held Bruker XRF Tracer III-SD. The limit of determination of a method (LDM) for elements was calculated by Rowe et al. (2012) according

to Rousseau (2001) for pellets prepared from crushed samples of the Woodford Formation (Mississippian) and an internationally accepted standard SARM-41. The LDM is defined as the lowest concentration of an element that can be reliably quantified in a sample under specific analytical conditions with a 95.4% confidence level (Rousseau, 2001; Rowe et al., 2012). The LDMs for both samples are shown in Appendix A. Analysis by Rowe et al. (2012) was conducted using the same model instrument used in this study.

X-ray fluorescence was conducted at 1-cm intervals over the length of each of the four cores and vertical thickness of each roof sample. Each sample was scanned twice, once for major elements and once for trace elements. For analysis of major elements, samples were scanned for 60 seconds under vacuum. For analysis of trace elements, samples were scanned for 90 seconds without using the vacuum pump. The limestone nodules in cores C6848 and C7005 were scanned at 1-cm intervals and included in the data; the black shale adjacent to the limestone nodule in core C7003 was scanned but the nodule was not. Thirty-five trace and 9 major duplicate measurements were taken on 3 of the 4 cores and compared to the initial measurements taken over the same intervals. The difference between the initial and duplicate measurements was observed to confirm the precision of the initial measurements.

2.6 X-ray diffraction analysis

Samples from two pyrite suns were analyzed by X-ray diffraction at Southern Illinois University Carbondale to determine the minerology. Mineralogical analysis was conducted using a Rigaku Ultima IV X-ray diffractometer. Three samples from each of the pyrite suns were prepared for analysis. Each sample was hand crushed to minus 100-mesh using a mortar and pestle. Powder mounts and glass slides were washed with 100% ethyl alcohol before use. The

powdered samples were loaded into a shallow cavity powder mount (20 mm x 20 mm). Samples were run at 40 kV and 44 mA, between 2 and 65° 2θ, at a scan speed of 2°/minute.

2.7 Electron Probe Microanalysis (EPMA)

Micro-probe analysis was conducted using a CAMECA SX50 electron probe micro-analyzer at the University of Kentucky by Dr. David Moecher. Vertical and horizontal point traverses were conducted on one sample prepared from each of two pyrite suns, samples 1A-2 and 2B-1. In the vertical traverse along the short axis, 75 point measurements were taken and in the horizontal along the long axis 100 points were taken.

A count time of 20 seconds and a 50 nano-amp beam current for point traverses. Elements analyzed include Mo, Cu, Zn, As, Pb, and Cd. Detection limits for trace element analysis are estimated at 0.05 wt.% (D. Moecher, personal communication).

CHAPTER 3

RESULTS

3.1 TOC/Rock-Eval Analysis

Total organic carbon (TOC) of all analyzed intervals ranges from 2.2% to 37.0% (Appendix B). The three values below 4.9% TOC are from the thin, calcareous shale transition to the overlying Brereton Limestone. The highest TOC values in cores C6848, C7003, and C7009 are in the bottom 30 cm (1 ft) of the Anna Shale; there are also TOC values > 20% in the middle and top of each core. Total organic carbon versus depth for each core is shown in Figures 10-13. The highest TOC values of core C7005 are in the top 30 cm (1 ft) of Anna Shale; there is also one value near 20% in the middle. All but two samples show fair (2-5 mg HC/g TOC) to excellent (> 5 mg HC/g TOC) source potential with S2 values ranging from 1.2 to 159.0 mg HC/g TOC with an average of 45.9 mg HC/g TOC. Type II kerogen source rocks are within the oil window with Tmax values of 425-450°C (Espitalié et al., 1985). The Tmax values for the samples range from 411-432°C, with an average of 422°C, indicating that the Anna Shale is immature to marginally mature at this location. Figure 14 shows a pseudo van Krevelen diagram that indicates a Type II marine kerogen for the Anna Shale.

3.2 Petrographic Analysis

Visual estimates of maceral content are provided in Appendix C. Maceral composition is plotted in vertical profiles shown in Figure 15. Micrinite in the Anna Shale is composed of high-reflectance, grains that occur as ovoid-shaped bodies (Figure 16A), layers (Figure 16C), finely disseminated material (Figure 16E, or disseminated in other partially micrinized macerals. Micrinite is the most common maceral ranging from 49% to 89% in all but the two lowermost

samples from core C7005, which contain 1.5% and 2.8%. Intervals of the Anna Shale with > 20% TOC contain > 60% micrinite and have substantially higher hydrogen indices than lower TOC intervals (Figures 14 and 15). Fusinite and inertodetrinite in the Anna Shale have a high reflectance and occur as bodies containing cell structure and homogenous fragments, respectively. Other inertinites, including fusinite and inertodetrinite, vary between 1% and 25%.

Bituminite in the Anna Shale can be dark brown with weak, pale yellow fluorescence (Figure 18A and 18B) and dark gray little to no fluorescence (Figure 18C and 18D). It occurs as thin wisps and layers that can contain micrinized material. Bituminite contents range from 0% to 34%; the lower portions of each core have higher bituminite contents. Other liptinites vary between 0% and 12%. Bituminite is especially abundant in the lower samples of cores C6848, C7003, and C7009 where it comprises up to 34% of the organic matter.

Solid bitumen comprises between 1% and 34% in all but the two lowermost samples from core C7005 which contain > 75% solid bitumen (Appendix C). Cores C6848, C7003, and C7009 contain < 20% solid bitumen. The upper black shale samples of core C7005 contain 20% and 34% solid bitumen, whereas the organic matter in the lower dark-gray shale samples is comprised of > 75% solid bitumen. The dark-gray shale interval can be seen below the limestone nodule in core C7005 (Figure 8). Other data from core C7005 also differs from the other cores.

Solid bitumen has a low reflectance and can range from dark to medium gray. Solid bitumen fills voids (Figure 19A and 19B), occurs along bedding (Figure 19C and 19D), and can be seen wrapping around grains of pyrite and other macerals (Figure 19E). Some solid bitumen shows weak fluorescence (Figure 19B), and some pieces of solid bitumen are partially micronized (Figure 19E and 19F).

Vitrinite composition varies between 0% and 7% in the Anna Shale. Vitrinite has a moderate reflectance, does not fluoresce, and is medium gray. Collotelinite occurs as large fragments and layers. Some collotelinite is completely homogenous while some exhibits poorly-defined cell structure.

Other liptinite macerals, including sporinite, cutinite, resinite, and liptodetrinite, make up a small percentage of the organic matter in each sample, < 4% with the exception of the lowermost sample from C7005 that contains 12%. Sporinite has a dark appearance in white light and fluoresces weakly to strongly yellow in blue light. It often occurs as single spore bodies and in sporangia in some samples. Cutinite has a dark appearance in white light and has a bright yellow fluorescence in blue light. It is derived from the waxy cuticles of plants and can exhibit the outline of cell structure. Resinite has a dark brown milky texture in white light and has bright yellow to green fluorescence in blue light; it occurs as small void fillings. Liptodetrinite occurs as small, fluorescing fragments of other liptinite macerals.

Maceral point count data collected on 3 samples are highlighted in gray in Appendix C. The point counts agree well with the visual estimates. The average difference between the two methods is 2%, suggesting visual estimates are an effective approach to quantifying the fraction of organic matter each maceral comprises in a sample.

Vitrinite reflectance analysis was conducted on one sample of Herrin (No. 6) Coal from the Lively Grove Mine. The 100 measurements indicate a mean random reflectance of 0.43%, which places the shale below the oil window and is in agreement with the Rock-Eval Tmax data. The vitrinite reflectance of the underlying Herrin (No. 6) Coal and Tmax of the Anna Shale, 0.43%

Ro random and average Tmax 422°C, respectively, indicate the shale has not entered the oil window.

3.3 Carbon-Sulfur-Iron Relationships

Total sulfur contents for cores C6848, C7003, C7009, and the roof samples are between 1.61% and 3.25%, whereas sulfur contents of core C7005 are as high as 5.38% (Appendix D). In core C7005, sulfur contents are the highest in the lower 61 cm (2 ft) and decrease up section. Total iron contents for core C6848, C7003, C7009, and the roof samples are between 3.00% and 4.26% whereas core C7005 has higher values ranging from 3.53% to 5.51%.

Total organic carbon from Rock-Eval and total sulfur data from carbon-sulfur analysis were used to make a carbon-sulfur plot (Figure 19). The data do not correlate significantly with a trend line, $r = 0.22$ $n = 43$. The trend-line does have a positive intercept on the sulfur axis suggesting anoxic to euxinic conditions.

Total organic carbon, total sulfur, and iron were normalized to 100% and plotted on a C-S-Fe ternary diagram (Figure 20). The 5 iron values from XRF measurements taken over each of the sample intervals were averaged to provide an average iron weight percent for that interval. The data used in the C-S-Fe ternary diagram are shown in Appendix D. The data display two trends corresponding to different DOPs. The data from the roof samples, and cores C6848, C7003, and C7009 plot along a constant S/Fe ratio corresponding to a DOP of 0.51. The data from core C7005 and some data from other samples plot along a S/Fe ratio corresponding to a DOP of 0.73.

3.4 Trace-element paleo-redox proxies

All trace element data are shown in Appendix E. Thirty-five duplicate trace element measurements from three of the four cores are compared to the original measurements in Appendix F.

Redox sensitive trace-element profiles for each core are shown in Figures 10-13. Three intervals of elevated concentrations of redox-sensitive elements are shown highlighted in gray for cores C6848, C7003, and C7009. Core C7005 has only one interval where concentrations of redox-sensitive elements are elevated. All these enriched intervals correspond to high TOC values.

Trace-element paleo-redox ratios for each core are shown in Figures 21-24. Plots of TE paleo-redox proxies and TOC are shown in Figure 25; there is a significant correlation at a significance level of $\alpha = 0.01$ between the TE paleo-redox ratios and TOC (Figure 25). The correlation between paleo-redox proxies and TOC suggests that with a decreasing amount of oxygen in the environment, organic matter preservation increased. The V/(V+Ni) ratios suggest anoxic to euxinic conditions for the intervals with the highest TOC of each core (Figures 21-24). The V/(V+Ni) ratios also indicate primarily strong anoxic to euxinic conditions for high TOC intervals (>15%) and weaker anoxic to marginally dysoxic conditions for lower TOC intervals (<15%) (Figure 25). The V/Cr ratios suggest anoxic conditions for the intervals with the highest TOC of each core and oxic to dysoxic conditions for the rest of the sequence in each core (Figures 21-24). The V/Cr ratios suggest primarily oxic conditions for intervals with < 15% TOC but no other clear distinctions can be made (Figure 25). The Ni/Co ratios for cores C6848, C7003, and C7009 suggest anoxic conditions for the three highest TOC intervals in each core and dysoxic to oxic conditions for the rest of the sequence (Figures 21, 22, 24). Ni/Co ratios for

core C7005 suggest highly variable redox conditions ranging from oxic to anoxic (Figure 23). Generally, the Ni/Co ratios for all cores suggest dysoxic conditions for intervals containing > 20% TOC and primarily oxic conditions for intervals containing < 20% TOC for all cores (Figure 25).

The paleo-redox proxy ratio was calculated for each measurement taken at 1-cm intervals on the roof samples. The average was taken of the ratios for each sample producing an estimation of the paleo-redox conditions for the interval of the roof sample. Plots of the roof sample paleo-redox proxies are shown in Figure 26. The V/Cr ratios suggest oxic conditions for four of the roof samples and dysoxic for the other two. The Ni/Co ratios suggest marginally dysoxic conditions for all the samples. The V/(V+Ni) ratios suggest anoxic conditions for four samples and euxinic conditions for the same two samples the V/Cr ratio suggested more restricted conditions.

3.5 Clastic influx

All major element data are shown in Appendix G. Nine duplicate major element measurements are compared to the original measurements is Appendix H.

Clastic sedimentation ratios are shown plotted vs. depth in Figures 27-30. Plots of clastic sedimentation ratios and TOC are shown in Figure 25; there is a significant positive correlation at a significance level of $\alpha = 0.01$ between the clastic sedimentation ratios and TOC (Figure 25). The highest TOC value in each core corresponds to the highest ratio for each proxy, and other high TOC intervals in each core correspond with increases in each ratio as shown highlighted in light gray (Figures 27-30). Intervals highlighted in dark gray are limestone nodules. The increases in the Ti/Al ratio with TOC suggest periods of higher clastic influx while organic matter rich

intervals were being deposited (Figure 25). The Si/Al and K/Al ratios also correlate with TOC (Figure 25). The Si/Al ratio suggests an increase in quartz relative to clays and the K/Al ratio may indicate relatively more micaceous clays or more fine-grained K-feldspar were being deposited while organic matter rich intervals were being deposited. Conversely, lower TOC intervals correlate with lower clastic sedimentation ratios, suggesting these are relatively low periods of clastic influx with less quartz relative to clays.

3.6 X-ray diffraction

X-ray diffraction patterns for samples taken from pyrite suns were not notably different from each other. Diffraction patterns for all 3 samples from pyrite sun 1 indicate the sample was composed of pyrite and a small amount of quartz. The diffraction pattern for pyrite sun sample 1C is shown in Figure 31. Diffraction patterns for all 3 samples from pyrite sun 2 indicate the sample was composed of pyrite and contain a peak at 29.4° that does not correspond to pyrite. The diffraction pattern for pyrite sun sample 2B has the largest peak at 29.4° and is shown in Figure 32. This peak corresponds with the largest peak in the diffraction pattern of chalcopyrite, initially suggesting this pyrite sun could contain a small amount of chalcopyrite. Concentrations of Cu in pyrite sun 2 were not detectable by EPMA suggesting there is not any chalcopyrite in the sample. Other iron sulfide minerals include pyrrhotite, greigite, and troilite. The diffraction patterns of pyrrhotite and troilite do not match the extra peak observed in pyrite sun sample 2B. The largest peak in the diffraction pattern of greigite does correspond with the extra peak in the diffraction pattern of pyrite sun sample 2B suggesting this pyrite sun may contain some greigite.

3.7 EPMA

Pyrite sun samples 1B and 2A were analyzed by EPMA for Mo, Cu, Zn, As, Cd, and Pb. Concentrations of these elements are not above the detection limits of the method used. Other samples were not analyzed because no detectable amount of any trace element was found.

CHAPTER 4

DISCUSSION

4.1 Source, type, and quality of organic matter

The Anna Shale is a source rock with excellent potential as indicated by the high average S2 of 45.9 mg HC/g and an average hydrogen index of 225 mg HC/g TOC. The Anna Shale may serve as an excellent source rock in the more thermally mature regions of the Illinois Basin to the east and southeast of the study area where it is likely further into the oil window. The source rock quality of the Anna Shale may be similar across the Illinois Basin because it is similar over 190 km (~120 miles) to the southeast in Hopkins County, Kentucky (Eble and Greb, 2018). The Anna Shale is characterized by an average TOC of 23.4% with a maximum value of 38.97% TOC in the western Kentucky region of the Illinois Basin (Eble and Greb, 2018).

Other studies of cyclothemic black shales across the midcontinent have reported micrinite as a major organic constituent. The Anna Shale in western Kentucky contains an average of ~42% inertinite, which is primarily micrinite (Eble and Greb, 2018). The description of the primary organic constituent (maceral) in the Little Osage Shale of the Western Interior Basin cyclothems (Wenger and Baker, 1986) suggests a comparable texture and distribution of micrinite as seen in the current Anna Shale study. The primary organic constituent of the Little Osage Shale is characterized as a material with pin-points of high and low reflectivity, suggesting this maceral is likely micrinite (Wenger and Baker, 1986).

The highest TOC intervals of both the Anna Shale in this study and the Little Osage Shale contain abundant large, ovoid-shaped and/or layered micrinite that parallel bedding (Figure 16A and 16C), whereas the lower TOC intervals contain disseminated micrinite (Figure 16E) (Wenger

and Baker, 1986). Degraded humic matter from coastal swamps was suggested as the source of this organic matter in the Little Osage Shale (Wenger and Baker, 1986).

Vitrinite reflectance from the underlying Herrin (No. 6) Coal and Tmax from Rock-Eval pyrolysis indicate that the Anna Shale is immature to marginally mature in this study area, therefore the solid bitumen observed in the Anna Shale is likely pre-oil solid bitumen generated during early maturity thermal alteration. The generation of hydrocarbons from liptinitic organic matter is thought to be one of the mechanisms of micrinite formation (Teichmüller and Ottenjahn, 1977; Teichmüller and Wolf, 1977; Taylor and Liu, 1989; Pickel et al., 2017). The abundance of micrinite may be the result of early hydrocarbon generation from more hydrogen-rich liptinitic materials like bituminite.

4.2 Paleo-redox conditions

C-S-Fe ternary diagrams allow recognition of consistent Fe/C, S/C, or S/Fe ratios and can be used to estimate DOP from TOC, total Fe, and total S (Dean and Arthur, 1989; Arthur and Sageman, 1994). Sediments deposited under oxic conditions can be distinguished from those deposited under dysoxic conditions at a boundary of 0.42 DOP (Raiswell et al., 1988). Some overlap in DOP occurs between dysoxic and anoxic categories from 0.55 - 0.93 DOP; a DOP of > 0.75 separates more than 90% of anoxic from dysoxic samples (Raiswell et al., 1988). Estimations of paleo-redox conditions made from C-S and C-S-Fe relationships have been shown to agree well and produce more reliable estimates (Ocubalidet et al., 2018). Estimations made from trace-element ratios have been shown to differ slightly with V/(V+Ni) indicating more oxygen restricted conditions than Ni/Co and V/Cr which tend to produce similar estimations of

paleo-redox conditions (Rimmer, 2004; Ocubalidet et al., 2018). Therefore, interpretations should be made using multiple paleo-redox proxies.

Paleo-weathering caused by the infiltration of oxidizing fluids has been shown to lower concentrations of TEs used in paleo-redox assessments and replace pyrite with hematite and goethite (Marynowski et al., 2017). There are no signs of paleo-weathering as concentrations of Mo, Cu, and Ni are high in some intervals on the order of several hundred parts per million, and concentrations of V and Zn are on the order of several thousand parts per million in some intervals. Additionally, pyrite nodules and pyritized fossils occur throughout the Anna Shale samples and have not been replaced by iron oxide minerals. Another process that could potentially effect TE paleo-redox proxies is post-depositional TE mobilization by hydrothermal fluids. The Anna Shale has a very low permeability and acts as an impermeable layer preventing the migration of any fluids through the shale. Also, secondary mineralization related to hydrothermal fluids is not observed in the Anna Shale or underlying coal in this area of the basin. No evidence for trace element mobilization by hydrothermal fluids is observed.

The C-S-Fe ternary diagram (Figure 20) shows two distinct trends in the data that can be used to estimate DOP. Data for cores C6848, C7003, C7009, and the roof samples plot along a constant S/Fe ratio that has an estimated DOP of 0.51. The DOP for these samples suggests deposition under dysoxic conditions. Data for core C7005 and one data point from cores C6848, C7003, and C7009 plot along a constant S/Fe ratio that has an estimated DOP of 0.73. The DOP for these samples suggests marginally anoxic conditions. The samples from C6848, C7003, and C7009 that plot along the 0.73 DOP line are the lowest TOC and upper-most sample from each core. The V/Cr and Ni/Co proxies suggest oxic conditions for these samples whereas the

V/(V+Ni) proxy suggests anoxic conditions. The lower TOC and trace-element proxies suggest these intervals may not have been deposited under anoxic conditions.

The Anna Shale paleo-redox conditions assessed from TE redox proxies in southwestern Illinois (this study) share few similarities with those in western Kentucky. In western Kentucky, V/Cr ratios suggest oxic conditions, and Ni/Co ratios suggest anoxic conditions (Eble and Greb, 2018). The V/(V+Ni) ratios suggest oxic conditions at the start of deposition that shifted to anoxic conditions during deposition of the middle and upper Anna Shale (Eble and Greb, 2018). The TE proxies do not indicate cyclic redox conditions during deposition in western Kentucky.

In southwestern Illinois, the Anna Shale was deposited under cyclic paleo-redox conditions. Three periods of more restricted redox conditions are shown in the plots of all three TE proxies for cores C6848, C7003, and C7009 (Figures 21, 22, 24). The V/Cr ratios suggest strongly anoxic conditions during the first restricted period and dysoxic to oxic conditions for the upper two low-oxygen periods. The Ni/Co ratios suggest similar dysoxic to anoxic conditions during each restricted period. The V/(V+Ni) ratios suggest anoxic to euxinic conditions for the entire interval with three periods of increased oxygen restriction and conditions becoming less restricted vertically. The V/Cr and Ni/Co ratios likely provide the more accurate estimation of paleo-redox conditions as V/(V+Ni) has been shown to be an outlier in other black shales (Rimmer, 2004; Ocubalidet et al., 2018). The TE proxies generally suggest the same redox conditions for core C7005 but the most restricted conditions occurred during deposition of the upper Anna Shale, not the lower intervals. The Ni/Co and V/(V+Ni) ratios show some cyclic redox conditions during deposition but restricted intervals do not correspond to organic matter accumulation as clearly as in other cores. The differences in trace element concentrations and

organic matter composition between the lower portion of core C7005 and the other cores suggest different depositional conditions.

Variations in geochemistry and organic matter have also been studied at a centimeter scale in the Hushpuckney Shale Member of the Late Pennsylvanian Swope Formation (Western Interior Basin). The paleo-redox conditions were also cyclic during deposition of the Late Pennsylvanian Hushpuckney Shale (Algeo et al., 2004). The cycles have been separated into low-order, eustatically controlled cycles and high-order, climatically controlled cycles (Algeo et al., 2004). High-order, climato-environmental fluctuations identified in the Hushpuckney Shale are 2-7cm thick cycles that are estimated to have lasted ~2,000-9,000 years; the high-frequency of these cycles suggest sub-Milankovitch climate fluctuations (Algeo et al., 2004). These high-order cycles more closely resemble the redox cycles observed in the Anna Shale. These may be the result of subtle shifts between wet, weakly seasonal climates and more seasonal precipitation that would increase and decrease runoff, which would ultimately strengthen and weaken the freshwater-sustained pycnocline (Algeo et al., 2004; Holterhoff and Cassady, 2012). Eustatic changes have also been suggested as a possible mechanism for these high-order cycles (Algeo et al., 2004).

Paleo-redox conditions during the deposition of cyclothemic black shales in the Western Interior Basin (Hushpuckney, Stark, and Muncie Creek shales) have been assessed using TOC-TE relationships (Algeo and Maynard, 2004). The relationship between TOC and TEs with a strong euxinic affinity has been observed to change between facies with < 10% and > 10% TOC (Algeo and Maynard, 2004). Trace element concentrations that do not correlate with TOC above this threshold have been associated with euxinic conditions (Algeo and Maynard, 2004).

Plots of aluminum-normalized TEs and TOC are shown in Figures 33 and 34. Under dysoxic conditions TEs are deposited mainly in detrital sediments and have no correlation with organic matter content (Algeo and Maynard, 2004). Trace elements are deposited predominantly as organometallic complexes under anoxic conditions so the concentration of TEs is related to the amount of organic matter deposited (Pratt and Davis, 1992). Trace elements with strong euxinic affinities are reduced to their lowest valence state under euxinic conditions, allowing the precipitation of sulfides and oxyhydroxides from the water column or at the sediment-water interface, which allows deposition of TEs independent of organic matter (Morse and Luther, 1999). According to Algeo and Maynard (2004), samples assigned to euxinic facies would have high concentrations of TEs with strong euxinic affinity (Mo, V, and Zn) that do not correlate with TOC. The five samples with high concentrations of V and the four samples with high concentrations of Mo have high correlation coefficients (Figure 33). The three samples with high concentrations of Zn do not show a correlation as expected for euxinic samples (Figure 33). However, the small populations of samples with high concentrations of TEs with strong euxinic affinity does not allow a clear population of samples indicative of euxinic conditions to be identified. For Mo and Zn, there is not a clear population of samples that have a strong correlation with TOC. However, there is a population of samples with V concentrations that correlate significantly with TOC at a significance level of $\alpha = 0.05$, indicating a population of samples that represent anoxic facies (Figure 33). For TEs with weak euxinic affinity, there are two distinct populations of samples (Figure 34). The population of 14 samples with concentrations of weak euxinic affinity elements Cu, Ni, and Cr show a significant correlation with TOC at a significance level of $\alpha = 0.01$ and Co shows a correlation at a significance level of

$\alpha = 0.02$, suggesting this population of samples represents anoxic conditions. With the exception of Ni, the other population of samples does not have a significant correlation with TOC and suggests dysoxic conditions. The two samples that are not assigned a facies are not clearly associated with either population.

The anoxic threshold for the Anna Shale may not be similar to those for the black shales of the Western Interior Basin studied by Algeo and Maynard (2004). The population of dysoxic samples has TOC contents as high as 13.3% and the anoxic population has values as low as 21.5% TOC, suggesting the dysoxic, anoxic threshold for the Anna Shale may not be at 10% TOC like as reported for other cyclothemic black shales by Algeo and Maynard (2004). The anoxic threshold for the Anna Shale may be between 15 - 20% TOC. More data should be gathered to evaluate the threshold.

4.3 Clastic influx

Influxes of sediment can interrupt organic matter preservation and can dilute organic matter (Murphy et al., 2000). Sediment influxes may also increase preservation through either physical protection (Salmon et al., 2000) or adsorption onto the surface of clay minerals (Kennedy et al., 2002). Rimmer et al. (2004) suggested that a change in the total supply of sediment, which would include the amount of clays, may affect the preservation of organic matter through these mechanisms. Changes in the K/Al ratio also may suggest a change in the minerology of sediments during clastic influxes (Rimmer et al., 2004). An increase in the K/Al ratio may indicate an increase in illite, which is K- rich (Kennedy et al., 2002).

Ti/Al and Si/Al ratios indicate three intervals of increased clastic influx and siliclastic sedimentation in cores C6848, C7003, and C7009 that correspond with the highest TOC intervals

as shown in Figures 27, 28, and 30. Two intervals of core C7005 with increased clastic influx correspond to high TOC intervals in Figure 29; only the upper high TOC interval shows an increase in quartz relative to clays. Increases in clastic influx also correspond with an increase in the K/Al ratio which may indicate a change in mineralogy of sediments. Influxes of clastic sedimentation correspond with high TOC intervals which suggest an increase in organic matter preservation during periods of increased sedimentation. This may be the result of physical protection by or adsorption onto the surface of clay minerals.

The corresponding cyclicity of organic matter preservation, deposition of trace-elements, paleo-redox conditions, and clastic influx suggest these were driven by a common mechanism (climatic or eustatic). The same observation was made in the geochemical study of the Hushpuckney Shale (Algeo, 2004).

4.4 X-ray diffraction and EPMA of pyrite suns

Pyrite sun 1 is composed entirely of pyrite; the minor amount of quartz is likely from remaining shale that was not removed from the surface during sample preparation. The anomalous peak at 29.4° in the diffraction patterns of pyrite sun 2 may indicate a small amount of chalcopyrite since this corresponds to the largest peak in the diffraction pattern of chalcopyrite, but no other chalcopyrite peaks appear in the diffraction pattern.

Any concentration of TEs in the pyrite suns analyzed (Mo, Cu, Zn, As, Cd, and Pb) is below the detection limits for EPMA which were estimated to be 0.05 wt%. Any zoning of TEs may still provide further insights into their formation so it is suggested that laser ablation inductively couple mass spectrometry (LA-ICP-MS) be conducted due to the significantly lower detection limits of the analysis.

4.5 Pyrite sun distribution and formation

The paleo-redox conditions of the roof samples of Anna Shale were investigated using TE paleo-redox proxies to determine if there were any relationships with the occurrence of pyrite suns. Plots of the roof sample paleo-redox proxies are shown in Figure 26. There are no clear relationships between paleo-redox conditions of the Anna Shale where pyrite suns occur and where they do not occur. The V/Cr and V/(V+Ni) ratios do suggest more restricted conditions for roof samples from locations where pyrite suns do occur (Roof 1, 2, 6, 7) compared to samples from locations they do not (Roof 4, 5). Further investigation with more samples should be conducted to elucidate any possible relationships.

Field observations at the Lively Grove Mine near Marissa, IL, suggest there is a clear relationship between the extent and type of bioturbation in the lower most portion of Anna Shale where pyrite suns occur. Some locations where pyrite suns do not occur are extensively bioturbated with burrows 1.6 mm (1/16 in) in diameter (Figure 35A) whereas others may not have any bioturbation at all. These burrows may have been produced by a worm-like phylum (J. Devera, ISGS, personal communication). Burrows of polycheate worms have been observed in "quasi-anaerobic" laminated sediments that were deposited under a water column with < 0.2 mL O_2/L H_2O (Tyson and Pearson, 1991). These small burrows have not been observed in areas where pyrite suns occur. Instead, larger burrows 3.8-5.7 cm (1 ½ -2 ¼ in) in diameter occur in the same areas as pyrite suns and are partially pyritized (Figures 35B-35E). Pyrite branches off the burrows in between shale bedding planes with pyrite petals that splay out at the end shown in Figure 35B. The burrow cast filled in with pyrite and Brereton Limestone that is shown in Figures 35D and 35E was surrounded by slickensides and oriented parallel with bedding at the

Herrin (No. 6) Coal and Anna Shale contact. Some burrows terminate in large (up to 20.3 cm (8 in) and greater) nodular pyrite concretions that are surrounded by slickensides, such as the burrow shown in Figure 35C and the pyrite nodule in Figure 35F.

The occurrence of these two concretions together has been described as pyrite flowers (Seilacher, 2001). The morphology of these concretions and mechanisms of their formation have been described in the Lower Jurassic Posidonia Shales of Germany (Seilacher, 2001). The nodular concretions would have formed when the mud was still soft and isotropic, while later compaction formed slickensides around the concretion (Seilacher, 2001). The petals branching off the earlier formed nodular concretion formed by displacing cohesive beds after compaction made the mud anisotropic (Seilacher, 2001). This area at the terminus of the burrow filled in by the nodular pyrite concretion may have been a dwelling chamber where the burrowing organism died or deposited fecal pellets (Zangerl et al., 1969; Carvalho et al., 2016). The decay of the organic matter in the burrow released fluids and gases containing hydrogen sulfide in all directions which contributed to pyrite petal formation in surrounding sediments (Zangerl et al., 1969; Carvalho et al., 2016).

Pyrite suns may have formed similarly to pyrite flowers. Pyrite suns likely formed after compaction made the muds anisotropic. The disk-shape originated from radial crack propagation as pyrite crystals nucleated at the midline on the interior of the concretion, displacing mud along bedding planes in a circular shape (Figure 36A and 36B) (Seilacher, 2001). The mirror image of relief on each face of a pyrite sun agrees with radial crack propagation (Figure 36C and 36D) (Seilacher, 2001). A broken surface cross-section shows pyrite crystals grew to form fibrous

cone-in-cone structures on either side of the midline as they displaced stiff beds of mud (Figure 36A and 36B) (Seilacher, 2001).

Burrows penetrating the Anna Shale from the Brereton Limestone where pyrite suns are found may have served as a conduit for sea-water sulfate to be transported to the base of the Anna Shale. Anaerobic conditions would likely have been present in the partially compacted Anna Shale sediments from the decay of organic matter. The sulfate could have then been reduced through bacterial activity, producing hydrogen sulfide that then reacted with iron in the sediments to form the pyrite concretions. The release of fluids and gases from the decay of organisms or fecal pellets at the bottom of burrows also may have contributed to the formation of pyrite suns (Zangerl et al., 1969; Carvalho et al., 2016).

Pyrite suns are only known to occur in the lowermost Anna Shale where the Herrin (No. 6) Coal is mined underground, therefore only the lowermost Anna Shale is typically observed. This limits observation of the middle and upper Anna Shale. Small roof falls do occur in these areas and sometimes several centimeters of shale can be broken off along bedding planes to expose more Anna Shale that does not contain pyrite suns. Pyrite sun occurrence may not be restricted to the base of the Anna Shale. The conditions present for their formation may also have been present in other intervals of the Anna Shale that are not accessible in underground mines. If a large enough roof fall or future surface mine exposes all the Anna Shale in an area where pyrite suns occur, the middle and upper Anna Shale could be examined for pyrite suns.

CHAPTER 5

CONCLUSIONS

The hypothesis of this thesis was that the Anna Shale was deposited under an anoxic water column and under such conditions organic matter could accumulate and be preserved. However, trace element proxies and C-S-Fe relationships suggest redox conditions cycled between anoxic and dysoxic conditions.

1) Trace element paleo-redox proxies indicate the redox conditions were cyclic during deposition of the Anna Shale. During periods of anoxia, large amounts of organic matter accumulated and were preserved whereas less organic matter was deposited during the periods of dysoxic conditions. Trace element-TOC relationships also indicate cyclic redox conditions during deposition. These relationships indicate deposition occurred under dysoxic, anoxic, and euxinic conditions. C-S-Fe relationships suggest conditions were dysoxic during deposition of cores C6848, C7003, and C7009 and that conditions were anoxic during deposition of core C7005.
2) Pyrite suns do not contain concentrations of TEs detectable by EPMA. Detection of any TEs would require an instrument with lower detection limits. Pyrite suns are composed of entirely pyrite, based on X-ray diffraction data.
3) The organic matter in the Anna Shale is a marine Type II kerogen that consists mostly of micrinite and bituminite. These macerals are thought to be degradation products suggesting the organic matter in the Anna Shale was altered prior and subsequent to preservation.

4) The Anna Shale has excellent source rock potential with an average TOC of 15.9% and average S2 values of 45.9 mg HC/g. The Anna Shale is marginally mature in southwestern Illinois but it may serve as an excellent source rock in more thermally mature regions of the basin to the east and southeast.

Future Work

There are multiple opportunities for future work on the Anna Shale and pyrite suns. Additional cores should be analyzed in the locality of core C7005 to more clearly understand the discrepancies seen in trace element concentrations, organic matter distribution, and maceral content between this core and the other three cores. Additional cores from the surrounding region could be analyzed to evaluate the lateral continuity of the cycles in paleo-redox conditions and provide more data to better define the threshold for the dysoxic-anoxic and anoxic-euxinic boundaries observed in TOC-TE relationships.

X-ray diffraction should be conducted on the Anna Shale to investigate changes in sources of sediment as they may relate to the causes of cycles in redox conditions such as changes in climate or minor eustatic changes. X-ray diffraction should also be conducted on samples of Anna Shale from the immediate areas where pyrite suns occur and from stratigraphically equivalent areas where they do not occur. Composition of the sediments may have played a role in the mechanical properties of the muds that caused radial crack propagation during formation of pyrite suns.

Laser ablation ICP-MS should be conducted to further investigate concentrations of TEs in pyrite suns for zonation. The detection limits of this method are much lower than EPMA and may be able to detect the presence of TEs.

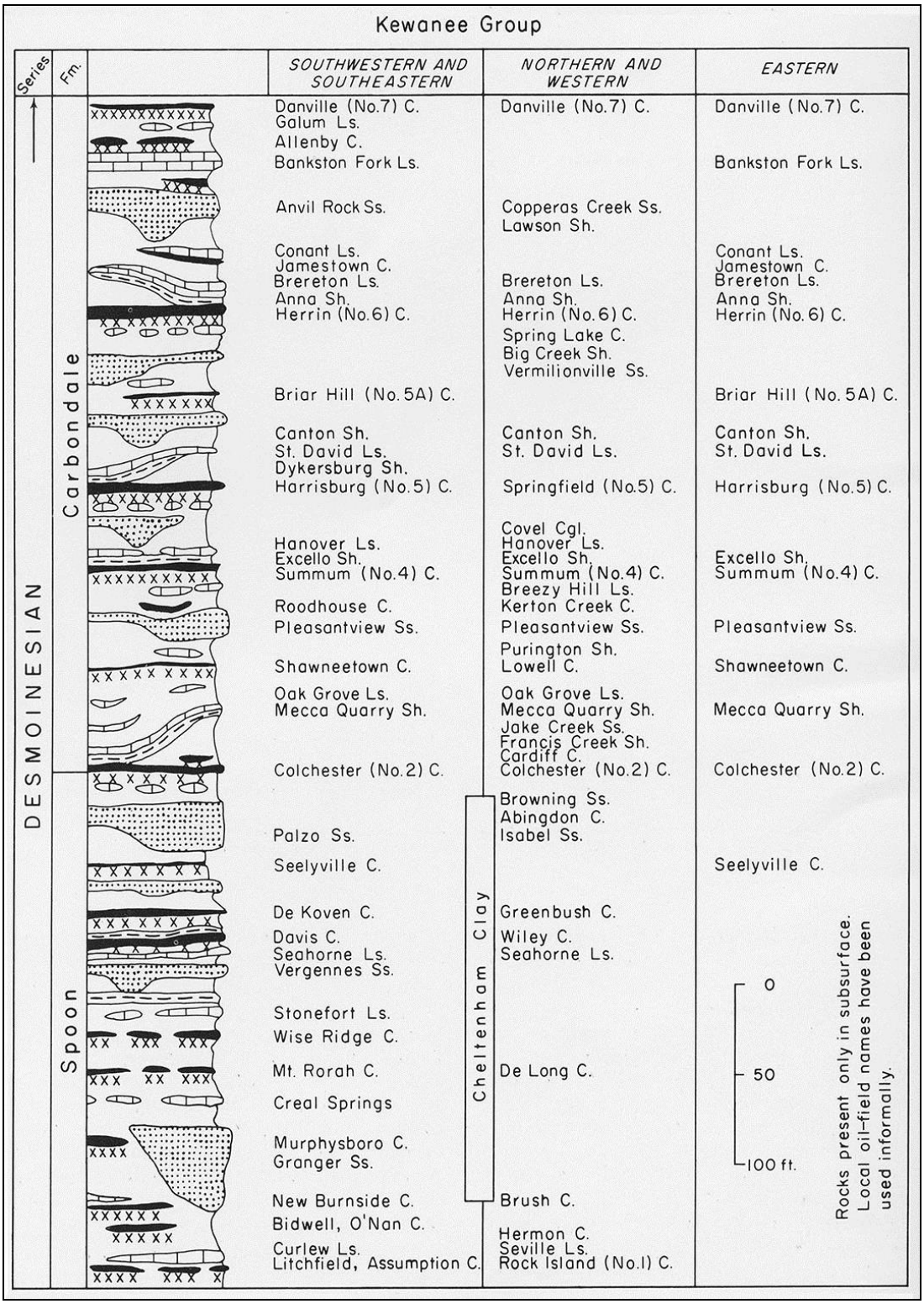

Figure 1: Stratigraphic column of the Carbondale Formation members, Illinois Basin (Willman et al., 1975).

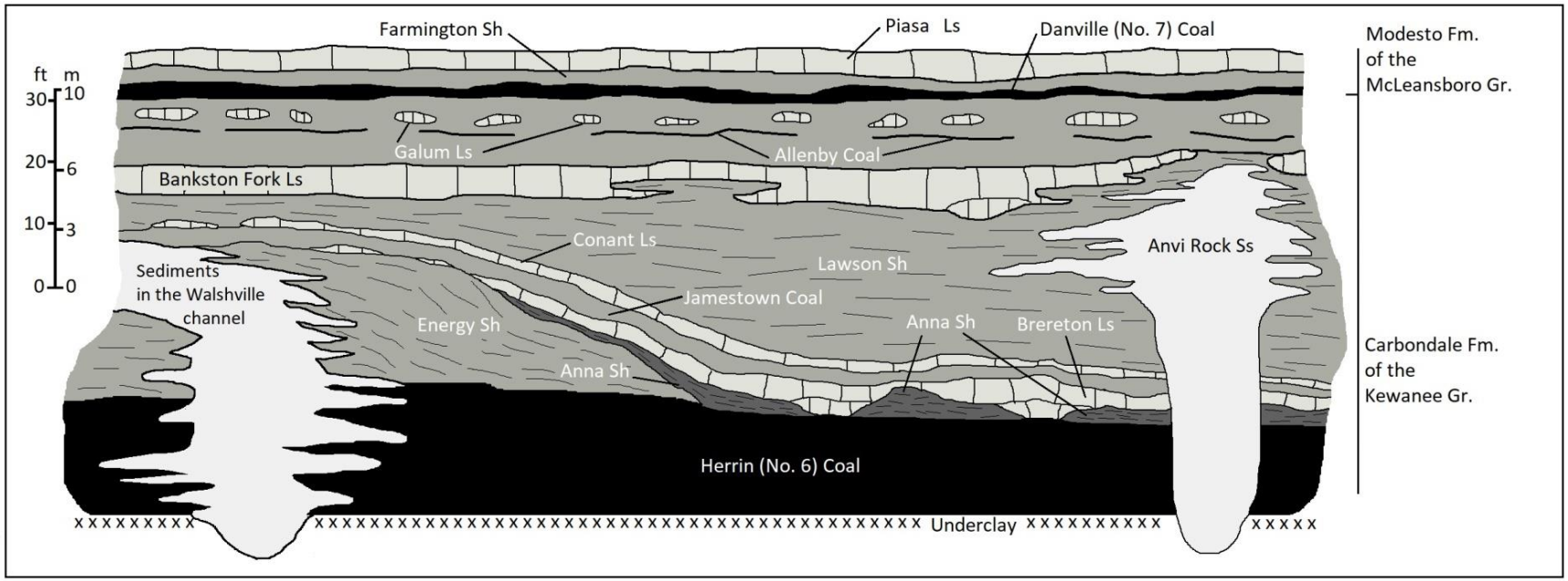

Figure 2: Representation of the relationships between units of the stratigraphic interval between the Herrin (No. 6) Coal and the Piasa Limestone (Redrafted from: Krausse et al., 1979, after Allgaier, 1974).

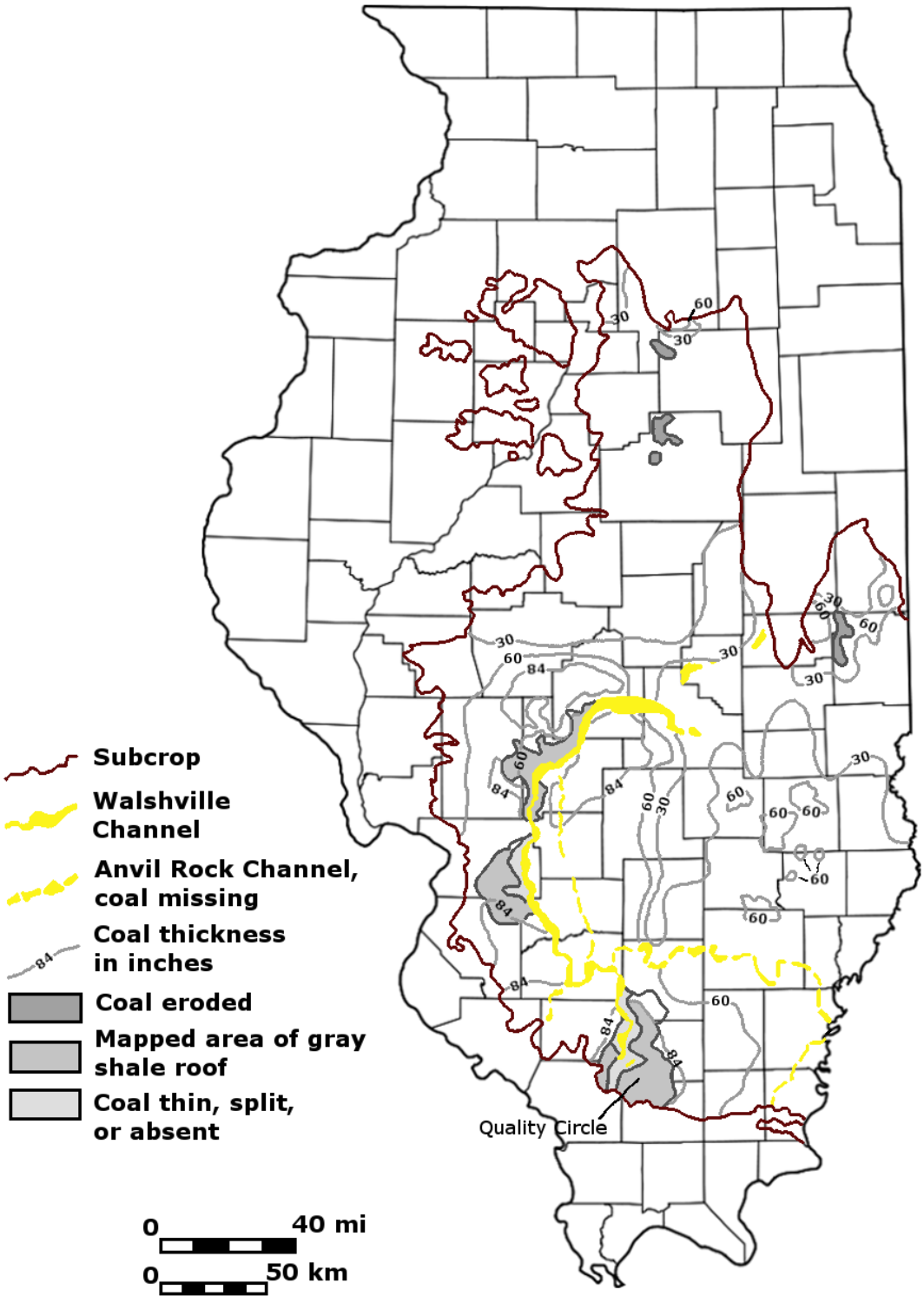

Figure 3: Distribution of the Herrin (No. 6) Coal, Walshville Channel, and gray Energy Shale (Redrafted from Krausse et al., 1979).

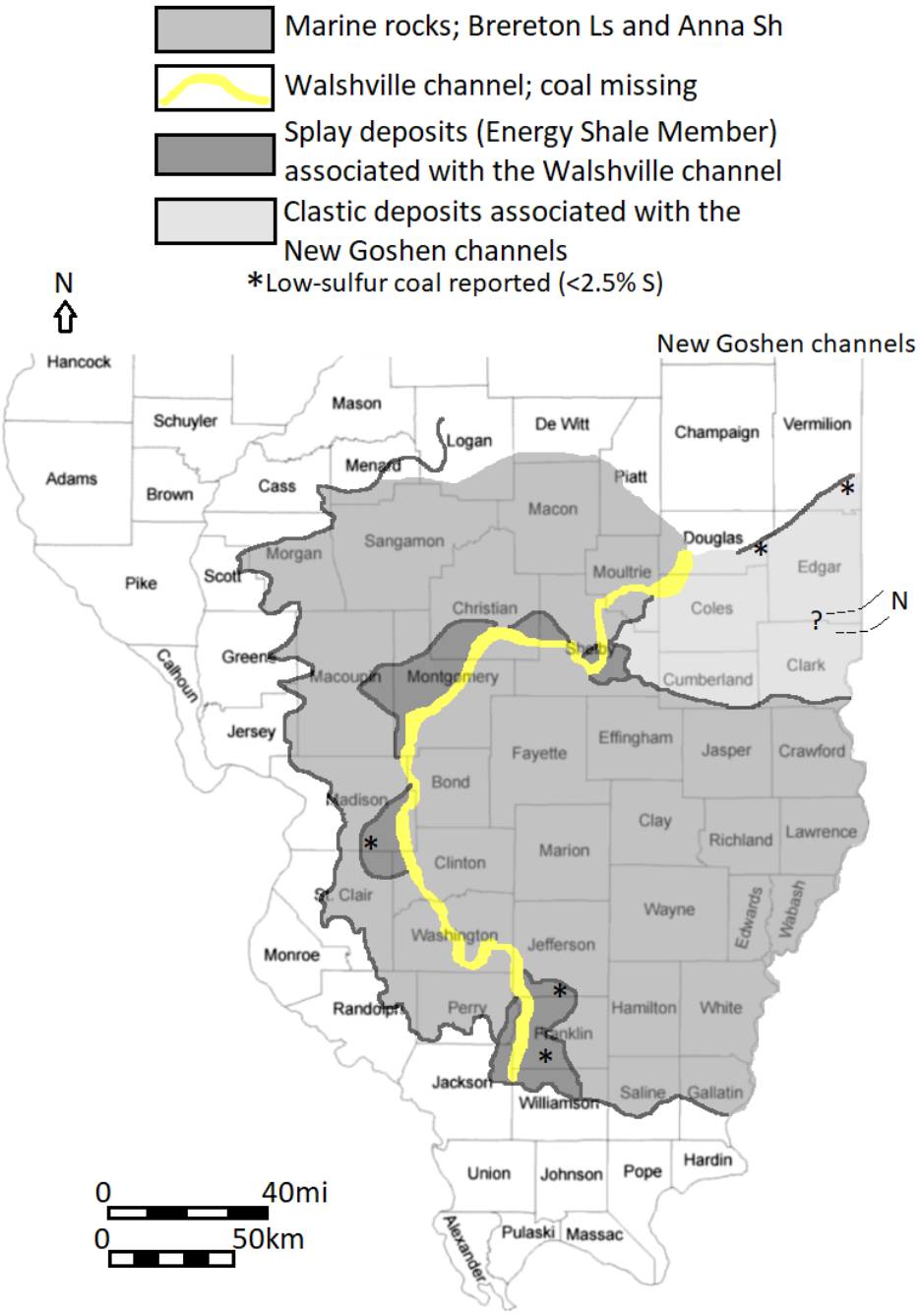

Figure 4: Distribution of roof lithologies of the Herrin (No. 6) Coal. Dark gray represents the gray Energy Shale and medium gray regions are where the Anna Shale or Brereton Limestone comprises the roof rock (Redrafted from Treworgy and Jacobson, 1979, modified from Krausse et al., 1979; Smith and Stall, 1975)

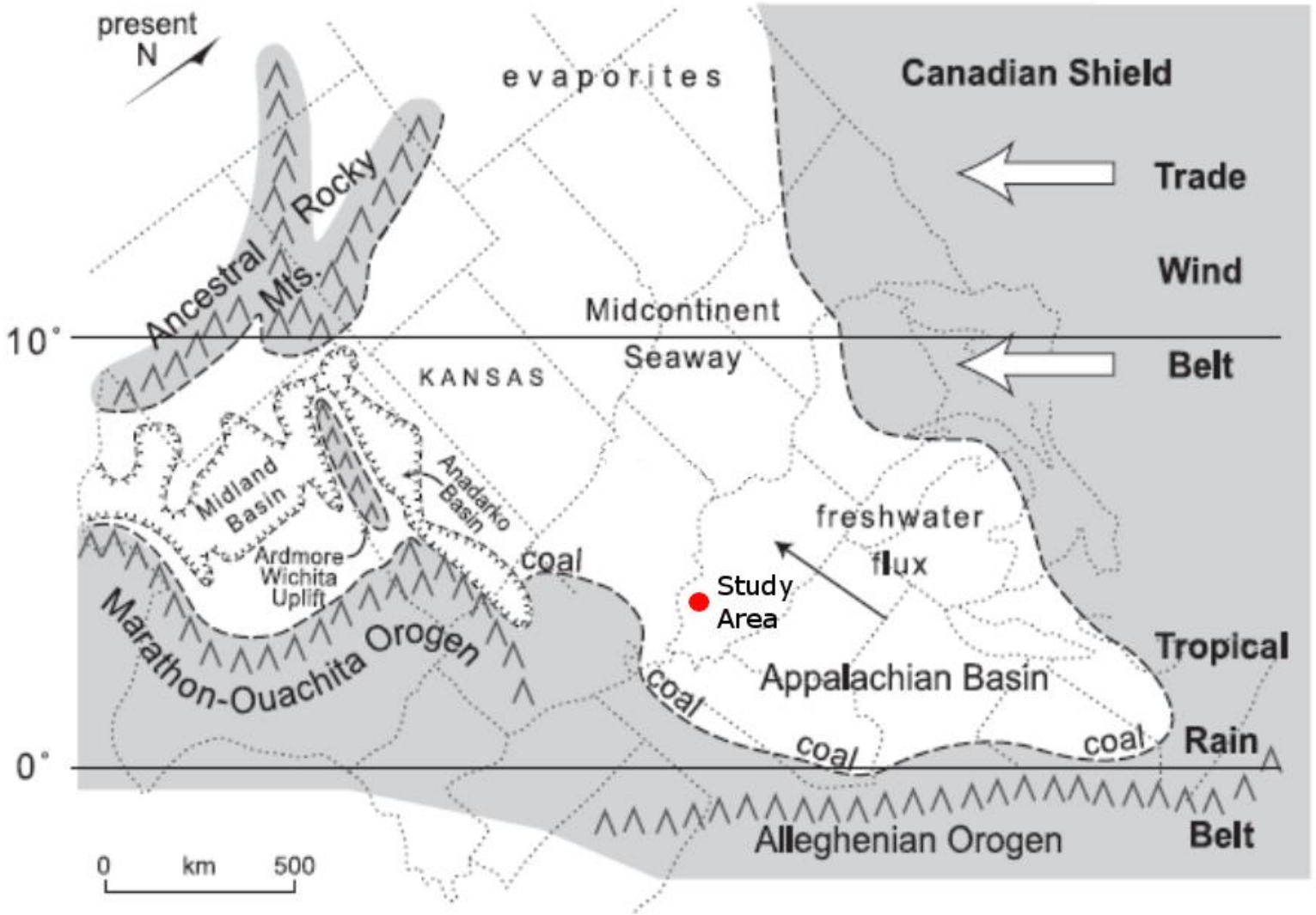

Figure 5: Paleogeography of the Late Pennsylvanian during the maximum transgression related to the deposition of the Hushpuckney Shale (modified from Algeo et al., 2004).

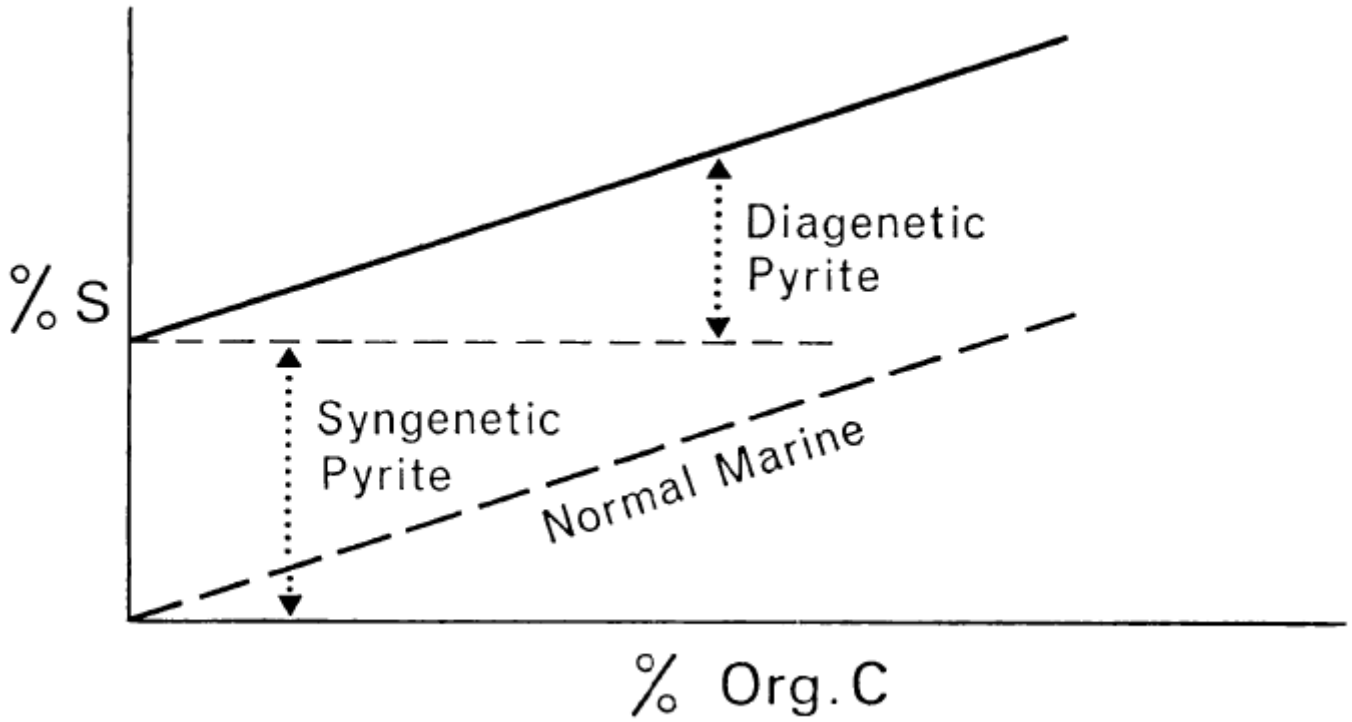

Figure 6: Idealized plot of pyrite sulfur (S) against organic carbon (C) for typical normal marine and euxinic sediments showing the syngenetic and diagenetic components of sedimentary pyrite (Raiswell and Berner, 1985).

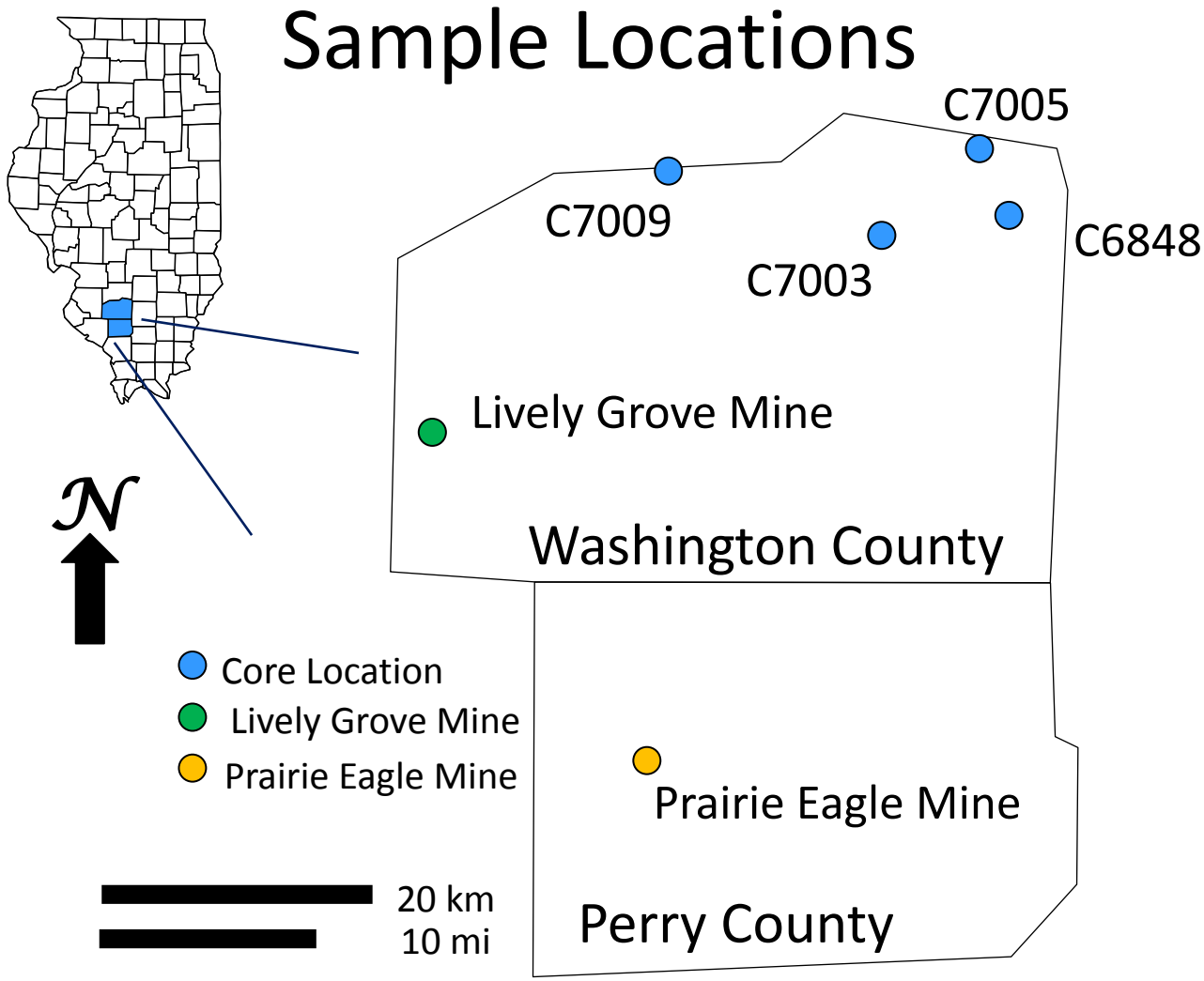

Figure 7: Map showing the core and mine locations in Washington County Illinois. Roof samples and pyrite suns were collected from the Prairie Eagle Mine. The sample of Herrin (No. 6) Coal was collected from the Lively Grove Mine.

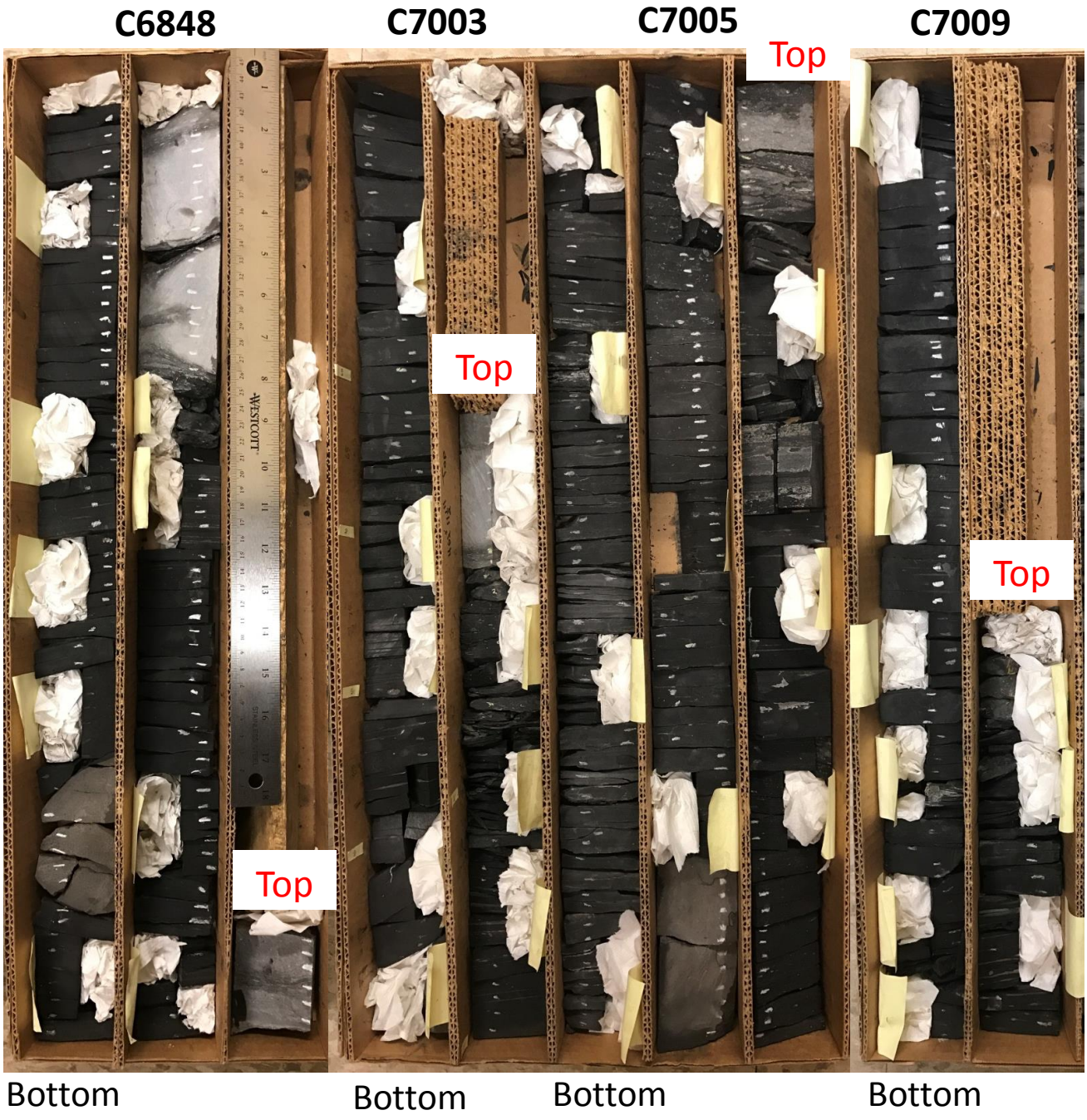

Figure 8: Sampled intervals of cores C6848, C7003, C7005, and C7009. The 5-cm intervals sampled from each core are marked with yellow Post-it notes. White chalk marks indicate 1-cm intervals for XRF analysis

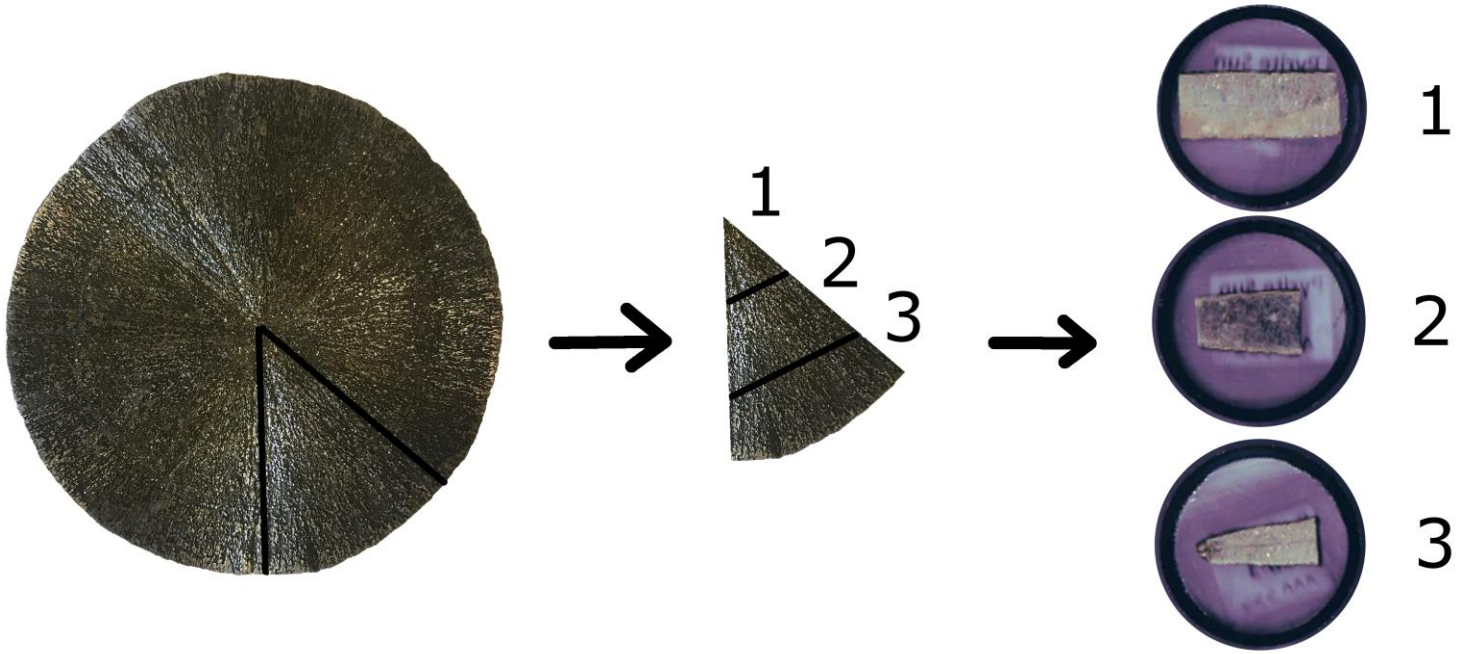

Figure 9: Pellets were prepared by first cutting a wedge out of the pyrite sun and then cutting the wedge into three pieces. The pieces were set in epoxy in 1-inch pellets to allow analysis of a cross-section of the pyrite sun.

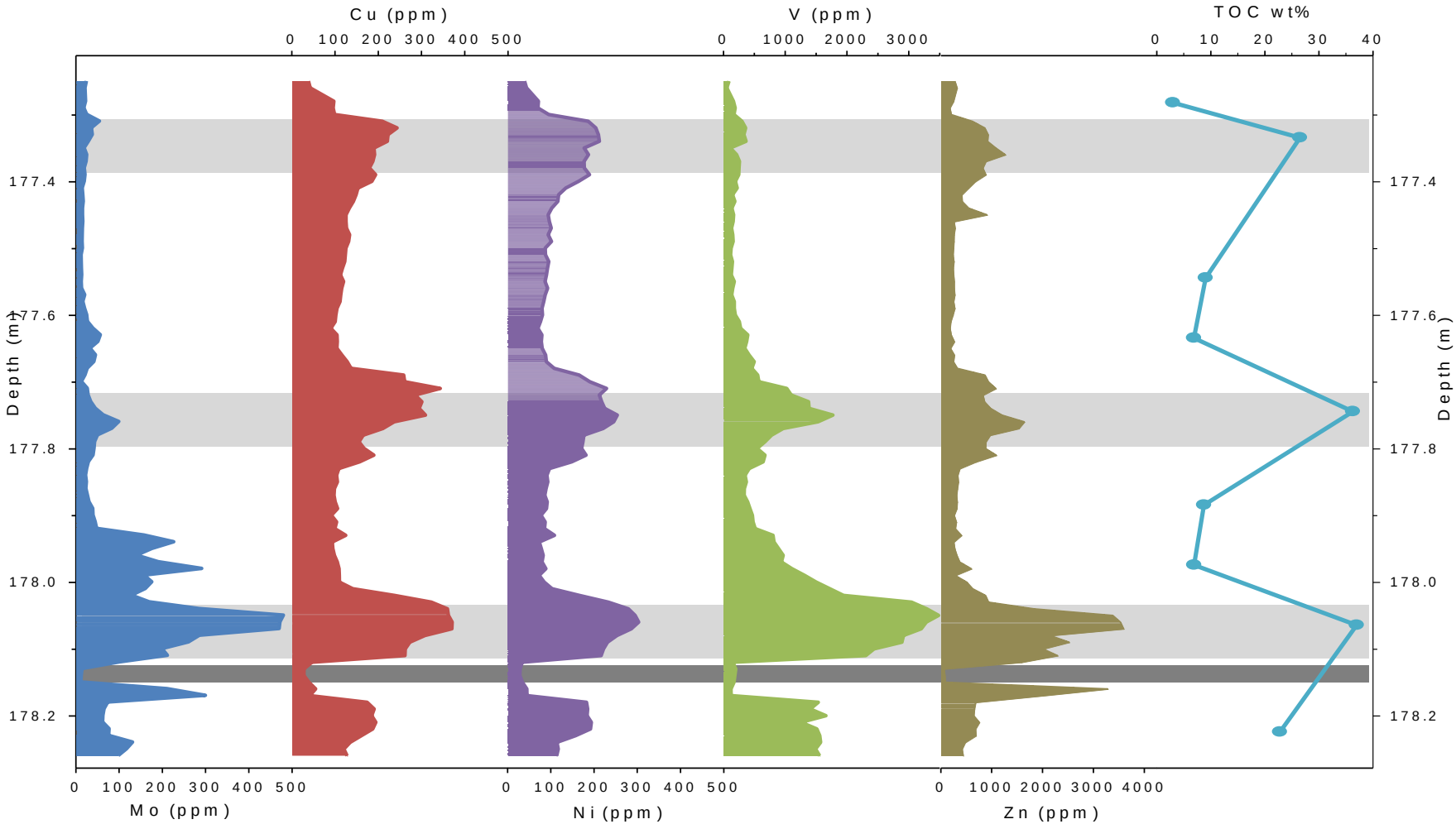

Figure 10: Plot of depth versus redox-sensitive elements (Mo, Cu, Ni, V, and Zn) and TOC for core C6848. Intervals with high concentrations of redox-sensitive elements, highlighted in light gray, correlate with high TOC intervals. The limestone nodule is highlighted in dark gray.

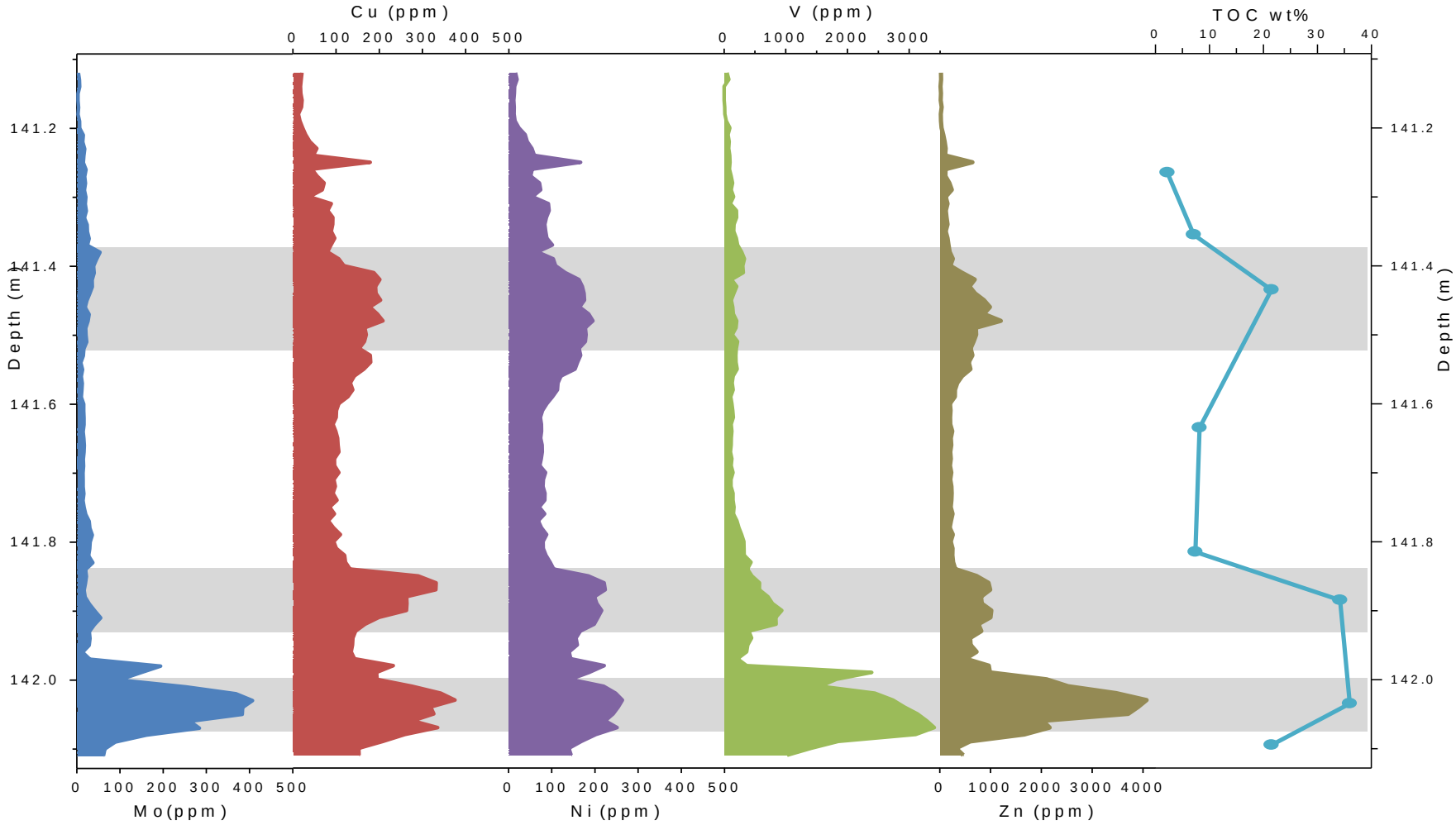

Figure 11: Plot of depth versus redox-sensitive elements (Mo, Cu, Ni, V, and Zn) and TOC for core C7003. Intervals with high concentrations of redox-sensitive elements, highlighted in light gray, correlate with high TOC intervals.

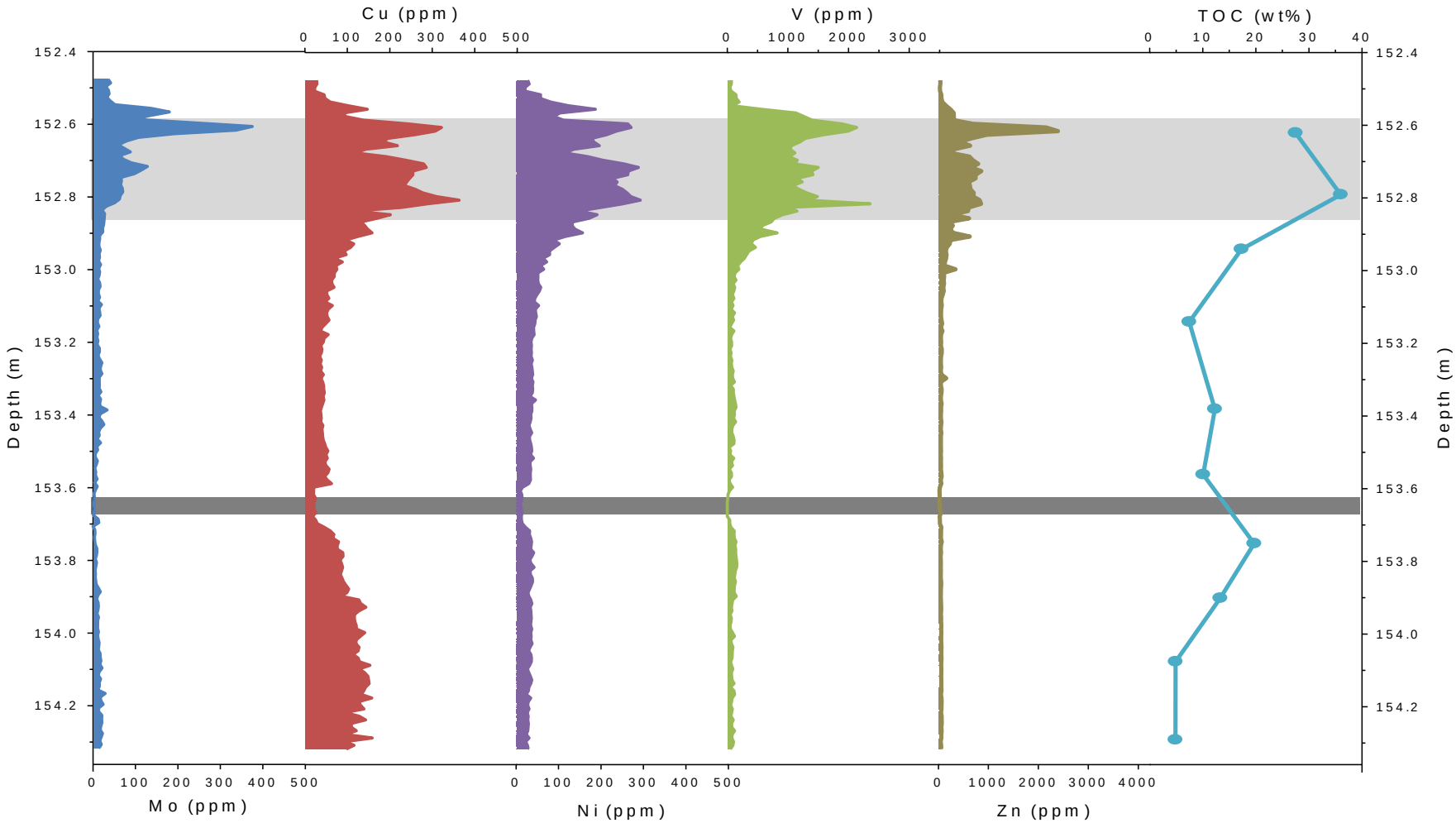

Figure 12: Plot of depth versus redox-sensitive elements (Mo, Cu, Ni, V, and Zn) and TOC for core C7005. Intervals with high concentrations of redox-sensitive elements, highlighted in light gray, correlate with high TOC intervals. The limestone nodule is highlighted in dark gray.

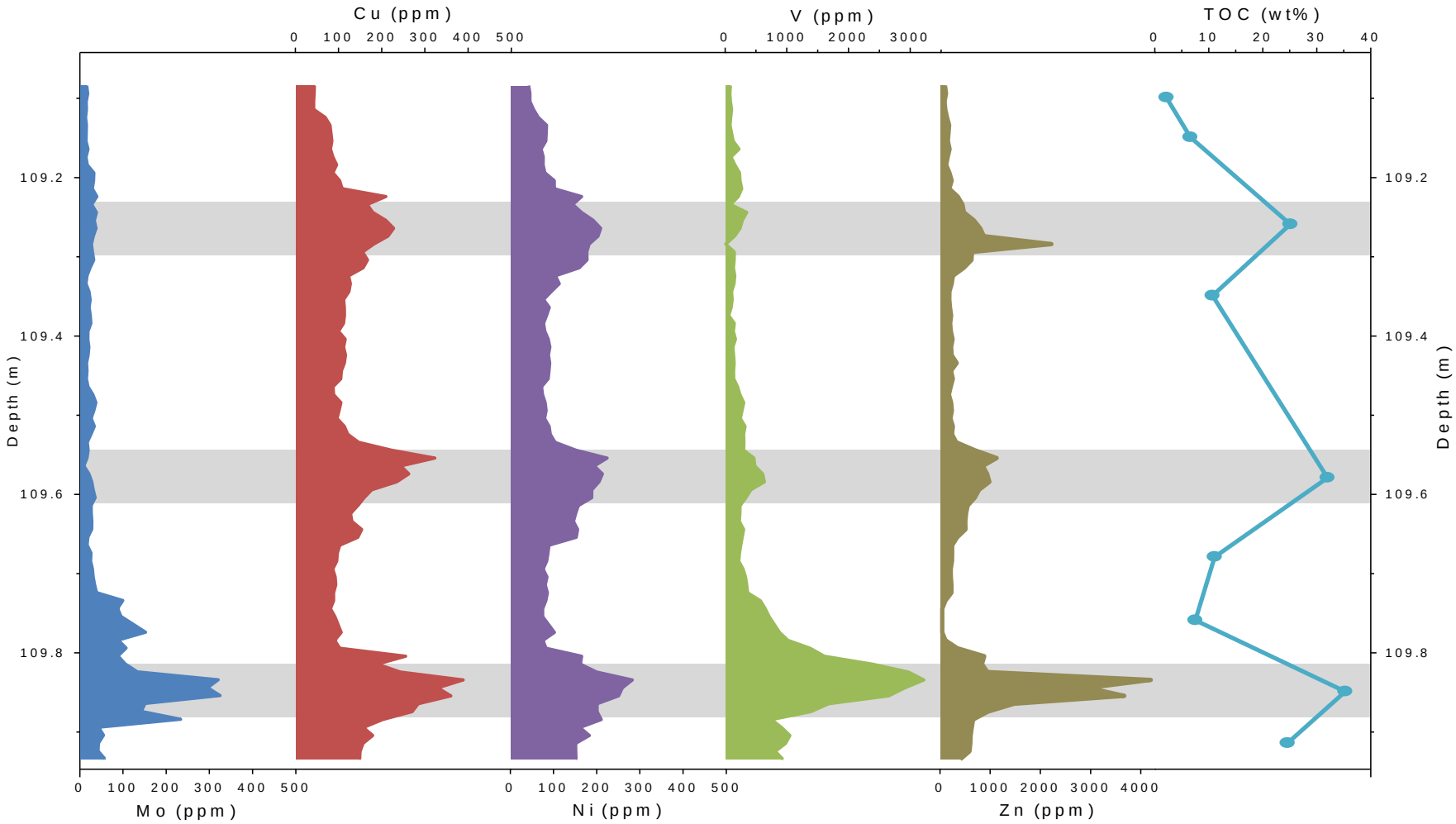

Figure 13: Plot of depth versus redox-sensitive elements (Mo, Cu, Ni, V, and Zn) and TOC for core C7009. Intervals with high concentrations of redox-sensitive elements, highlighted in light gray, correlate with high TOC intervals.

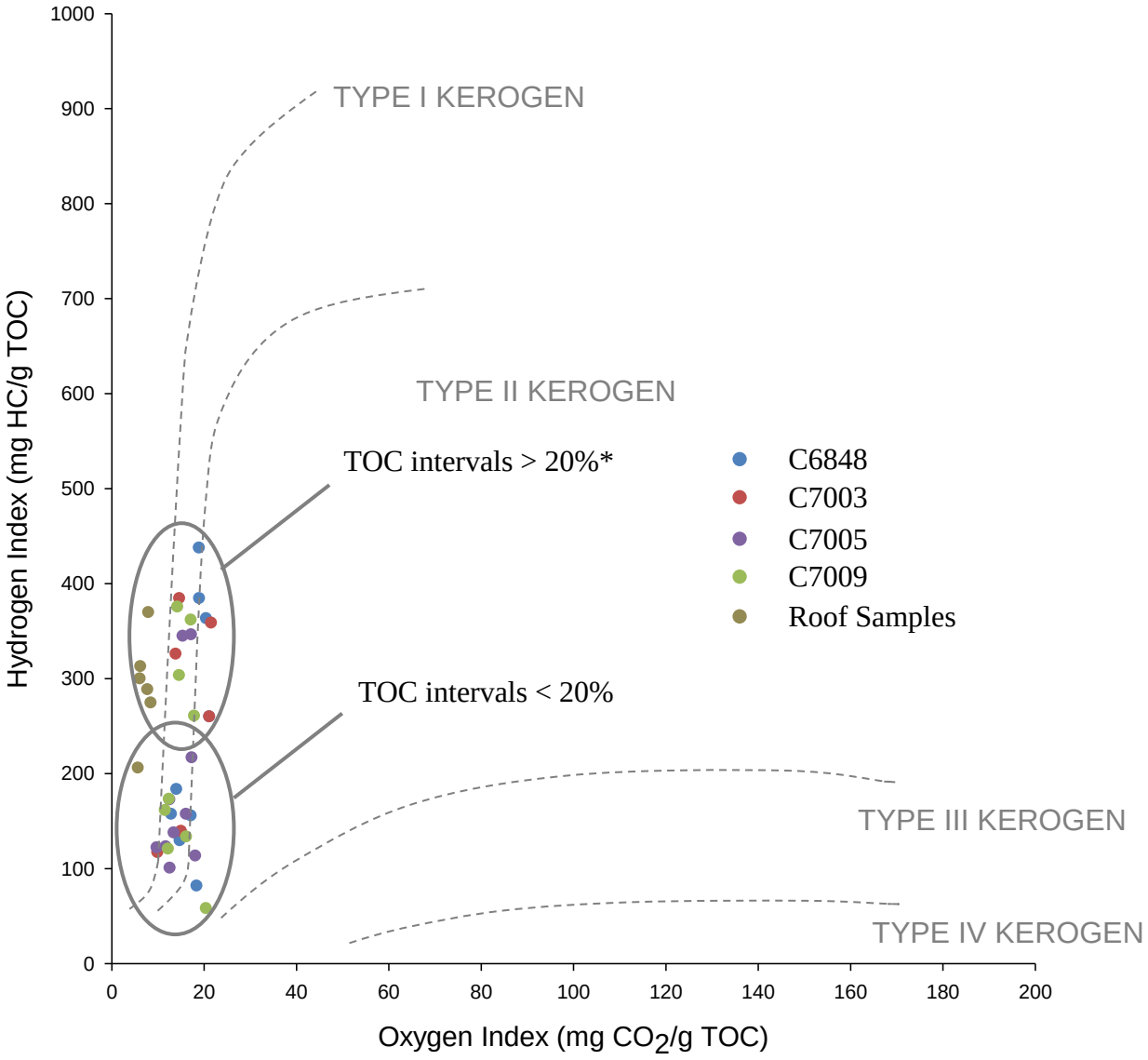

Figure 14: Pseudo van Krevelen diagram indicating a Type II marine kerogen for cores, C7003, C7005, C7009, and roof samples. *With the exception of roof samples 1, 2, 6, and 7, which all have < 10% TOC.

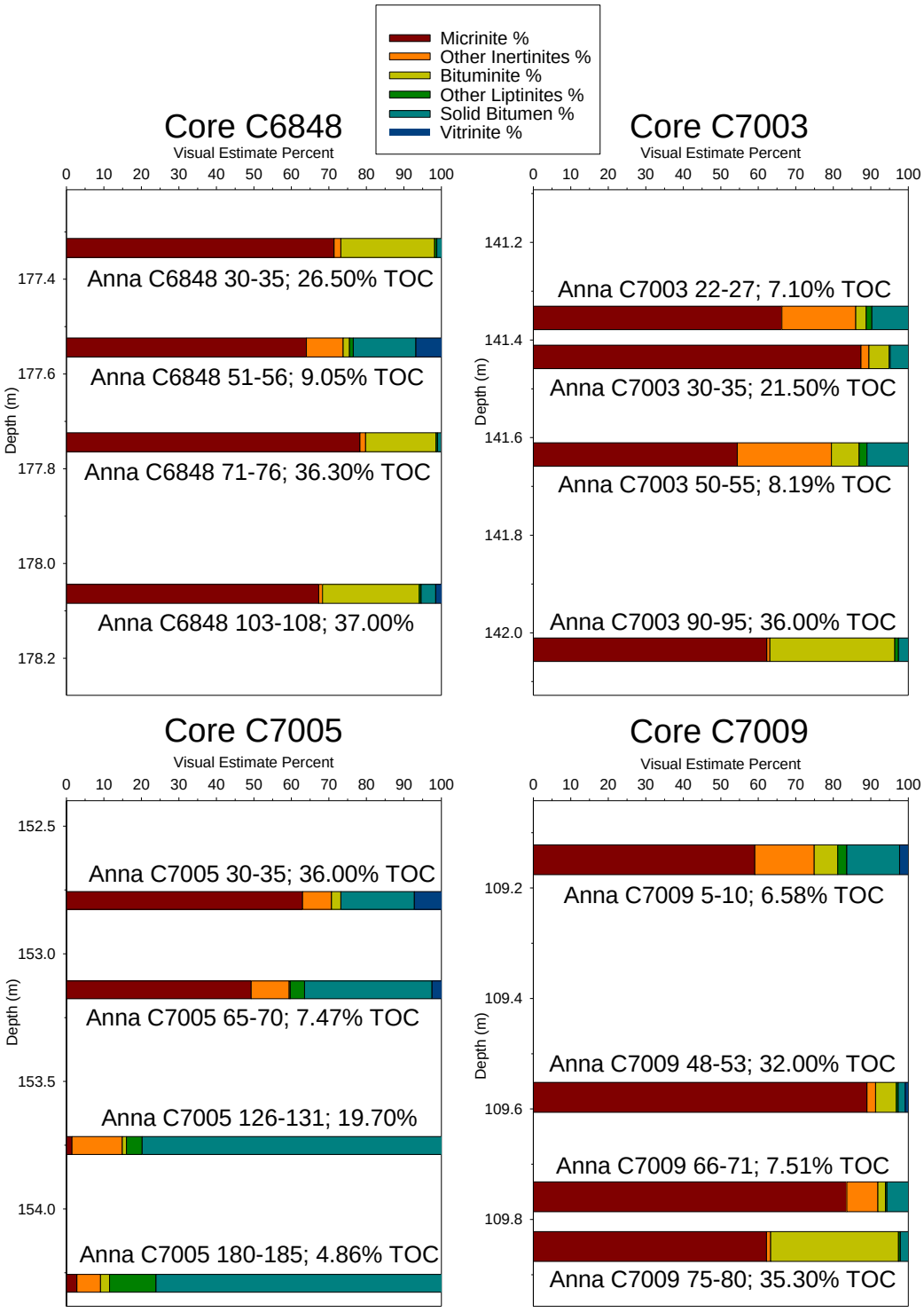

Figure 15: Profiles of petrographic data showing the portion each maceral contributes to TOC (on mineral-matter free, volume % basis).

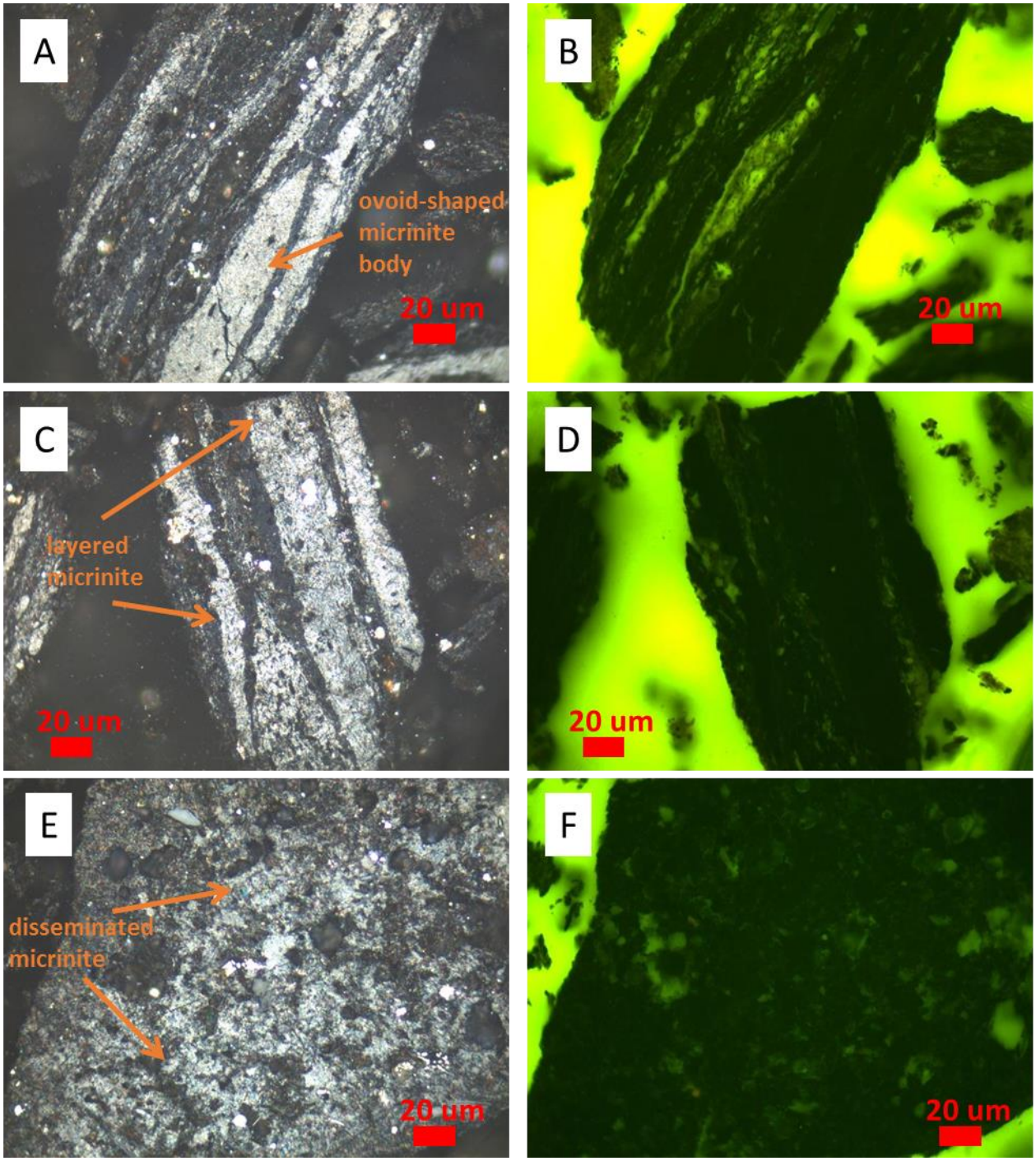

Figure 16: A) and B) White- and blue-light photomicrographs of ovoid-shaped micrinite body, sample C6848 71-76. C) and D) White- and blue-light photomicrographs of layered micrinite, sample C7003 90-95. E) and F) White- and blue-light photomicrographs of disseminated micrinite, sample C7003 30-35.

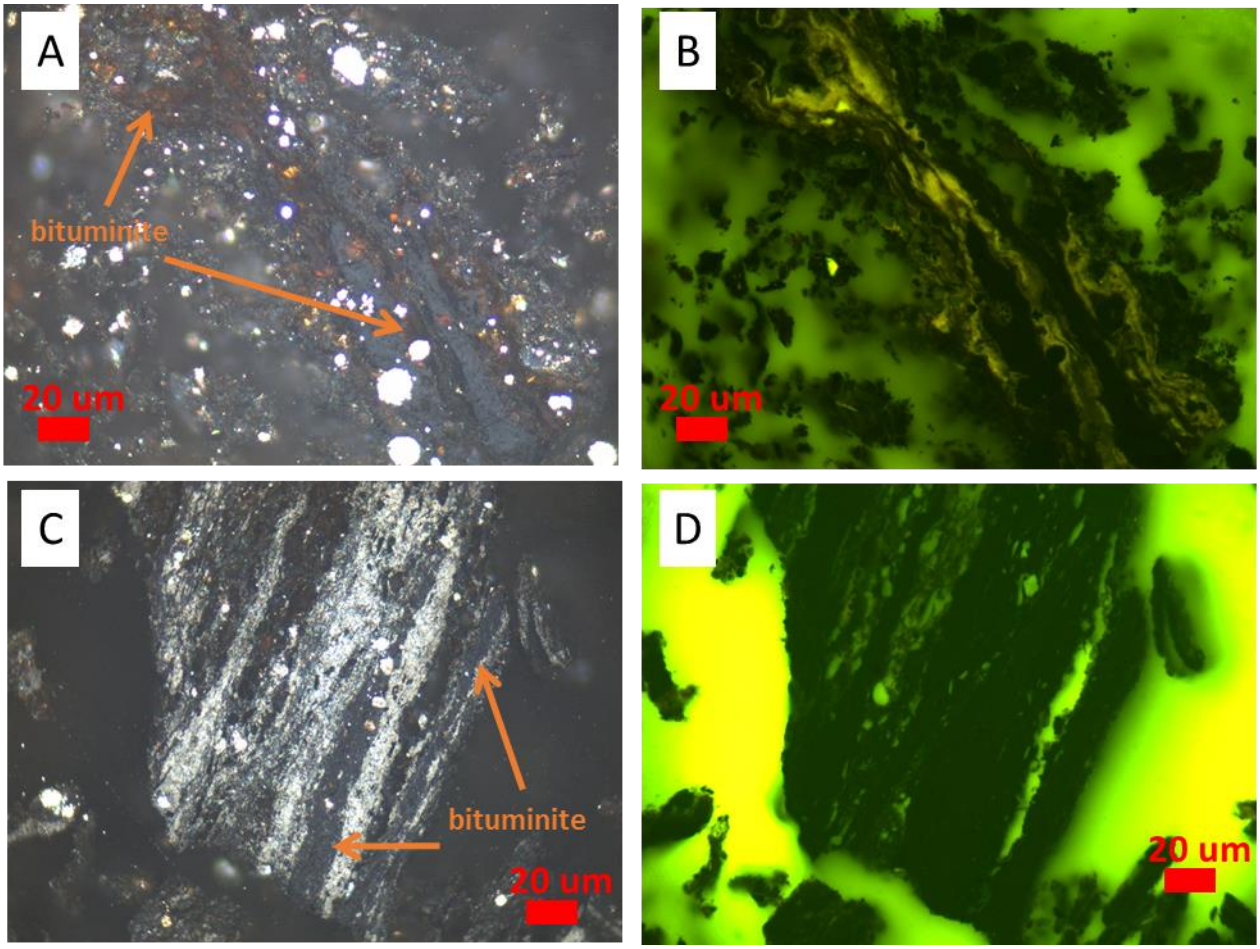

Figure 17: A) and B) White- and blue-light photomicrographs of dark brown bituminite with weak fluorescence, sample C7005 65-70. C) and D) White- and blue-light photomicrographs of dark gray bituminite with no fluorescence, sample C6848 103-108.

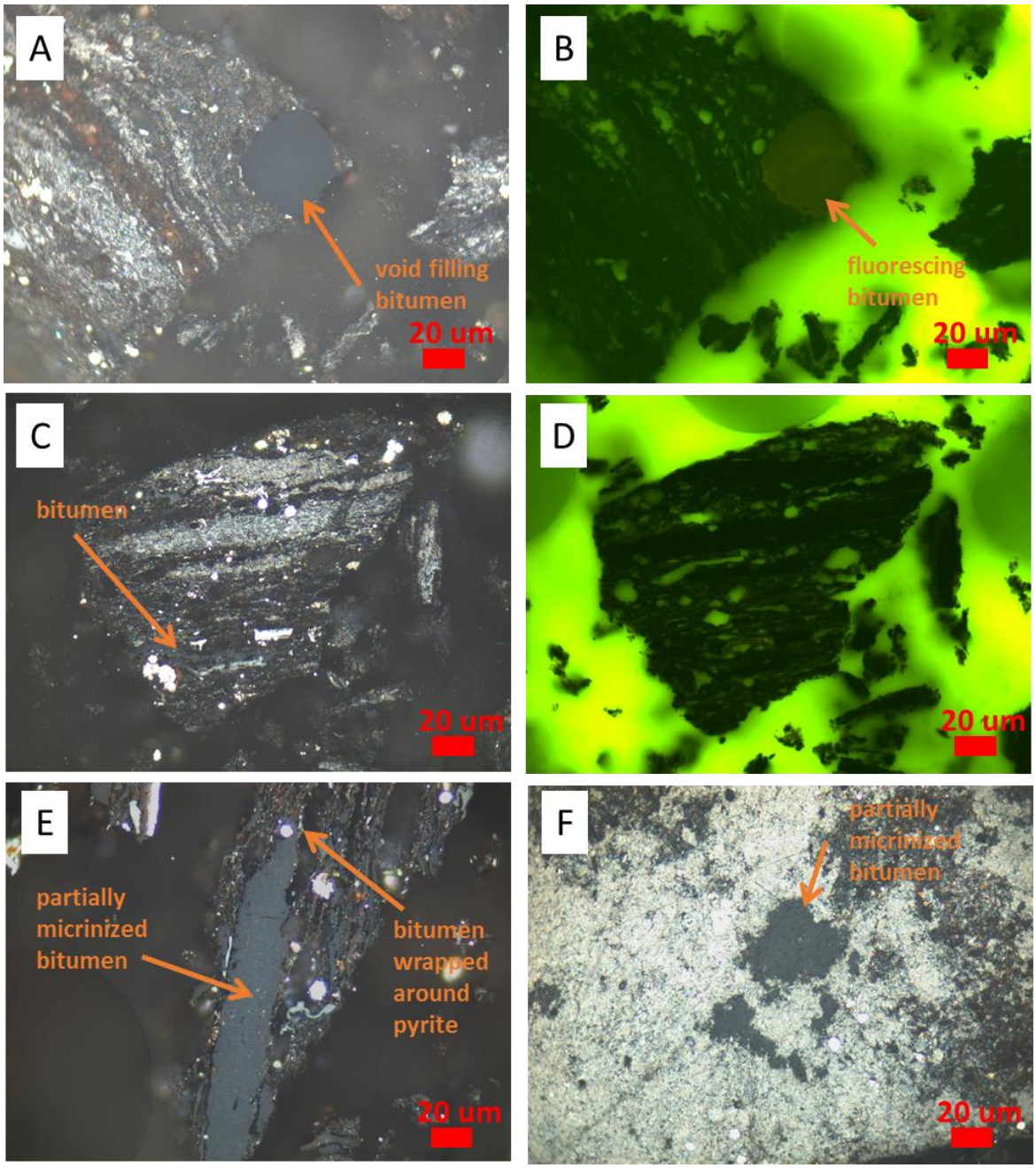

Figure 18: A) and B) White- and blue-light photomicrographs of void-filling solid bitumen (SB) with minor fluorescence, sample C6848 103-108. C) and D) White- and blue-light photomicrographs of SB along bedding, sample C6848 30-35. E) and F) White-light photomicrographs of partially micronized SB, samples C7005 126-131 and C7005 30-35, respectively.

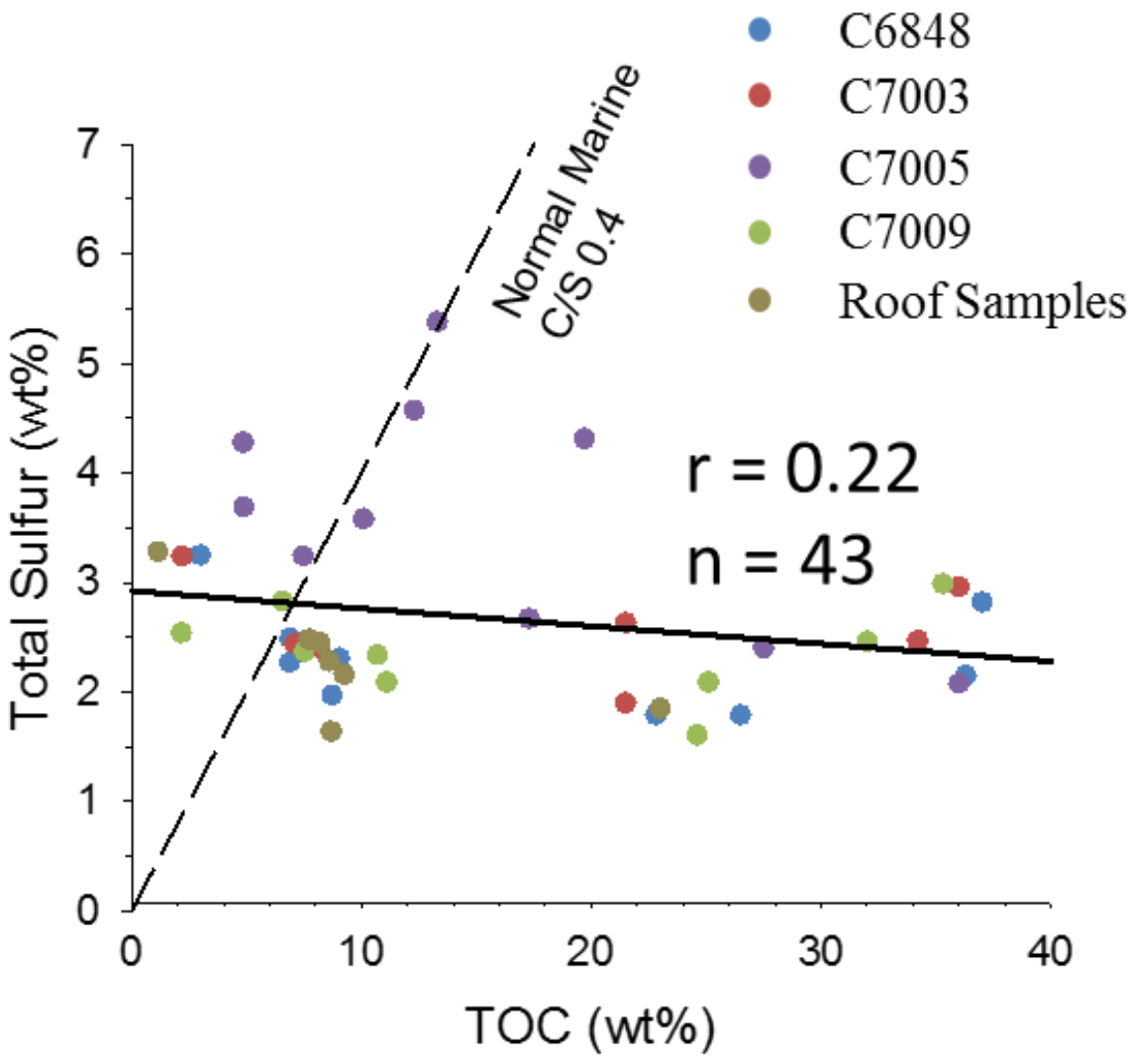

Figure 19: Carbon-sulfur plot of all core samples and roof samples. The C/S ratio for normal marine sediments of 0.4 is plotted for reference.

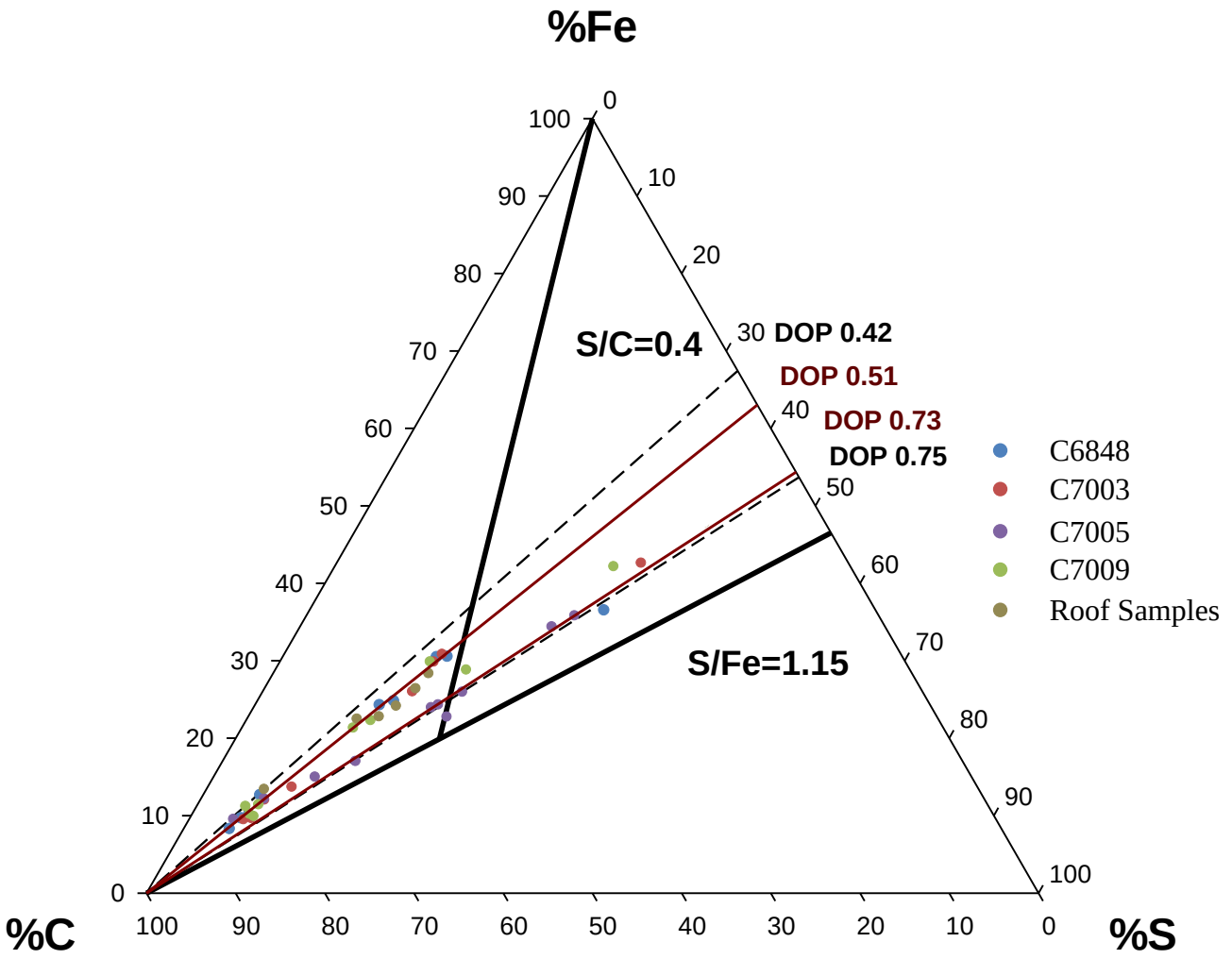

Figure 20: C-S-Fe ternary diagram for cores C6848, C7003, C7005, C7009, and roof samples, suggest two populations with approximated trend lines through 0.51 and 0.73 DOP.

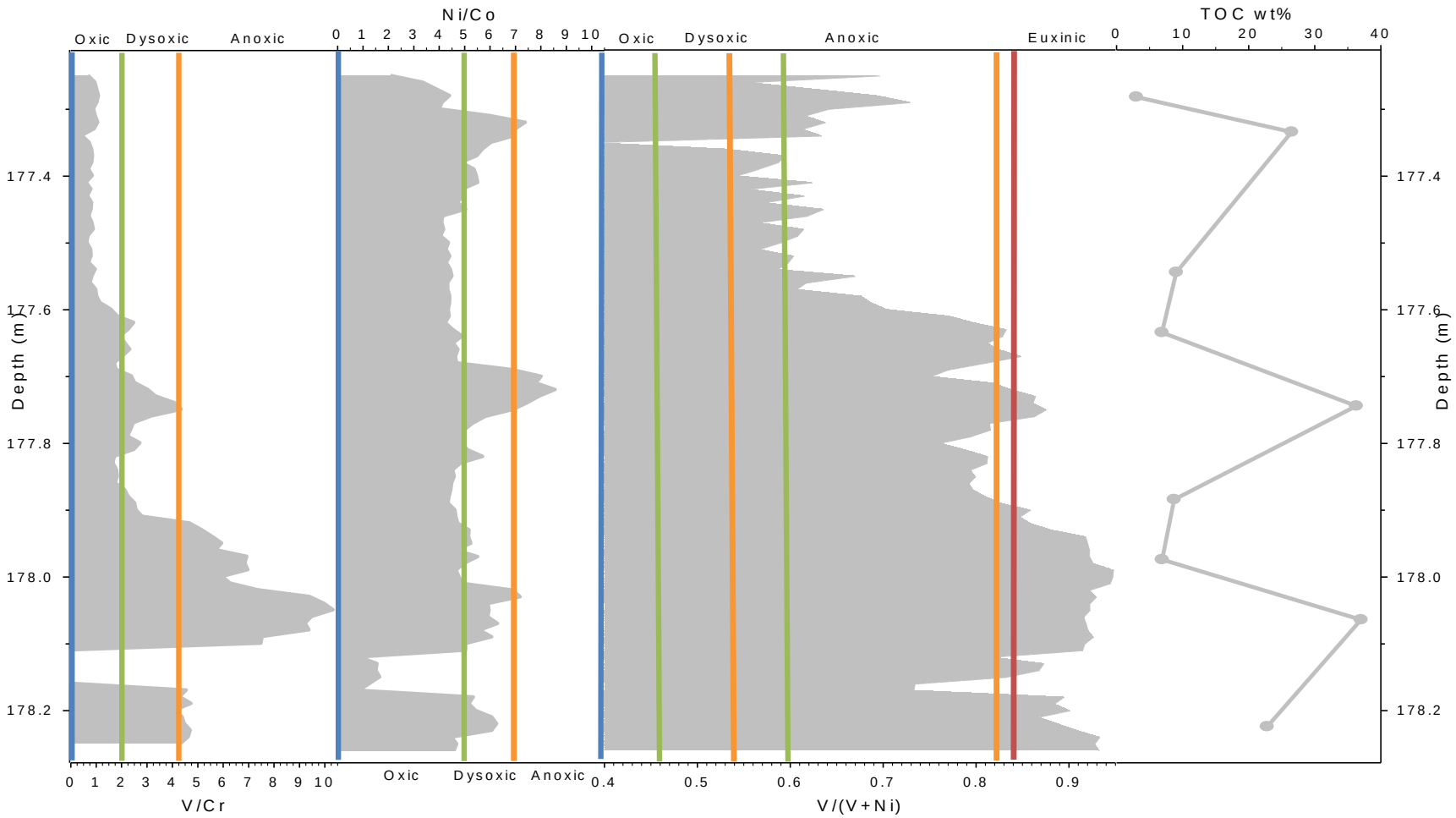

Figure 21: Trace element paleo-redox proxies and TOC plotted versus depth for core C6848. V/Cr <2.00 oxic, 2.00-4.25 dysoxic, >4.25 anoxic (Jones and Manning, 1994); Ni/Co <5.00 oxic, 5.00-7.00 dysoxic, >7.00 anoxic (Jones and Manning, 1994); V/(V+Ni) <0.46 oxic, 0.46-0.60 dysoxic, 0.54-0.82 anoxic, 0.84-0.89 euxinic (Hatch and Leventhal, 1992)

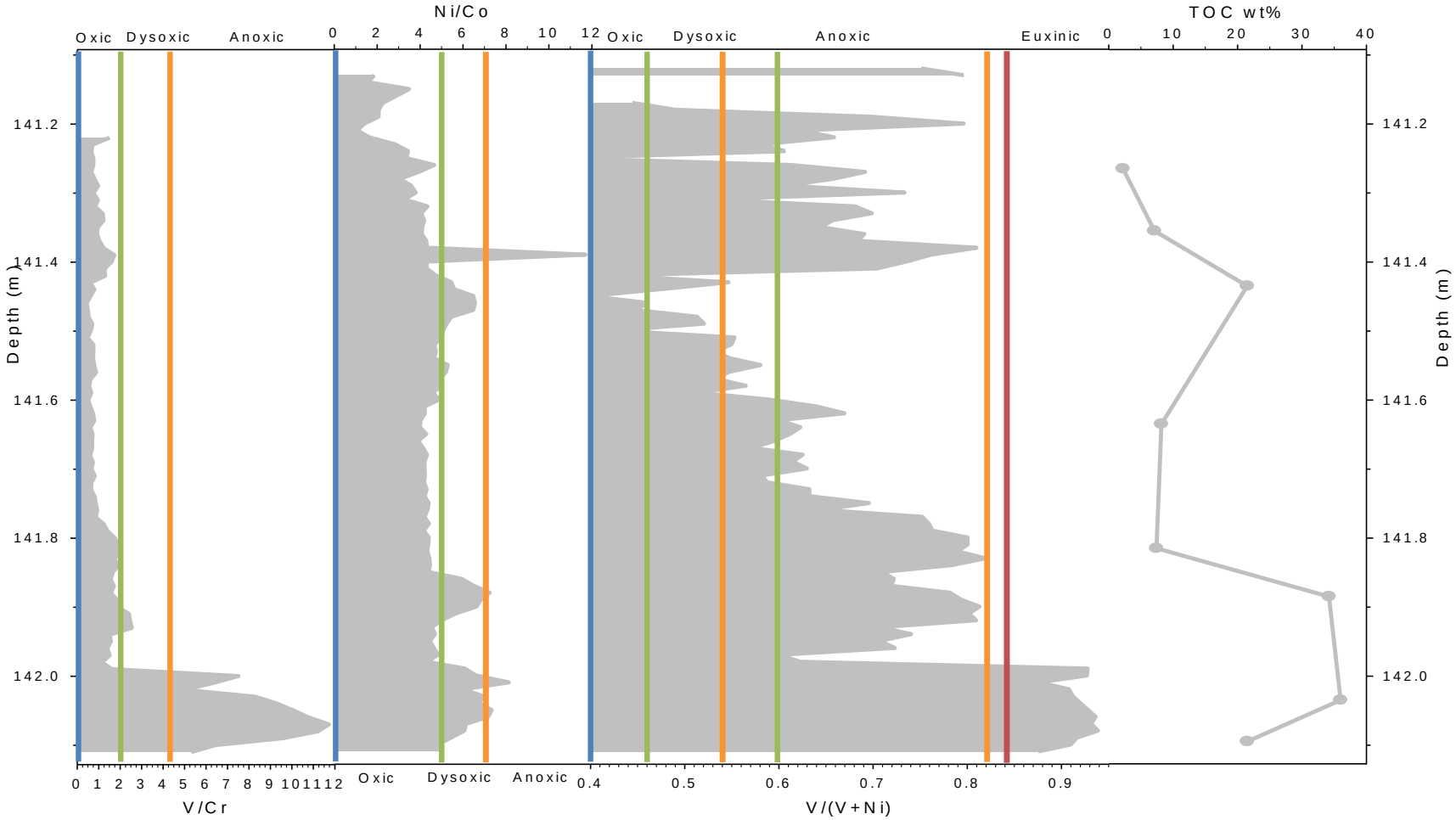

Figure 22: Trace element paleo-redox proxies and TOC plotted versus depth for core C7003. V/Cr <2.00 oxic, 2.00-4.25 dysoxic, >4.25 anoxic (Jones and Manning, 1994); Ni/Co <5.00 oxic, 5.00-7.00 dysoxic, >7.00 anoxic (Jones and Manning, 1994); V/(V+Ni) <0.46 oxic, 0.46-0.60 dysoxic, 0.54-0.82 anoxic, 0.84-0.89 euxinic (Hatch and Leventhal, 1992)

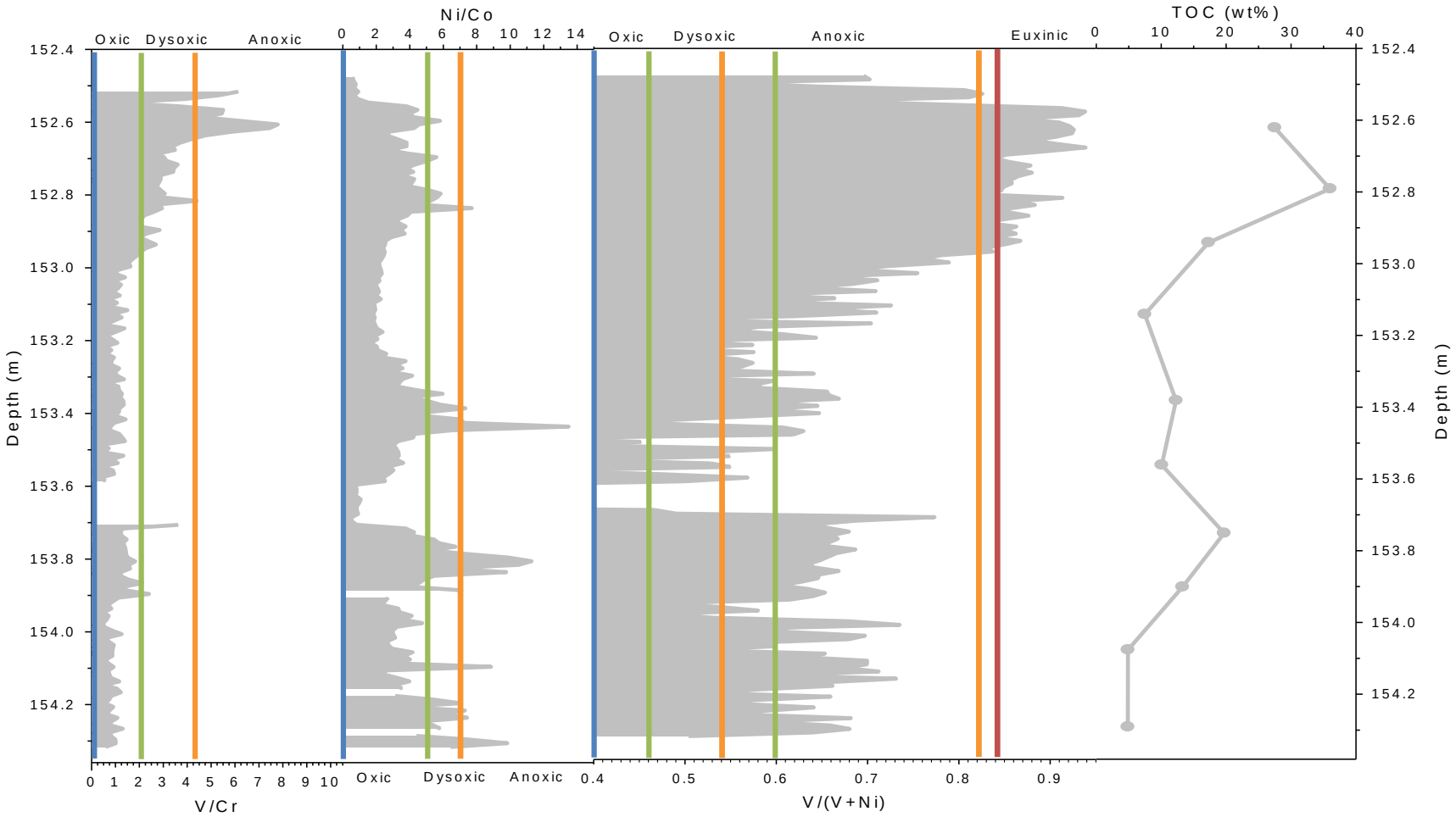

Figure 23: Trace element paleo-redox proxies and TOC plotted versus depth for core C7005. V/Cr <2.00 oxic, 2.00-4.25 dysoxic, >4.25 anoxic (Jones and Manning, 1994); Ni/Co <5.00 oxic, 5.00-7.00 dysoxic, >7.00 anoxic (Jones and Manning, 1994); V/(V+Ni) <0.46 oxic, 0.46-0.60 dysoxic, 0.54-0.82 anoxic, 0.84-0.89 euxinic (Hatch and Leventhal, 1992)

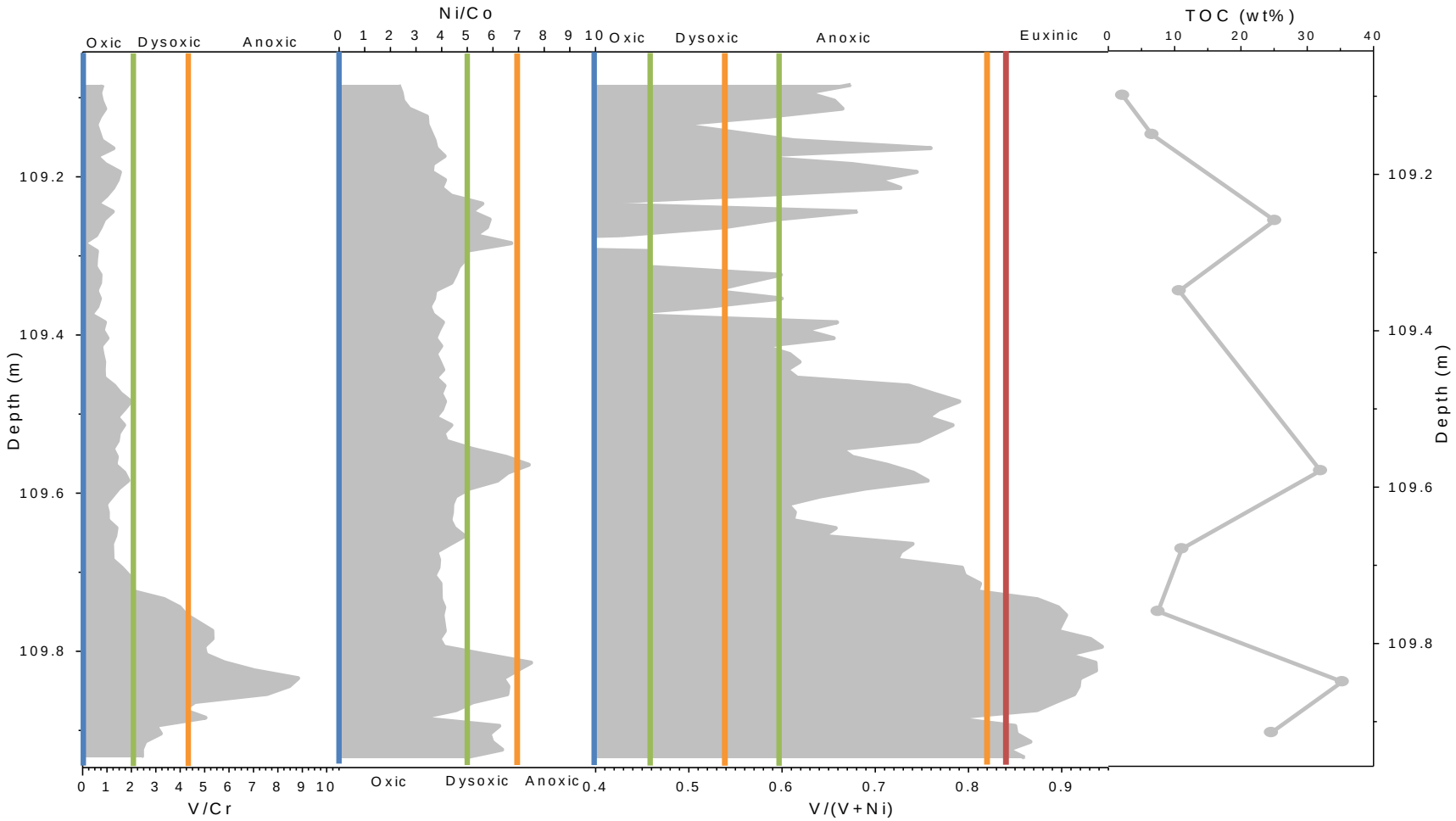

Figure 24: Trace element paleo-redox proxies and TOC plotted versus depth for core C7009. V/Cr <2.00 oxic, 2.00-4.25 dysoxic, >4.25 anoxic (Jones and Manning, 1994); Ni/Co <5.00 oxic, 5.00-7.00 dysoxic, >7.00 anoxic (Jones and Manning, 1994); V/(V+Ni) <0.46 oxic, 0.46-0.60 dysoxic, 0.54-0.82 anoxic, 0.84-0.89 euxinic (Hatch and Leventhal, 1992).

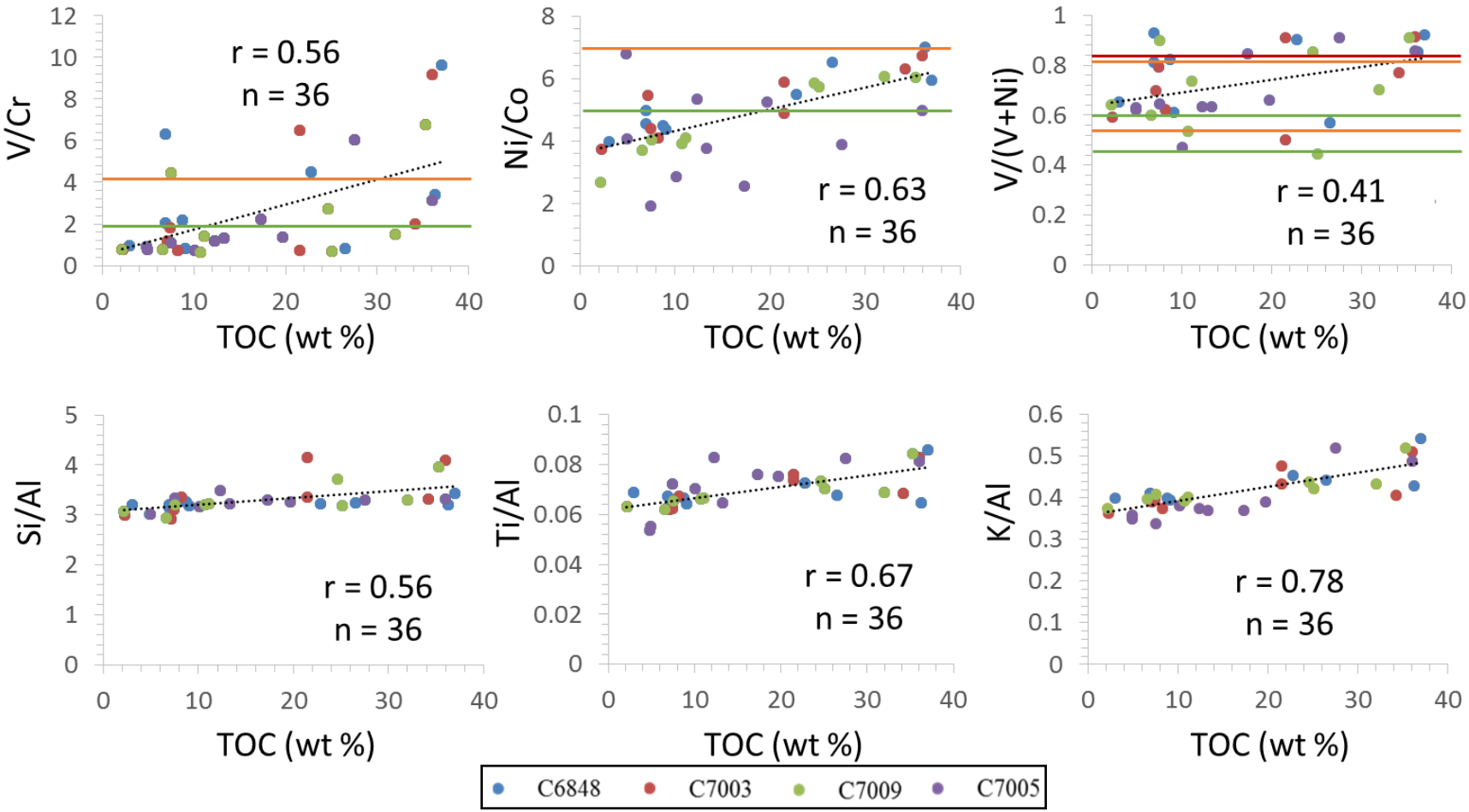

Figure 25: Plots of TE paleo-redox proxies and clastic proxies versus TOC. Green lines indicate thresholds for dysoxic conditions, orange lines indicate thresholds for anoxic conditions (Jones and Manning, 1994), and red lines indicate thresholds for euxinic conditions (Hatch and Leventhal, 1992).

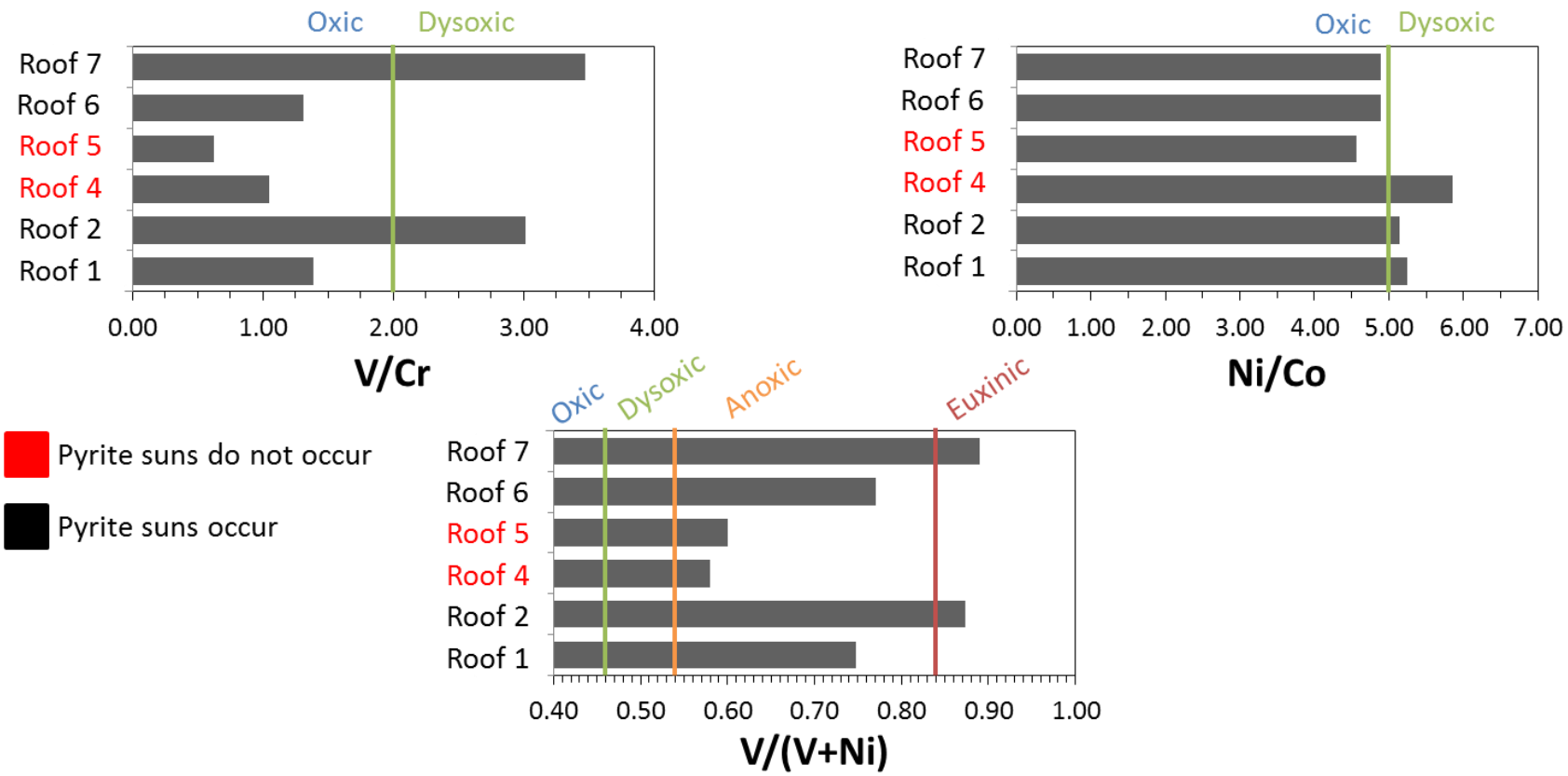

Figure 26: Trace element paleo-redox proxies for roof samples of Anna Shale from areas where pyrite suns do not occur (red) and where they do (black). *Roof sample 3 is Energy Shale and therefore not included in this study.

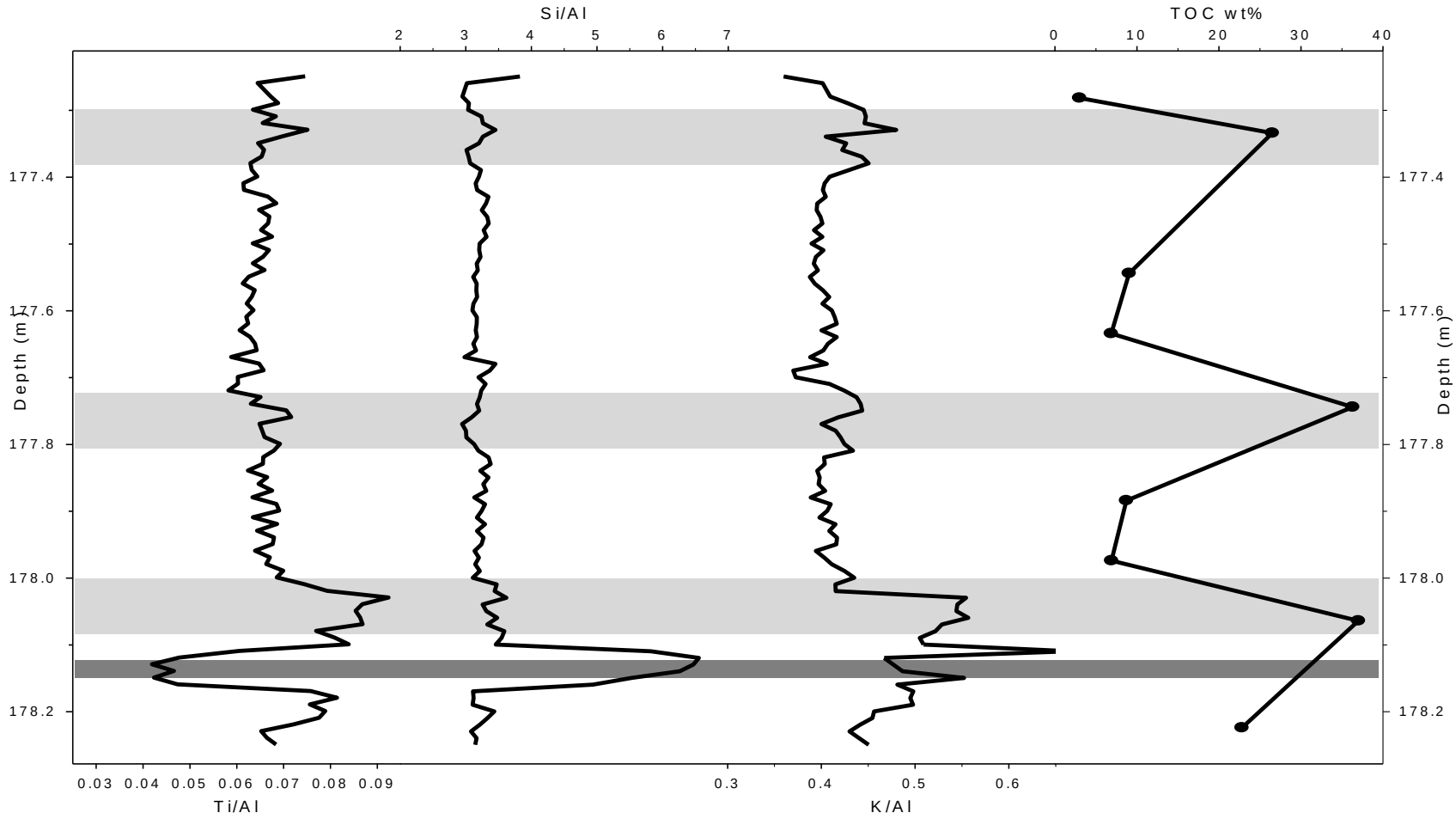

Figure 27: Proxies for clastic sedimentation and TOC plotted against depth for core C6848. Ti/Al is a proxy for sedimentation rate, Si/Al is a proxy for the amount of quartz relative to clays, and K/Al is a proxy for the amount of micaceous clays or fine grained K-feldspar. Highlighted in light gray and dark gray, respectively, intervals of increased clastic influx and the limestone nodule.

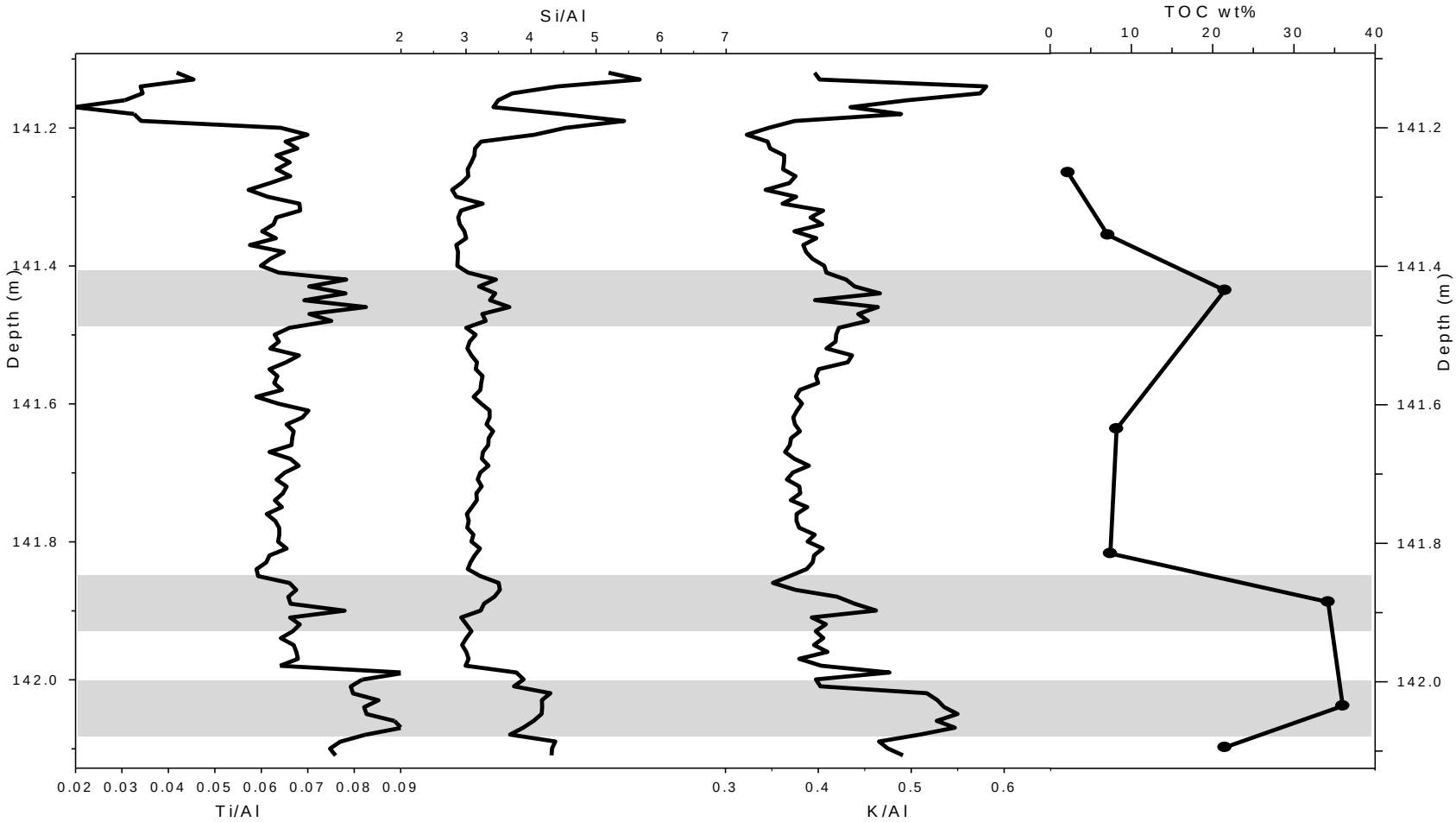

Figure 28: Proxies for clastic sedimentation and TOC plotted against depth for core C7003. Ti/Al is a proxy for sedimentation rate, Si/Al is a proxy for the amount of quartz relative to clays, and K/Al is a proxy for the amount of micaceous clays or fine grained K-feldspar. Highlighted in light gray, intervals of increased clastic influx.

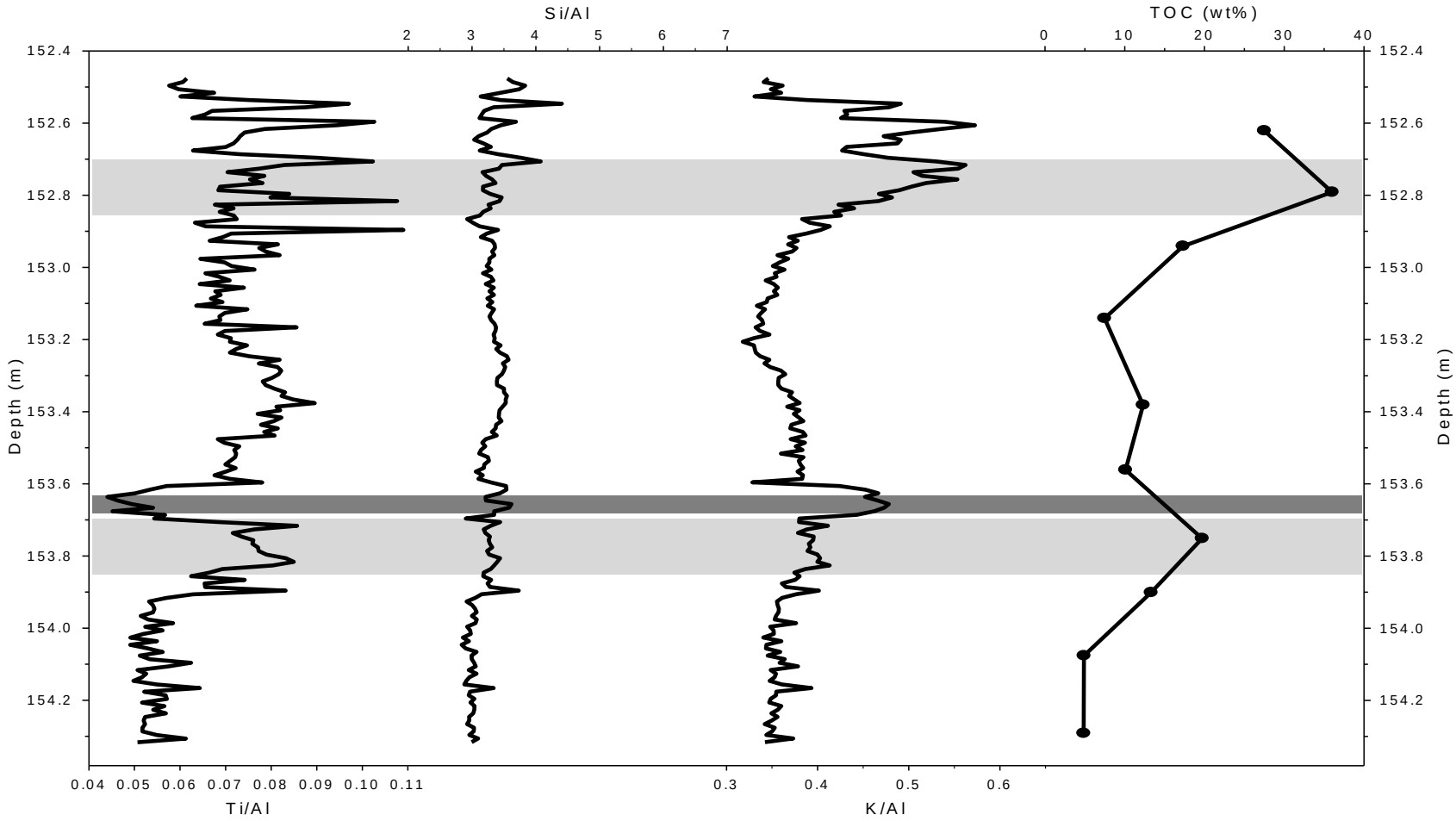

Figure 29: Proxies for clastic sedimentation and TOC plotted against depth for core C7005. Ti/Al is a proxy for sedimentation rate, Si/Al is a proxy for the amount of quartz relative to clays, and K/Al is a proxy for the amount of micaceous clays or fine grained K-feldspar. Highlighted in light gray and dark gray, respectively, intervals of increased clastic influx and the limestone nodule.

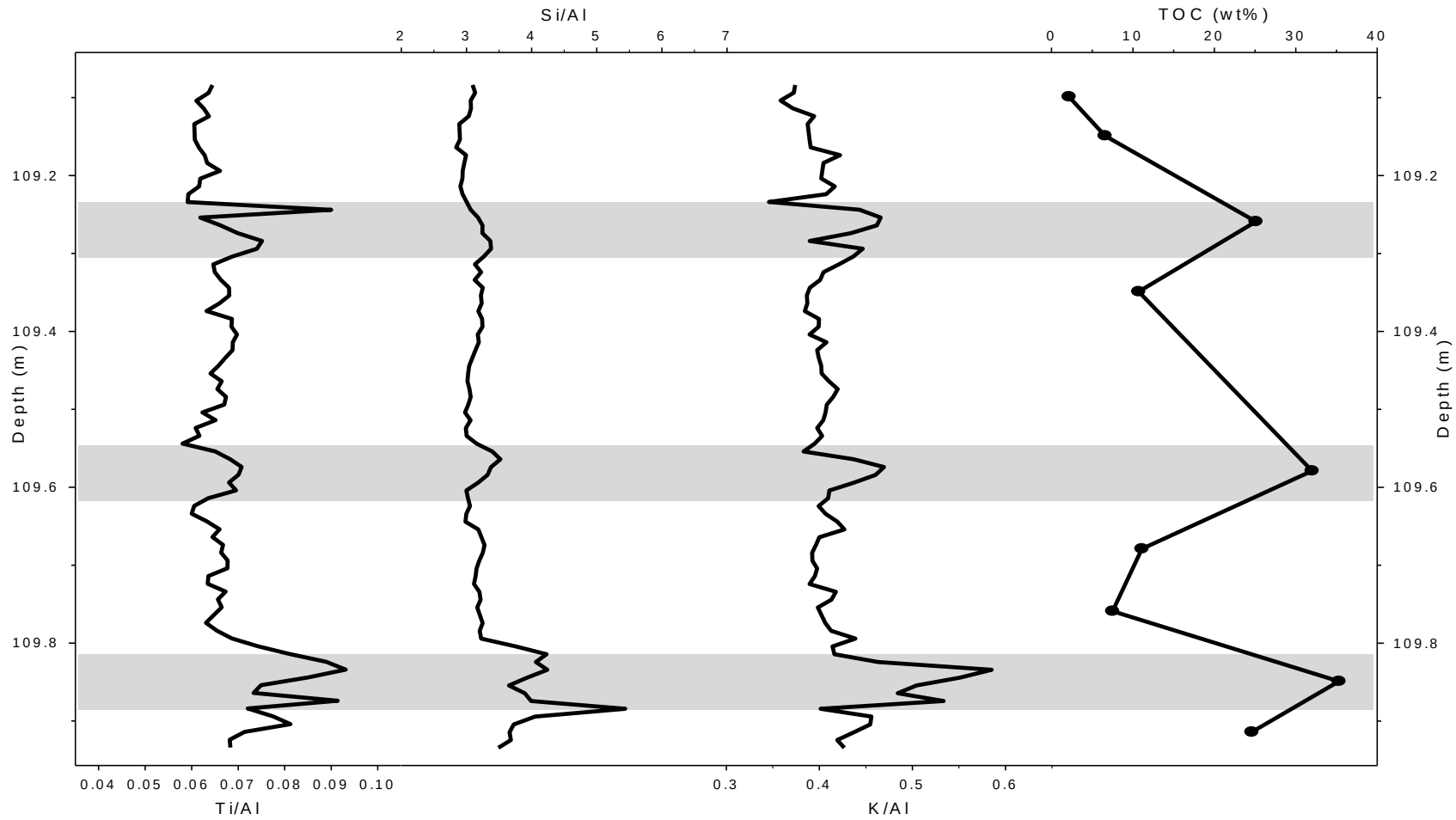

Figure 30: Proxies for clastic sedimentation and TOC plotted against depth for core C7009. Ti/Al is a proxy for sedimentation rate, Si/Al is a proxy for the amount of quartz relative to clays, and K/Al is a proxy for the amount of micaceous clays or fine grained K-feldspar. Highlighted in light gray, intervals of increased clastic influx.

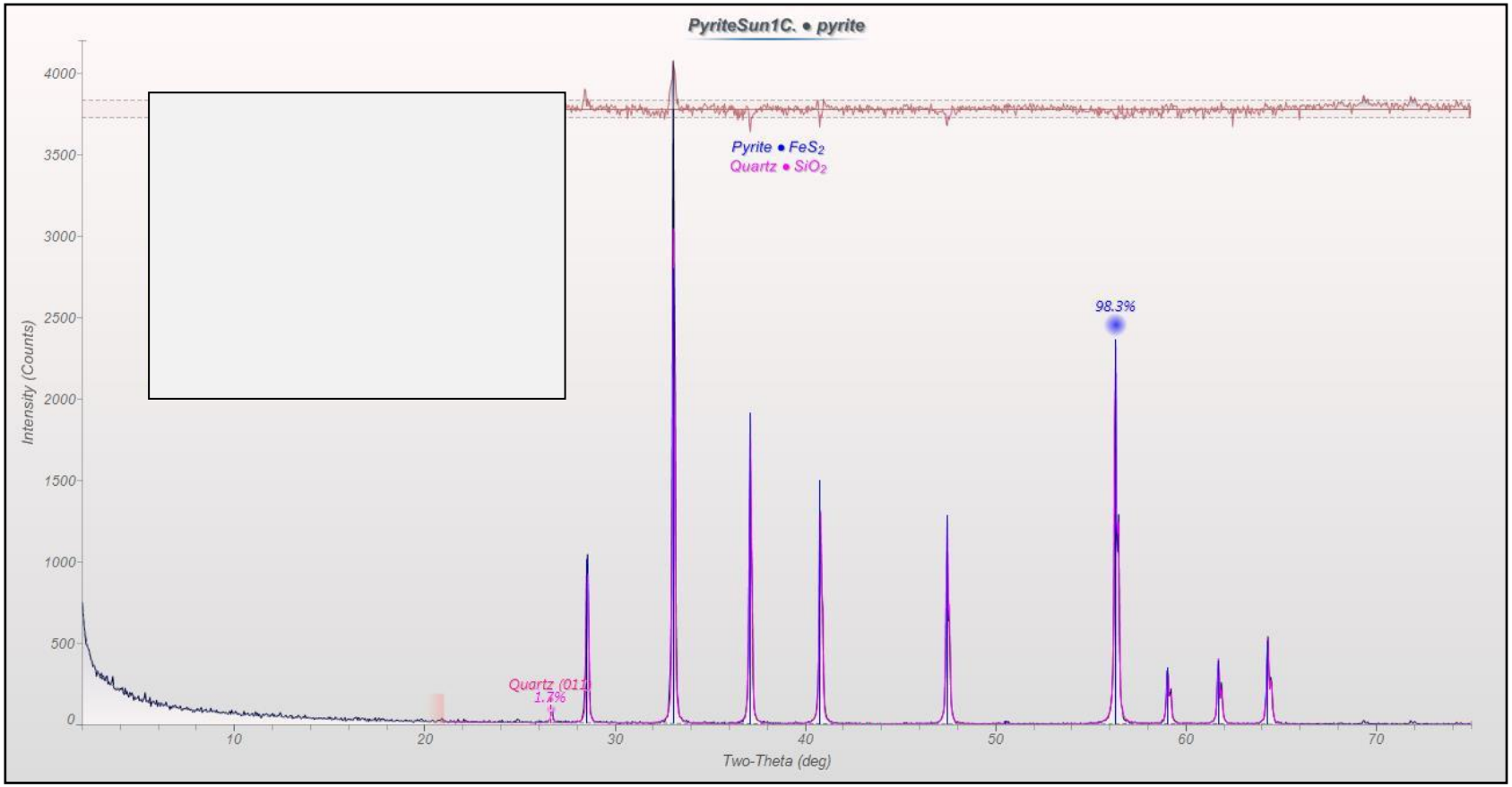

Figure 31: X-ray diffraction pattern for sample Pyrite Sun 1C. The sample is composed almost entirely of pyrite with one peak near 26.5° indicating a small amount of quartz is present.

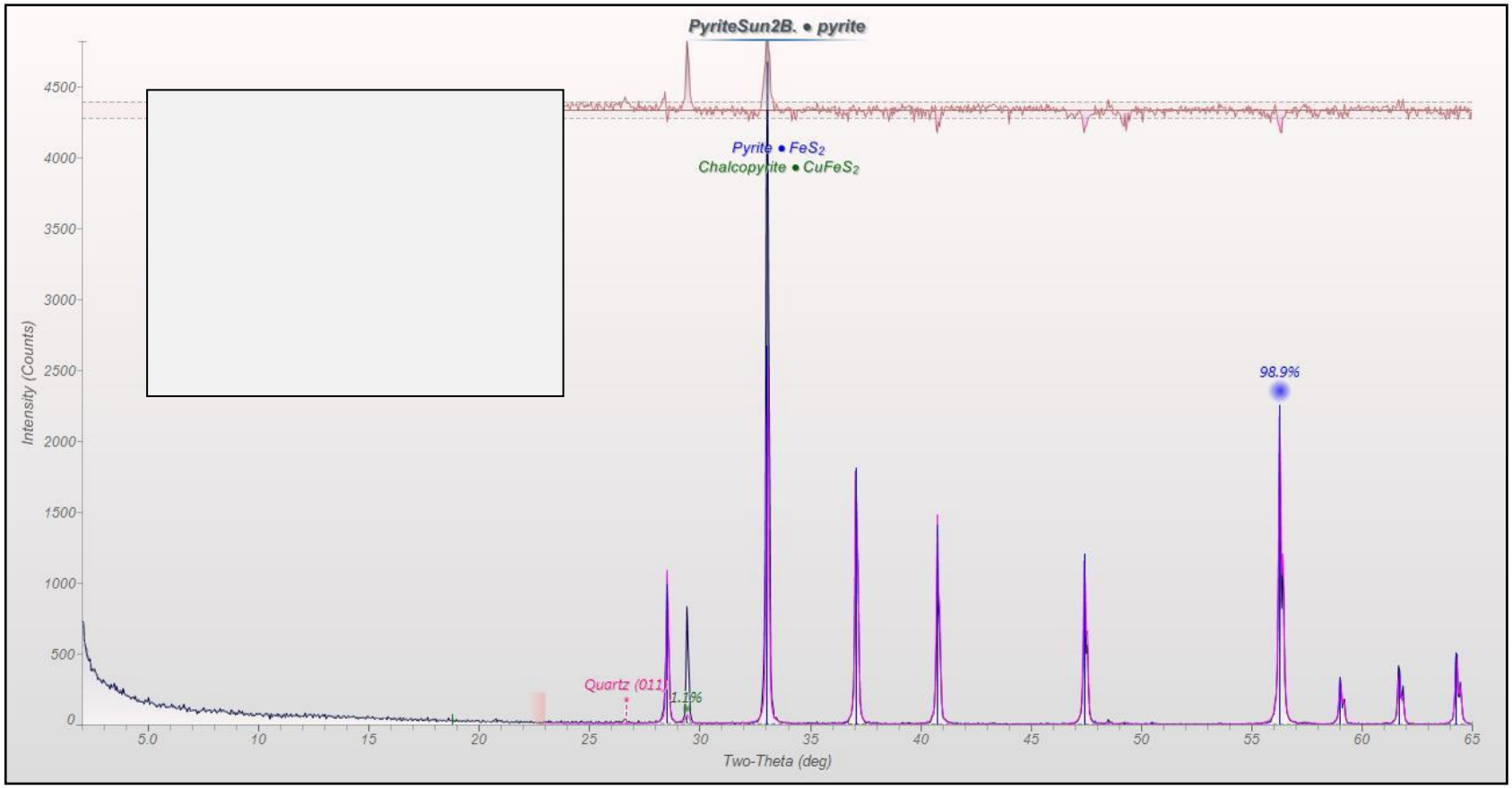

Figure 32: X-ray diffraction pattern for sample Pyrite Sun 2B. The sample is composed almost entirely of pyrite with one peak near 29.4° that may be the result of a small amount of chalcopyrite.

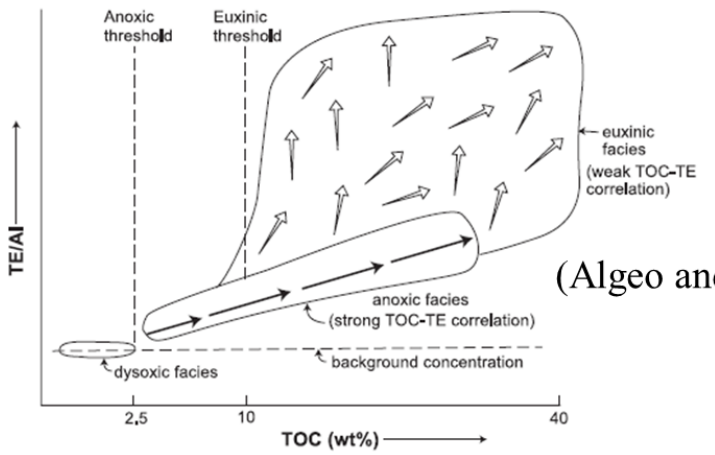

(Algeo and Maynard, 2004)

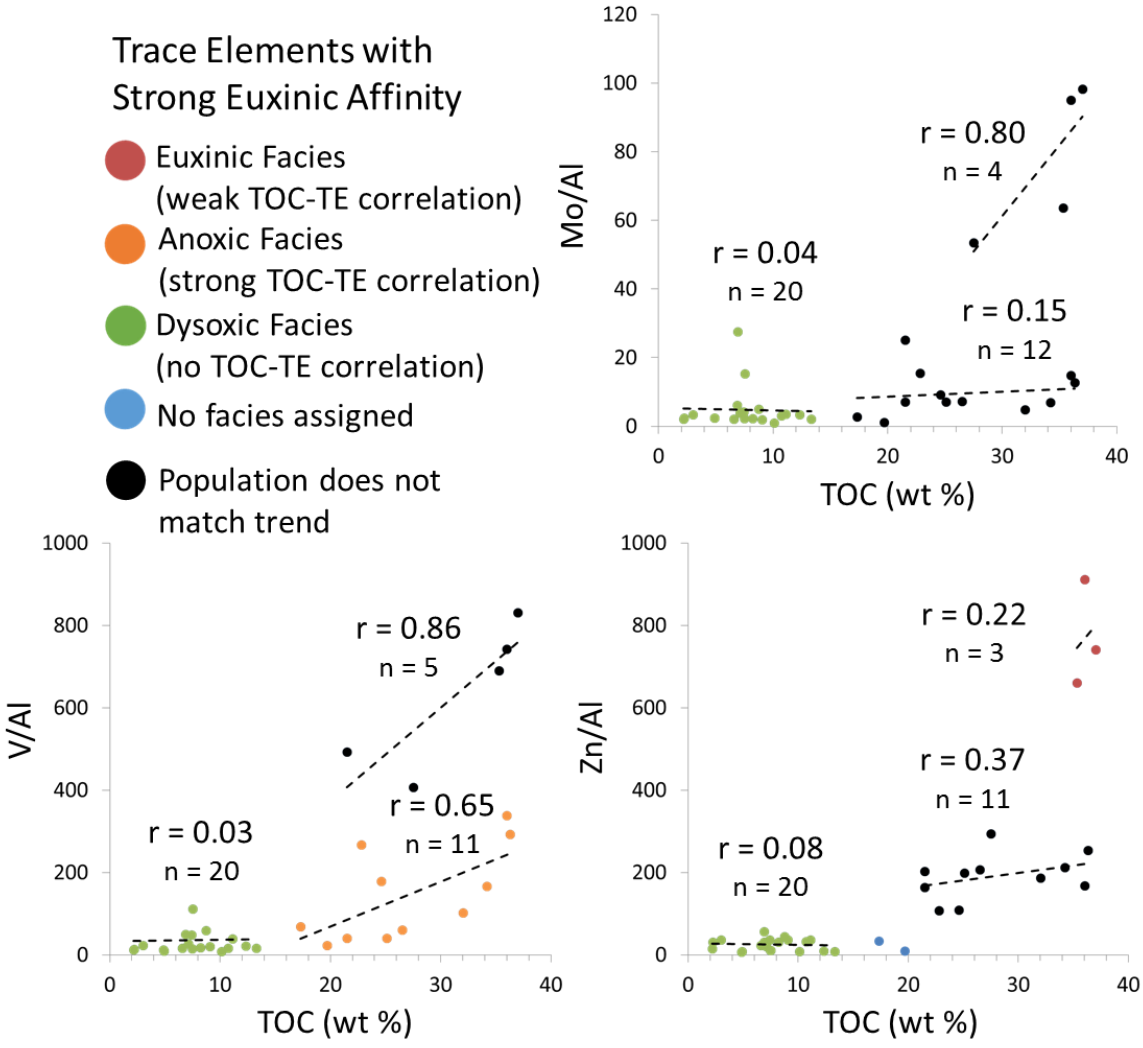

Figure 33: Aluminum-normalized trace elements with strong euxinic affinities showing distinct relationships with TOC for dysoxic, anoxic, and euxinic conditions.

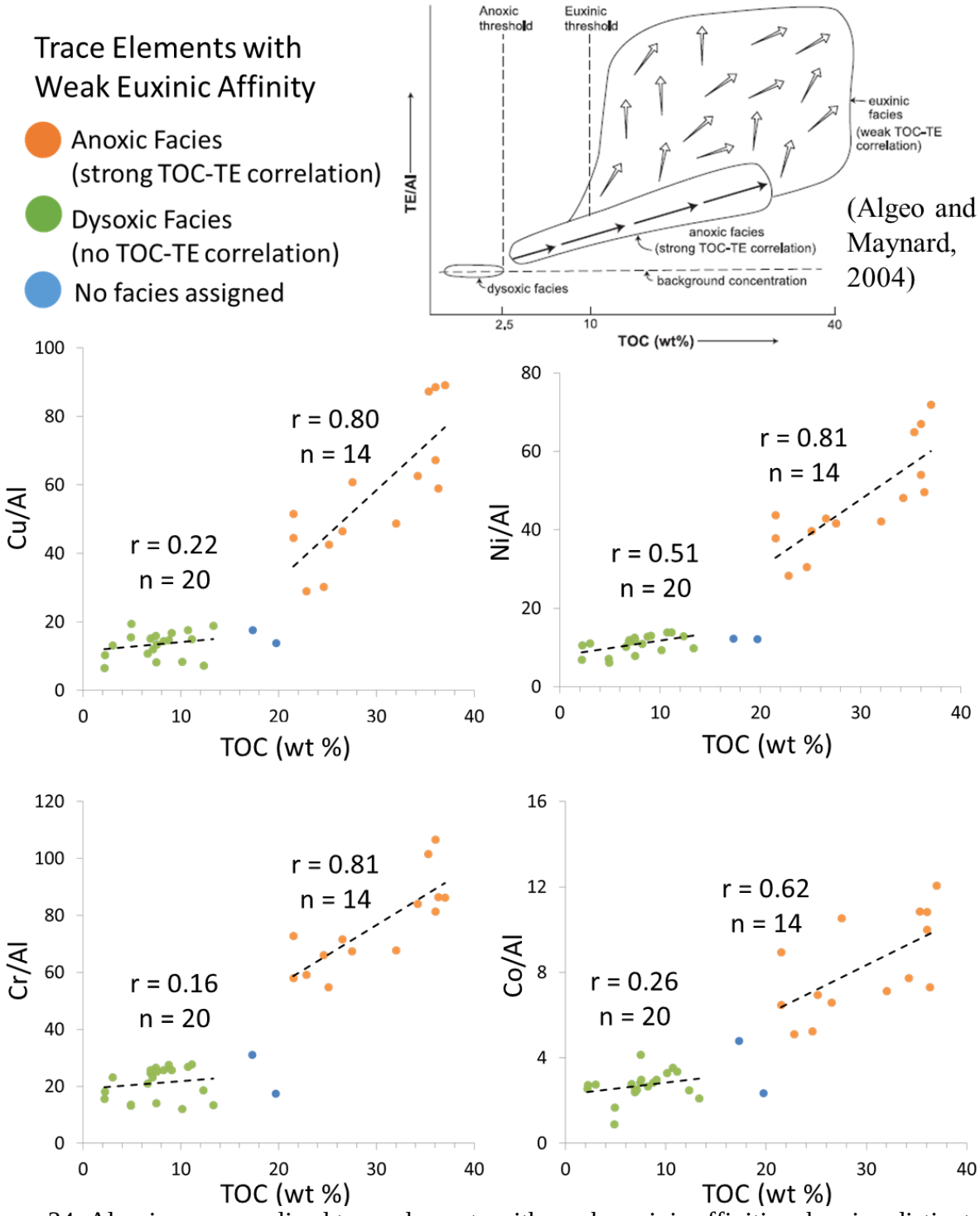

Figure 34: Aluminum normalized trace elements with weak euxinic affinities showing distinct relationships with TOC for dysoxic and anoxic.

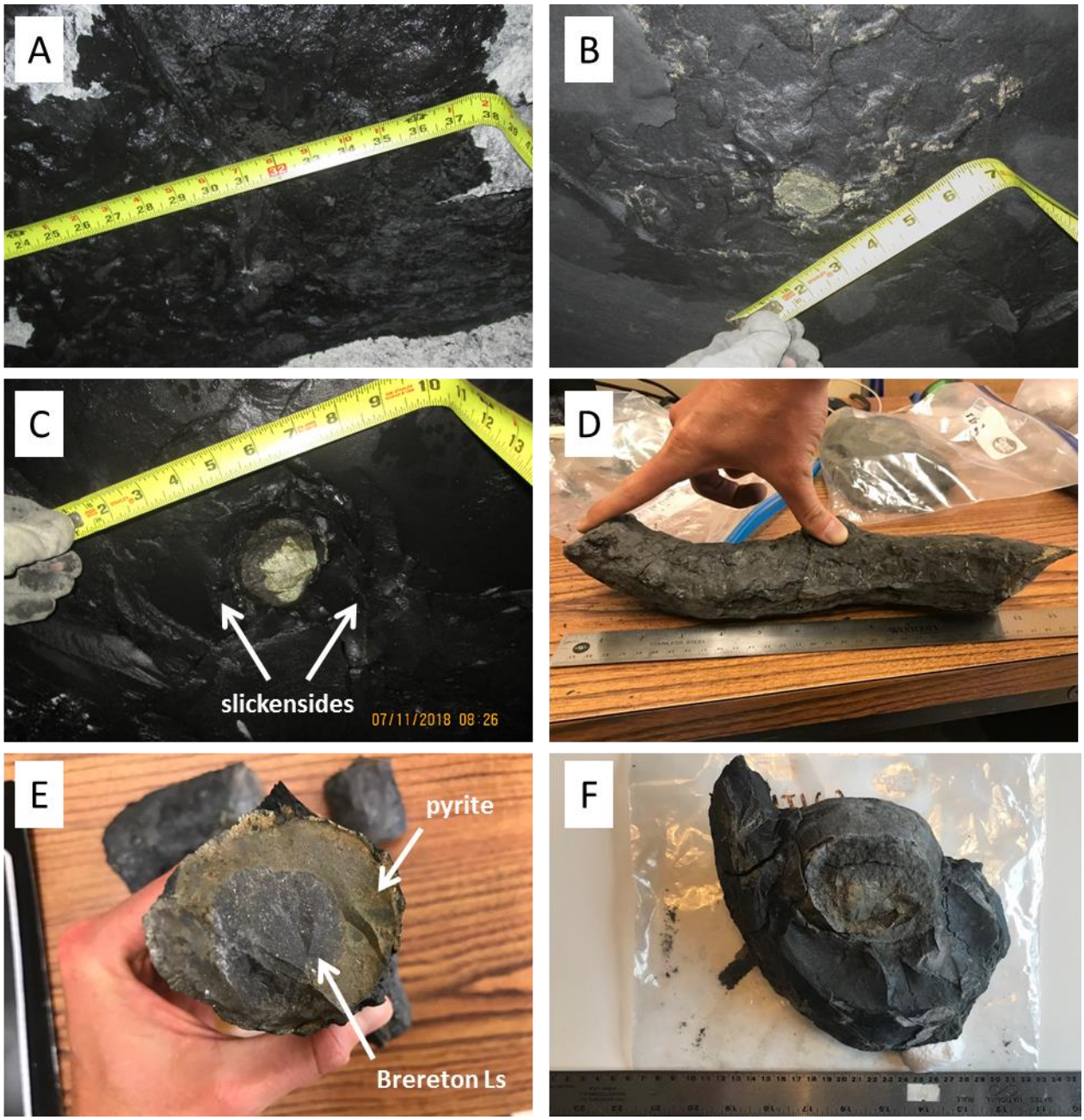

Figure 35: All samples are from the Lively Grove Mine. A) Highly bioturbated area at the base of the Anna Shale. B) and C) Burrows penetrating the Anna Shale into the roof of the mine. D) and E) Burrow cast showing pyrite and Brereton Limestone infill from the base of the Anna Shale. F) Nodular pyrite concretion from a large burrow terminus of in the lowermost Anna Shale.

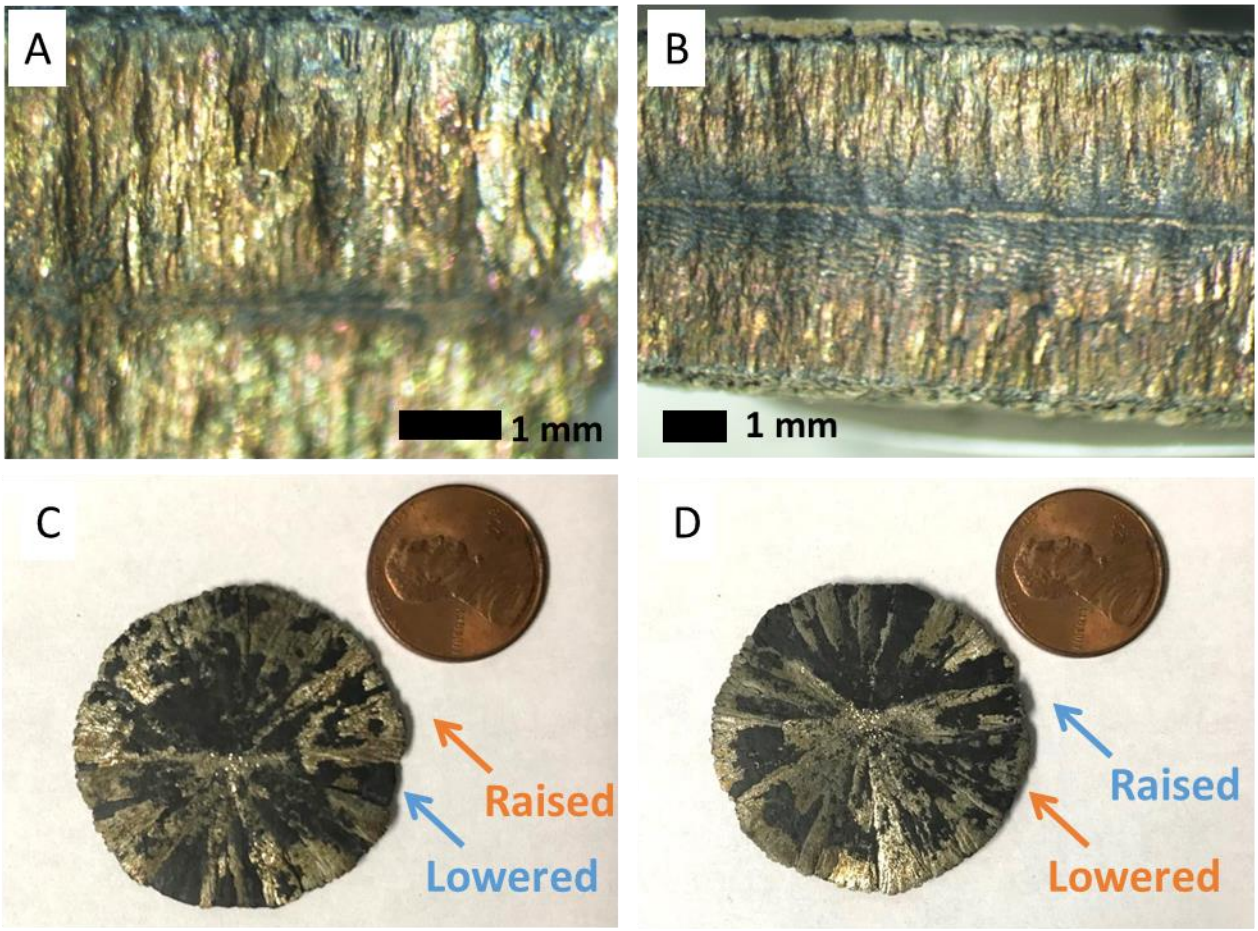

Figure 36: A) and B) Broken cross-section of a pyrite sun from the Prairie Eagle Mine showing fibrous cone-in-cone concretions growing outward (up and down) from the midline of the concretion. C) and D) Pyrite sun from the Lively Grove Mine showing the mirror image relief on each face. The sample was flipped along the horizontal axis from image C to D; the portions that are lowered on one face are raised on the other face and vice versa. The color of the label corresponds to the same portion of the sample.

REFERENCES

Algeo, T. J., Maynard, J. B., 2004. Trace-element behavior and redox facies in core shales of Upper Pennsylvanian Kansas-type cyclothems. Chemical Geology 206, 289-318.

Algeo, T. J., Shwark, L., Hower, J. C., 2004. High-resolution geochemistry and sequence stratigraphy of the Hushpuckney Shale (Swope Formation, eastern Kansas): implications for climo-environmental dynamics of the Late Pennsylvanian Midcontinent Seaway. Chemical Geology 206, 259-288.

Algeo, T. J., Heckel, P. H., 2008. The Late Pennsylvanian Midcontinent Sea of North America: A review. Paleogeography, Paleoclimatology, Paleoecology 268, 205-221.

Allgaier, G. J., 1974. Reserves of the Herrin (No. 6) Coal in the Fairfield Basin in southeastern Illinois. Illinois State Geological Survey Circular 489, pp. 31.

Anthony, J. W., Bideaux, R. A., Bladh, K. W., Nichols, M. C., 1990. Handbook of Mineralogy Volume I. Mineralogical Society of America. Chantilly, Virginia, pp. 588.

Archer, A. W., Elrick, S., Nelson, J. W., DiMichele, W. A., 2016. Cataclysmic burial of Pennsylvanian Period coal swamps in the Illinois Basin: Hypertidal sedimentation during Gondwanan glacial melt-water pulses. In: Contributions to Modern and Ancient Tidal Sedimentology: Proceedings of the Tidalites 2012 Conference, First Edition. pp. 217-231.

Arthur, M. A., Sageman, B. B., 1994. Marine black shales: Depositional mechanisms and environments of ancient deposits. Annual Review of Earth and Planetary Sciences 22, 499-551.

ASTM D5373-08, 2008. Standard test methods for instrumental determination of carbon, hydrogen, and nitrogen in laboratory samples of coal, ASTM International, West

Conshohocken, PA.

ASTM D4239-02, 2002. Standard test methods for sulfur in the analysis of coal and coke using high temperature tube furnace combustion methods, ASTM International, West Conshohocken, PA.

Berner, R. A., 1970. Sedimentary pyrite formation. American Journal of Science 268, 1-23.

Berner, R. A., Raiswell, B., 1983. Burial of organic carbon and pyrite sulfur in sediments over Phanerozoic time: a new theory. Geochimica et Cosmochimica Acta 47, 5, 855-862.

Berner, Z. A., Puchelt, H., Noltner, T., Kramar, U., 2013. Pyrite geochemistry in the Toarcian Posidonia Shale of southwest Germany: Evidence for contrasting trace-element patterns of diagenetic and syngenetic pyrites. Sedimentology 60, 548-573.

Bertrand, P., Shimmield, G., Martinez, P., Grousset, F., Jorissen, F., Paterne, M., Pujol, C., Bouloubassi, I., Menard, P. B., Peypouquet, J. P., Beaufort, L., Sicre, M. A., Lallier-Verges, E., Foster, J. M., Ternois, Y., 1996. The glacial ocean productivity hypothesis: the importance of regional temporal and spatial studies. Marine Geology 130, 1-9.

Caplan, M. L., Bustin, R. M., 1998. Paleoceanographic controls on geochemical characteristics of organic-rich Exshaw mudrocks: role of enhanced primary production. Organic Geochemistry 30, 161-188.

Cardott, B. J., Landis, C. R., Curtis, M. E., 2015. Post-oil solid bitumen network in the Woodford Shale, USA – a potential primary migration pathway. International Journal of Coal Geology 139, 106-113.

Carvalho, C., Couto, H., Figueiredo, M., Baucon, A., 2016. Microbial-related biogenic structures from the Middle Ordovician slates of Canelas (northern Portugal). Communicaçõ̃es

Geológicas 103, 23-38.

Cecil, C. B., Dulong, F. T., West, R. R., Stamm, R., Wardlaw, B., Edgar, N. T., 2003. Climate controls on the stratigraphy of a Middle Pennsylvanian cyclothem in North America. In: Cecil, C. B., Edgar, N. T., Climate Controls on Stratigraphy. SEPM (Society for Sedimentary Geology) Special Publication No. 77, pp. 151-180.

Chou, M. M., Dickerson, D. R., Chou, S. J., Sargent, M. L., 1991. Hydrocarbon source potential and organic geochemical nature of source rocks and crude oils in the Illinois Basin. Illinois Petroleum Report No. 136, Department of Energy and Natural Resources, Illinois State Geological Survey. pp. 39.

Curiale, J. A., 1986. Origin of solid bitumens, with emphasis on biological marker results. Organic Geochemistry 10, 559-580.

Dean, W. E., Arthur, M. A., 1989. Iron-sulfur-carbon relationships in organic-carbon-rich sequences I: Cretaceous Western Interior Seaway. American Journal of Science 289, 708-743.

Dunham, R. J., 1962. Classification of carbonate rocks according to depositional texture. In: Ham, W. E. (Ed.), Classification of Carbonate Rocks, American Association of Petroleum Geologists, Tulsa, pp. 108-121.

Eble, C. F., Greb, S. F., 2018. Geochemical, petrographic and palynologic characteristics of two late middle Pennsylvanian (Asturian) coal-to-shale sequences in the eastern Interior Basin, USA. International Journal of Coal Geology 190, 99-125.

Edwards, B. D., 1985. Bioturbation in a dysaerobic, bathyal basin: California borderland. In: Curran, H. A., (Ed.), Biogenic Structures: Their Use in Interpreting Depositional

Environments. Special Publication SEPM, Vol. 35, pp. 309-331.

Espitalié, J., Deroo, G., Marquis, F., 1985. Rock-Eval pyrolysis and its applications. Revue de l'Institut Francais du Petrole 40, 563-579.

Givens, T. J., 1968. Paleoecology and environment of deposition of part of the Brereton and Jamestown Cyclothems (Middle Pennsylvanian) of Williamson County, Illinois. M.S. Thesis, Department of Geology, Southern Illinois University, Carbondale, IL, pp. 182.

Greb, S. F., Andrews W. M., Eble, C. F., DiMichele, W., Cecil, C. B., Hower, J. C., 2003. Desmoinesian coal beds of the Eastern Interior and surrounding basins: The largest tropical peat mires in Earth history. Extreme depositional environments: Mega end members in geologic time: Boulder Colorado, Geological Society of America Special Paper 370, pp. 127-150.

Hatch, J. R., Leventhal, J. S., 1992. Relationship between inferred redox potential of the depositional environment and geochemistry of the Upper Pennsylvanian (Missourian) Stark Shale Member of the Dennis Limestone, Wabaunsee County Kansas, USA. Chemical Geology 99, 65-82.

Heckel, P. H., 1977. Origin of phosphatic black shale facies in Pennsylvanian cyclothems of mid-continent North America. American Association of Petroleum Geologist Bulletin 61, 1045-1068.

Heckel, P. H., 1994. Evaluation of evidence for glacial-eustatic control over marine Pennsylvanian cyclothems in North America and consideration of possible tectonic effects. In: Dennison, J. M., Ettensohn, F. R. (Eds.), Tectonic and Eustatic Controls on Sedimentary Cycles. Society for Sedimentary Geology, Concepts in Sedimentology and Paleontology No.

4, pp. 65-87.

Holterhoff, P., Cassidy, K., 2012. Late Pennsylvanian and Early Permian black shale-limestone bed-set couplets of the Eastern Shelf, Midland Basin (Texas): climate-driven redox cycles of the inner platform realm. American Association of Petroleum Geologist Annual Meeting, Search and Discovery Article #90142.

International Committee for Coal and Organic Petrology (ICCP), 2001. The new inertinite classification (ICCP system 1994). Fuel 80, 459-471.

International Committee for Coal and Organic Petrology (ICCP), 1998. The new vitrinite classification (ICCP system 1994). Fuel 77, 349-358.

James, G. W., 1970. Stratigraphic geochemistry of a Pennsylvanian black shale (Excello) in the Mid-Continent and Illinois Basin. Ph.D. Dissertation, Rice University, Houston, TX, pp. 92.

Jewett, J. M., 1941. Classification of the Marmaton group, Pennsylvanian, in Kansas. Kansas Geological Survey Bulletin 38, pt. 11, pp. 285-344.

Johnson, D. O., 1972. Stratigraphic analysis of the interval between the Herrin (No. 6) Coal and the Piasa Limestone in southwestern Illinois. M.S. Thesis, Department of Geology, Southern Illinois University, Carbondale, IL, pp. 105.

Jones, B., Manning, D. A. C., 1994. Comparison of geochemical indices used for the interpretation of paleoredox conditions in ancient mudstones. Chemical Geology 111, 111-129.

Kennedy, M. T., Pevear, D. R., Hill, R. J., 2002. Mineral surface control of organic carbon in black shale. Science 295, 657-660.

Krausse, H. F., Damberger, H. H., Nelson, W. J., Hunt, S. R., Ledvina C. T., Treworgy, C. G., White, W. A., 1979. Roof strata of the Herrin (No. 6) coal member in mines of Illinois: Their geology and stability. Illinois Minerals Note 72, Illinois State Geological Survey. pp. 54.

Kravits, C. M., Crelling, J. C., 1981. Effects of overbank deposition on the quality and maceral composition of the Herrin (No. 6) Coal (Pennsylvanian) of Southern Illinois. International Journal of Coal Geology 1, 195-212.

Langrand, E. L., 1977. A petrologic study of the upper portion of the Herrin (No. 6) Coal Member in relation to roof lithology. M.S. Thesis, Department of Geology, Southern Illinois University, Carbondale, IL, pp. 55.

Lewan, M. D., 1983. Effects of thermal maturation on stable organic carbon isotopes as determined by hydrous pyrolysis of Woodford Shale. Geochimica et Cosmochimica Acta 47, 1471-1479.

Liu, B., Schieber, J., Mastalerz, M., 2017. Combined SEM and reflected light petrography of organic matter in the New Albany Shale (Devonian-Mississippian) in the Illinois Basin: a perspective on organic pore development with thermal maturation. International Journal of Coal Geology 184, 57-72.

Marynowski, L., Pisarzowska, A., Derkowski, A., Rakocinski, M., Szaniawski R., Srodon, J., Cohen, A., 2017. Influence of paleo-weathering on trace metal concentrations and environmental proxies in black shales. Palaeogeography, Palaeoclimatology, Palaeoecology 472, 177-191.

Mastalerz, M., Drobniak, A., Stankiewicz, A. B., 2018. Origin, properties, and implications of

solid bitumen in source-rock reservoirs: a review. International Journal of Coal Geology 195, 14-36.

Morse, J, W, Luther, G. W. III, 199. Chemical influences on trace metal-sulfide interactions in anoxic sediments. Geochimica et Cosmochimica Acta 63, 3373-3378.

Murphy, A. E., Sageman, B. B., Hollander, D. J., 2000. Black shale deposition and faunal overturn in Devonian Appalachian Basin: Clastic starvation, seasonal water-column mixing, and efficient biolimiting nutrient recycling. Paleoceanography 15, 280-291.

Nelson, W. J., 1979. Geologic effects of the Walshville channel on coal mining conditions in Southern Illinois. In: Palmer, J. E., and Dutcher, R. R. (Eds.), Depositional and Structural history of the Pennsylvanian System of the Illinois Basin, Part 2: Invited papers, Field Trip 9/Ninth International Congress of Carboniferous Stratigraphy and Geology, pp. 151-158.

Ocubalidet, S. G., Rimmer, S. M., Conder, J. A., 2018. Redox conditions associated with organic carbon accumulation in the Late Devonian New Albany Shale, west-central Kentucky, Illinois Basin. International Journal of Coal Geology 190, 42-55.

Palmer, J. E., Jacobson, R. J., Trask, C. B., 1979. Depositional environments of strata of late Desmoinesian age overlying the Herrin (No. 6) Coal Member in southwestern Illinois. In: Palmer, J. E., Dutcher, R. R. (Eds.), Depositional and Structural History of the Pennsylvanian System of the Illinois Basin, Part 2: Invited papers, Field Trip 9/Ninth International Congress of Carboniferous Stratigraphy and Geology, pp. 92-102.

Pickel, W., Kus, J., Flores, D., Kalaitzidis, S., Christanis, K., Cardott, B. J., Misz-Kennan, M., Rodrigues, S., Hentschel, A., Hamor-Vido, M., Crosdale, P., Wagner, N., ICCP, 2017. Classification of liptinite – ICCP system 1994. International Journal of Coal Geology 169, 40-

61.

Pratt, L. M., Davis, C. L., 1992. Intertwined fates of metals, sulfur, and organic carbon in black shales. In: Pratt, L. M., Comer, J. B., Brassell, S. C., Droppo, R. (Eds.), 1992. Geochemistry of Organic Matter in Sediments and Sedimentary Rocks, SEPM Short Course No. 27, pp. 1-27.

Raiswell, R., Berner, R. A., 1985. Pyrite formation in euxinic and semi-euxinic sediments. American Journal of Science 285, 710-724.

Raiswell, R., Buckley, F., Berner, R. A., Anderson, T. F., 1988. Degree of pyritization of iron as a paleoenvironmental indicator of bottom-water oxygenation. Journal of Sedimentary Petrology 58, 812-819.

Rimmer, S. M., Geochemical paleoredox indicators in Devonian-Mississippian black shales, Central Appalachian Basin (USA). Chemical Geology 206, 373-391.

Rimmer, S M., Thompson, J. A., Goodnight, S. A., Robl, T. L., 2004. Multiple controls on the preservation of organic matter in Devonian-Mississippian marine black shales: geochemical and petrographic evidence. Paleogeography, Paleoclimatology, Paleoecology 215, 125-154.

Rousseau, R. M., 2001. Detection limit and estimate of uncertainty of analytical XRF results. The Rigaku Journal 18, 33-47.

Rowe, H., Hughes, N., Robinson, K., 2012. The quantification and application of handheld energy-dispersive x-ray fluorescence (ED-XRF) in mudrock chemostratigraphy and geochemistry. Chemical Geology 324-325, 121-131.

Salmon, V., Derenne, S., Lallier-Vergés, E., Largeau, C., Beaudoin, B., 2000. Protection of organic matter by mineral matrix in a Cenomanian black shale. Organic Geochemistry 31,

463-474.

Seilacher, A., 2001. Concretion morphologies reflecting diagenetic and epigenetic pathways. Sedimentary Geology 143, 41-57.

Smith, W. H., Stall, J. B., 1975. Coal and water resources for coal conversion in Illinois. Illinois State Water Survey and Illinois State Geological Survey, Cooperative Resources Report 4. pp. 79.

Taylor, G. H., Liu, S. Y., 1989. Micrinite – its nature, origin and significance. International Journal of Coal Geology 14, 29-46.

Teichmüller, M., 1974. Übuer neu macerale der iptinit-gruppe und die entstehung des micrinits. Fortschr. Geol. Rheinld. Westfalen, 243, 49-73.

Teichmüller, M., Ottenjann, K., 1977. Art und diageneses von liptiniten und lipoiden stiffen in einem erdölmuttergestein auf grund fluoreszenzmikroskopischer untersuchungen. Erdöl Kohle, 30, 387-389.

Teichmüller, M., Wolf, M., 1977. Application of fluorescence microscopy in coal petrology and oil exploration. Journal Microscopy 109, 49- 73.

Terry, R. D., Chilingar, G. V., 1955. Summary of "Concerning some additional aids in studying sedimentary formations", by M. S. Shvestsov. Journal of Sedimentary Petrology 25, 229-234.

Tissot, B. P., Welte, D. H., 1984. Petroleum Formation and Occurrence, Second Enlarged Edition. Springer-Verlag, Berlin Heidelberg, pp. 699.

Treworgy, C. G., Jacobson, R. J., 1979. Paleoenvironments and distribution of low-sulfur coal in Illinois. Ninth International Congress on Carboniferous Stratigraphy and Geology. Reprint In: Cross, A. T. (Ed.), 1986. Economic Geology: Coal, Oil and Gas, Vol. 4,

pp. 349-359.

Tyson, R. V., Pearson, T. H., 1991. Modern and ancient continental shelf anoxia: an overview. In: Tyson, R. V., Pearson, T. H., (Eds.), Modern and Ancient Continental Shel Anoxia. Geological Society Special Publication, Vol. 58, pp. 1-26.

Utgaard, J., 1979. Paleoecology and depositional history of rock strata associated with the Herrin (No. 6) Coal Member, Delta Mine, Southern Illinois. In: Palmer, J. E., and Dutcher, R. R. (Eds.), Depositional and Structural history of the Pennsylvanian System of the Illinois Basin, Part 2: Invited papers, Field Trip 9/Ninth International Congress of Carboniferous Stratigraphy and Geology, pp. 86-92.

Wanless, H. R., 1955. Pennsylvanian rocks of Eastern Interior Basin. American Association of Petroleum Geologists Bulletin 39, 1753-1820.

Wenger, L. M., Baker, D. R., 1986. Variations in organic geochemistry of anoxic-oxic black shale-carbonate sequences in the Pennsylvanian of the Midcontinent USA. Organic Geochemistry 10, 85-92.

Wetendorf, F. H., 1967. Environment of deposition of parts of the Brereton, Jamestown, and Bankston Cyclothems (Middle Pennsylvanian) of Williamson County, Illinois. M.S. Thesis, Department of Geology, Southern Illinois University, Carbondale, IL, pp. 89.

Willman, H. B., Atherton, E., Buschbach, T. C., Collinson, C., Frye, J. C., Hopkins, M. E., Lineback, J. A., Simon, J. A., 1975. Pennsylvanian Subsystem. Handbook of Illinois Stratigraphy, Illinois State Geological Survey Bulletin 95. pp. 261.

Zangerl, R., Richardson, E. S. Jr., Woodland, B. G., Miller, R. L., Neavel, R. C., Tourtelot, H., A., 1963. The paleoecological history of two Pennsylvanian black shales.

Chicago Natural History Museum, Fieldiana series, Geology Memoirs v. 4. pp. 352.

Zangerl, R., Woodland, B. G., Richardson, E. S. Jr., Zachary, D. L., 1969. Early diagenetic phenomena in the Fayetteville black shale (Mississippian) of Arkansas. Sedimentary Geology 3, 87-119.

APPENDIX A

LIMIT OF DETERMINATION OF A METHOD (LDM) FOR TRACE ELEMENTS

Determined by Rowe et al. (2012) according to Rousseau (2001).

Sample	Co (ppm)	Ni (ppm)	Cu (ppm)	Zn (ppm)	As (ppm)	Pb (ppm)	Se (ppm)	Th (ppm)	Sr (ppm)	Y (ppm)	Zr (ppm)	Mo (ppm)
SARM-41	NA	34	48	14	NA	NA	NA	2	4	3	11	2
Woodford Fm.	NA	52	40	191	NA	NA	NA	2	10	5	13	9

LDM FOR MAJOR ELEMENTS

Determined by Rowe et al. (2012) according to Rousseau (2001).

Sample	Na (wt %)	Mg (wt %)	Al (wt %)	Si (wt %)	P (wt %)	S (wt %)	K (wt %)	Ca (wt %)	Ti (wt %)	V (ppm)	Cr (ppm)	Mn (wt %)	Fe (wt %)
SARM-41	NA	0.33	0.28	0.5	0.03	0.04	0.04	0.06	0.02	82	32	0.006	0.06
Woodford Fm.	NA	0.17	0.28	0.5	0.07	0.20	0.18	0.06	0.04	137	26	0.002	0.12

*NA not analyzed by Rowe et al. (2012)

APPENDIX B

ROCK-EVAL DATA FOR ANNA SHALE SAMPLES

Sample Name/ Marks from top of core	Depth (m below KB) /Description	TOC (wt%)	S1 (mg HC/g)	S2 (mg HC/g)	S3 (mg CO_2/g)	Tmax (°C)	HI (mg HC/g TOC) (S2x100/TOC)	OI (mg HC/g rock) (S3x100/TOC)	PI (S1/(S1+S2))
Core C6848									
Anna C6848 25-29cm	177.28	3.00	0.19	2.46	0.55	428	82	18	0.07
Anna C6848 30-35cm	177.33	26.50	3.39	96.33	5.41	427	364	20	0.03
Anna C6848 51-56cm	177.54	9.05	0.62	14.26	1.16	422	158	13	0.04
Anna C6848 60-65cm	177.63	6.88	0.49	8.93	1.01	420	130	15	0.05
Anna C6848 71-76cm	177.74	36.30	4.76	158.95	6.85	428	438	19	0.03
Anna C6848 85-90cm	177.88	8.73	0.63	16.04	1.22	420	184	14	0.04
Anna C6848 94-99cm	177.97	6.90	0.52	10.76	1.18	418	156	17	0.05
Anna C6848 103-108cm	178.06	37.00	4.30	142.30	7.00	424	385	19	0.03
Anna C6848 119-124cm	178.22	22.80	1.88	59.33	4.81	425	260	21	0.03
Core C7003									
Anna C7003 13-18cm	141.27	2.21	0.05	1.19	0.52	432	54	24	0.04
Anna C7003 22-27cm	141.35	7.10	0.25	7.12	0.87	417	100	12	0.03
Anna C7003 30-35 cm	141.43	21.50	1.35	60.29	3.33	426	280	15	0.02

Sample Name/ Marks from top of core	Depth (m below KB) /Description	TOC (wt%)	S1 (mg HC/g)	S2 (mg HC/g)	S3 (mg CO_2/g)	Tmax (°C)	HI (mg HC/g TOC) (S2x100/TOC)	OI (mg HC/g rock) (S3x100/TOC)	PI (S1/(S1+S2))
Anna C7003 50-55cm	141.63	8.19	0.28	9.61	0.81	421	117	10	0.03
Anna C7003 68-73cm	141.81	7.42	0.36	10.36	1.11	417	140	15	0.03
Anna C7003 75-80cm	141.88	34.20	2.93	111.54	4.73	426	326	14	0.03
Anna C7003 90-95cm	142.03	36.00	4.62	138.48	5.25	416	385	15	0.03
Anna C7003 97-100cm	142.09	21.50	1.92	77.13	4.62	422	359	21	0.02
Core C7005									
Anna C7005 13-18cm	152.62	27.50	2.24	95.28	4.72	415	346	17	0.02
Anna C7005 30-35cm	152.79	36.00	3.46	124.16	5.52	423	345	15	0.03
Anna C7005 45-50cm	152.94	17.30	0.90	37.55	2.99	427	217	17	0.02
Anna C7005 65-70cm	153.14	7.47	0.42	11.77	1.20	428	158	16	0.03
Anna C7005 89-94cm	153.38	12.30	0.61	13.98	2.22	426	114	18	0.04
Anna C7005 107-112cm	153.56	10.10	0.52	13.93	1.35	420	138	13	0.04
Anna C7005 126-131cm	153.75	19.70	1.02	34.04	2.46	412	173	12	0.03
Anna C7005 141-146cm	153.90	13.30	0.59	16.27	1.29	418	122	10	0.03
Anna C7005 160-165cm	154.08	4.89	0.24	6.03	0.57	413	123	12	0.04
Anna C7005 180-185cm	154.29	4.86	0.23	4.90	0.61	417	101	13	0.04

Sample Name/ Marks from top of core	Depth (m below KB) /Description	TOC (wt%)	S1 (mg HC/g)	S2 (mg HC/g)	S3 (mg CO_2/g)	Tmax (°C)	HI (mg HC/g TOC) (S2x100/TOC)	OI (mg HC/g rock) (S3x100/TOC)	PI (S1/(S1+S2))
Core C7009									
Anna C7009 0-5cm	109.10	2.16	0.08	1.26	0.44	431	58	20	0.06
Anna C7009 5-10cm	109.15	6.58	0.21	7.96	0.80	429	121	12	0.03
Anna C7009 16-21cm	109.26	25.10	1.67	76.22	3.66	420	304	15	0.02
Anna C7009 25-30cm	109.35	10.70	0.51	17.28	1.23	421	161	11	0.03
Anna C7009 48-53cm	109.58	32.00	3.40	120.22	4.54	420	376	14	0.03
Anna C7009 58-63cm	109.68	11.10	0.52	19.24	1.37	415	173	12	0.03
Anna C7009 66-71cm	109.76	7.51	0.38	10.04	1.21	411	134	16	0.04
Anna C7009 75-80cm	109.85	35.30	3.74	127.78	6.03	419	362	17	0.03
Anna C7009 82-86cm	109.91	24.60	1.43	64.18	4.38	419	261	18	0.02
Roof Samples									
Anna Roof 1	Pyrite Sun Horizon	8.61	0.57	25.84	0.52	426	300	6	0.02
Anna Roof 2	Pyrite Sun Horizon	8.20	0.65	23.68	0.63	417	289	8	0.03
Anna Roof 4	No Pyrite Suns	23.00	1.58	85.09	1.81	426	370	8	0.02
Anna Roof 5	No Pyrite Suns 30cm above coal	8.68	0.48	17.90	0.49	428	206	6	0.03
Anna Roof 6	Pyrite Sun Horizon	9.24	0.68	28.92	0.57	426	313	6	0.02

Sample Name/ Marks from top of core	Depth (m below KB) /Description	TOC (wt%)	S1 (mg HC/g)	S2 (mg HC/g)	S3 (mg CO_2/g)	Tmax (°C)	HI (mg HC/g TOC) (S2x100/TOC)	OI (mg HC/g rock) (S3x100/TOC)	PI (S1/(S1+S2))
Anna Roof 7	Pyrite Sun Horizon	7.73	0.59	21.24	0.65	417	275	8	0.03

KB = Kelly Bushing

APPENDIX C

PETROGRAPHIC DATA FOR ANNA SHALE SAMPLES

Data reported on a volume percent, mineral-matter free basis.

*Point count (PC) data are highlighted in gray

Sample Name/ Marks from top of core	Depth (m below KB)	Micrinite %	Other Inertinites %	Bituminite %	Other Liptinites %	Solid Bitumen %	Vitrinite %
Core C6848							
Anna C6848 30-35cm	177.33	71	2	25	1	1	0
Anna C6848 51-56cm	177.54	63	10	2	1	17	7
Anna C6848 71-76cm	177.74	78	2	19	0	1	0
Anna C6848 71-76cm	177.74	78	1	18	0	3	0
Anna C6848 103-108cm	178.06	66	1	26	1	4	2
Core C7003							
Anna C7003 22-27cm	141.35	65	20	3	2	10	0
Anna C7003 30-35 cm	141.43	88	2	5	0	5	0
Anna C7003 50-55cm	141.63	55	25	7	2	11	0
Anna C7003 90-95cm	142.03	62	1	33	1	3	0
Anna C7003 90-95cm	142.03	68	1	28	0	3	0
Core C7005							
Anna C7005 30-35cm	152.79	62	8	3	0	20	7
Anna C7005 65-70cm	153.14	49	10	0	4	34	3
Anna C7005 126-131cm	153.75	2	13	1	4	80	0
Anna C7005 180-185cm	154.29	3	6	2	12	77	0
Core C7009							
Anna C7009 5-10cm	109.15	60	16	6	2	14	2
Anna C7009 5-10cm	109.15	65	11	8	1	14	1

Sample Name/ Marks from top of core	Depth (m below KB)	Micrinite %	Other Inertinites %	Bituminite %	Other Liptinites %	Solid Bitumen %	Vitrinite %
Anna C7009 48-53cm	109.58	88	2	6	1	2	1
Anna C7009 66-71cm	109.76	84	8	2	0	6	0
Anna C7009 75-80cm	109.85	62	1	34	1	2	0

KB = Kelly Bushing

APPENDIX D

C-S-FE DATA FOR ANNA SHALE SAMPLES

Sample Name	Depth (m below KB) /Description	TOC (wt.%)	Fe (avg. wt.%)	TS (wt.%)
Core C6848				
Anna C6848 25-29cm	177.28	3.00	3.60	3.25
Anna C6848 30-35cm	177.33	26.50	3.04	1.79
Anna C6848 51-56cm	177.54	9.05	3.75	2.31
Anna C6848 60-65cm	177.63	6.88	4.02	2.27
Anna C6848 71-76cm	177.74	36.30	3.49	2.15
Anna C6848 85-90cm	177.88	8.73	3.44	1.97
Anna C6848 94-99cm	177.97	6.90	4.13	2.49
Anna C6848 103-108cm	178.06	37.00	4.52	2.82
Anna C6848 119-124cm	178.22	22.80	3.58	1.79
Core C7003				
Anna C7003 13-18cm	141.27	2.21	4.05	3.24
Anna C7003 22-27cm	141.35	7.10	4.26	2.44
Anna C7003 30-35 cm	141.43	21.50	3.21	1.9
Anna C7003 50-55cm	141.63	8.19	3.73	2.4
Anna C7003 68-73cm	141.81	7.42	4.19	2.42
Anna C7003 75-80cm	141.88	34.20	3.86	2.47
Anna C7003 90-95cm	142.03	36.00	4.18	2.96
Anna C7003 97-100cm	142.09	21.50	3.84	2.63

Sample Name	Depth (m below KB) /Description	TOC (wt.%)	Fe (avg. wt.%)	TS (wt.%)
Core C7005				
Anna C7005 13-18cm	152.62	27.50	4.15	2.4
Anna C7005 30-35cm	152.79	36.00	4.03	2.08
Anna C7005 45-50cm	152.94	17.30	3.53	2.67
Anna C7005 65-70cm	153.14	7.47	3.76	3.24
Anna C7005 89-94cm	153.38	12.30	5.43	4.57
Anna C7005 107-112cm	153.56	10.10	4.31	3.58
Anna C7005 126-131cm	153.75	19.70	4.94	4.31
Anna C7005 141-146cm	153.90	13.30	5.51	5.38
Anna C7005 160-165cm	154.08	4.89	4.50	3.69
Anna C7005 180-185cm	154.29	4.86	5.11	4.28
Core C7009				
Anna C7009 0-5cm	109.10	2.16	3.43	2.54
Anna C7009 5-10cm	109.15	6.58	3.82	2.83
Anna C7009 16-21cm	109.26	25.10	3.52	2.09
Anna C7009 25-30cm	109.35	10.70	3.75	2.34
Anna C7009 48-53cm	109.58	32.00	3.93	2.46
Anna C7009 58-63cm	109.68	11.10	3.58	2.09
Anna C7009 66-71cm	109.76	7.51	4.21	2.37
Anna C7009 75-80cm	109.85	35.30	4.23	2.99
Anna C7009 82-86cm	109.91	24.60	3.32	1.61

Sample Name	Depth (m below KB) /Description	TOC (wt.%)	Fe (avg. wt.%)	TS (wt.%)
Roof Samples				
Anna Roof 1	Pyrite Sun Horizon	8.61	3.47	2.28
Anna Roof 2	Pyrite Sun Horizon	8.20	3.83	2.45
Anna Roof 4	No Pyrite Suns	23.00	3.86	1.85
Anna Roof 5	No Pyrite Suns 30cm above coal	8.68	3.00	1.64
Anna Roof 6	Pyrite Sun Horizon	9.24	3.37	2.16
Anna Roof 7	Pyrite Sun Horizon	7.73	4.05	2.48

KB = Kelly Bushing; Total Organic Carbon (TOC), Fe, and Total Sulfur (TS) reported in weight percent; Fe weight percent is an average of the X-ray fluorescence measurements taken on the sampled interval

APPENDIX E

XRF DATA FOR ALL TRACE ELEMENTS

Marks from top of core (cm)	Depth (ft below KB)	Depth (m below KB)	Co (ppm)	Ni (ppm)	Cu (ppm)	Zn (ppm)	As (ppm)	Pb (ppm)	Se (ppm)	Th (ppm)	Sr (ppm)	Y (ppm)	Zr (ppm)	Mo (ppm)
C6848														
1	580.77	177.02	3	14	32	18	3	9	6	1	852	9	7	3
2	580.80	177.03	3	14	23	19	3	10	7	1	841	10	3	1
3	580.84	177.04	3	12	23	28	3	9	5	1	809	8	5	4
4	580.87	177.05	12	23	29	39	4	10	6	2	614	11	19	6
5	580.90	177.06	5	13	25	29	4	10	5	1	703	9	12	0
6	580.93	177.07	3	14	19	39	3	10	5	1	723	10	4	4
7	580.97	177.08	7	13	24	26	4	10	6	1	589	15	10	2
8	581.00	177.09	13	23	25	44	6	11	9	2	554	18	26	3
9	581.03	177.10	18	28	36	34	6	12	10	3	492	12	33	0
10	581.07	177.11	6	16	25	19	4	10	6	1	857	15	4	5
11	581.10	177.12	5	14	23	15	5	10	3	0	969	10	3	1
12	581.13	177.13	5	13	15	20	6	11	6	1	873	5	4	2
13	581.16	177.14	4	13	15	20	5	10	6	1	1006	8	3	6
14	581.20	177.15	4	16	23	22	3	10	6	0	1078	8	2	4
15	581.23	177.16	14	26	35	52	7	11	5	3	612	15	29	1
16	581.26	177.17	23	42	62	157	11	14	11	4	478	19	59	9
17	581.30	177.18	7	12	22	20	6	11	8	2	718	14	10	4
18	581.33	177.19	8	15	19	99	5	11	9	1	771	8	5	10
19	581.36	177.20	8	17	26	20	5	11	6	1	733	7	4	10
20	581.39	177.21	9	16	22	23	5	11	7	1	792	13	10	8

21	581.43	177.22	13	21	19	76	5	10	7	3	385	11	28	2
22	581.46	177.23	11	17	23	30	5	11	6	2	473	11	16	0
23	581.49	177.24	14	19	18	25	6	12	8	2	402	12	20	3
24	581.53	177.25	19	39	39	276	19	19	16	5	295	21	112	24
25	581.56	177.26	13	44	43	316	19	19	18	7	196	18	146	21
27	581.62	177.28	16	71	97	246	18	21	33	9	114	19	154	23
28	581.66	177.29	17	70	96	177	21	22	24	10	107	14	158	18
29	581.69	177.30	24	95	99	204	29	28	38	9	132	19	153	25
30	581.72	177.31	31	187	210	618	14	20	75	6	165	54	81	55
31	581.76	177.32	28	204	243	865	13	18	73	6	189	55	77	36
32	581.79	177.33	30	210	223	930	14	21	96	5	268	89	78	38
33	581.82	177.34	30	212	221	918	12	19	93	6	178	57	77	29
34	581.85	177.35	29	177	190	1080	17	22	98	5	306	99	75	19
35	581.89	177.36	33	187	191	1266	21	23	94	7	155	43	90	25
36	581.92	177.37	32	177	187	884	17	22	91	7	137	44	97	24
37	581.95	177.38	36	177	179	824	20	25	93	7	131	40	95	20
38	581.98	177.39	35	190	194	884	19	22	79	7	94	22	96	21
39	582.02	177.40	30	164	185	678	16	20	70	7	91	21	118	19
40	582.05	177.41	24	135	153	543	15	20	61	8	99	30	131	15
41	582.08	177.42	24	118	149	409	16	20	58	8	106	41	141	16
42	582.12	177.43	24	116	143	419	15	20	56	8	99	32	137	17
43	582.15	177.44	22	102	133	547	16	19	51	8	98	32	150	15
44	582.18	177.45	19	94	125	906	19	18	48	8	104	32	150	15
45	582.21	177.46	23	97	125	257	18	21	44	9	100	29	153	16
46	582.25	177.47	25	101	127	277	21	24	42	8	99	28	150	15
47	582.28	177.48	23	94	134	257	18	21	43	8	100	22	151	15
48	582.31	177.49	25	102	132	254	20	22	36	9	95	24	146	14
49	582.35	177.50	20	87	125	246	20	22	40	9	96	24	149	15

50	582.38	177.51	21	88	124	239	15	19	37	9	92	27	146	12
51	582.41	177.52	22	95	122	256	18	21	37	9	98	24	142	12
52	582.44	177.53	22	92	117	241	16	21	43	8	97	23	142	13
53	582.48	177.54	20	90	113	249	18	21	40	9	93	19	141	13
54	582.51	177.55	19	87	120	260	15	19	39	9	95	16	142	13
55	582.54	177.56	21	93	115	261	17	21	42	9	94	18	141	13
56	582.58	177.57	20	87	113	273	16	20	44	9	101	20	138	20
57	582.61	177.58	19	84	112	251	13	18	42	9	96	18	135	16
58	582.64	177.59	18	80	105	271	16	19	42	9	95	16	137	20
59	582.67	177.60	18	81	102	234	19	22	49	9	96	11	128	25
60	582.71	177.61	17	76	100	194	17	22	52	9	105	12	140	27
61	582.74	177.62	17	70	90	178	20	24	55	10	103	7	135	39
62	582.77	177.63	18	79	105	201	18	25	66	9	99	10	130	57
63	582.81	177.64	16	78	105	262	18	24	61	8	101	11	129	51
64	582.84	177.65	18	80	104	187	19	25	70	9	103	10	136	33
65	582.87	177.66	19	88	116	264	20	27	79	8	99	8	132	45
66	582.90	177.67	19	90	128	247	20	28	84	8	91	7	131	42
67	582.94	177.68	23	108	137	325	21	28	90	8	86	2	114	26
68	582.97	177.69	24	166	259	868	20	23	79	6	135	86	79	21
69	583.00	177.70	24	190	261	933	13	18	83	4	248	160	65	13
70	583.03	177.71	29	229	343	1080	13	19	102	5	48	1	64	26
71	583.07	177.72	25	212	285	828	11	17	92	5	114	63	69	28
72	583.10	177.73	27	218	301	859	11	19	98	5	65	22	69	34
73	583.13	177.74	30	225	295	979	14	22	123	5	107	85	74	45
74	583.17	177.75	37	254	309	1203	17	24	138	5	48	13	76	63
75	583.20	177.76	42	245	237	1640	28	32	154	5	68	14	82	99
76	583.23	177.77	41	221	211	1528	29	35	160	5	114	69	90	83
77	583.26	177.78	35	177	165	968	25	34	151	6	81	19	98	50

78	583.30	177.79	35	174	155	883	26	34	137	7	87	21	99	43
79	583.33	177.80	35	171	167	878	27	33	130	7	98	39	100	42
80	583.36	177.81	35	181	190	1090	26	30	117	7	79	16	105	40
81	583.40	177.82	26	148	157	687	17	22	83	7	74	20	114	29
82	583.43	177.83	20	97	109	372	16	23	84	8	106	44	147	25
83	583.46	177.84	20	91	104	331	16	24	82	8	104	38	147	22
84	583.49	177.85	20	93	106	342	18	25	80	9	97	26	140	24
85	583.53	177.86	20	89	98	321	17	25	77	8	100	34	145	23
86	583.56	177.87	19	86	98	309	21	29	84	8	113	42	144	27
87	583.59	177.88	21	92	100	319	20	27	80	9	106	40	141	30
88	583.63	177.89	21	90	106	310	18	26	83	9	103	37	148	39
89	583.66	177.90	17	77	92	262	21	28	80	8	99	22	140	40
90	583.69	177.91	19	87	104	303	18	24	76	9	100	18	141	45
91	583.72	177.92	18	85	100	282	19	26	80	9	97	16	131	48
92	583.76	177.93	21	109	125	405	24	32	103	8	90	14	124	158
93	583.79	177.94	14	74	94	253	25	32	94	8	102	12	136	226
94	583.82	177.95	15	78	95	271	23	34	103	8	95	12	131	176
95	583.85	177.96	18	82	99	313	23	32	104	8	101	14	132	140
96	583.89	177.97	14	80	105	371	24	33	111	8	99	15	136	191
97	583.92	177.98	18	89	109	598	25	34	120	8	96	15	140	291
98	583.95	177.99	16	73	110	281	21	33	118	9	102	10	143	158
99	583.99	178.00	18	85	110	507	26	35	121	9	98	12	143	176
100	584.02	178.01	21	103	141	626	25	33	127	8	91	12	134	161
101	584.05	178.02	24	166	238	877	14	22	108	6	62	16	82	129
102	584.08	178.03	32	233	323	936	15	25	139	4	56	35	61	170
103	584.12	178.04	47	279	360	1830	25	32	180	4	77	43	69	285
104	584.15	178.05	49	295	362	3380	44	39	214	4	92	22	75	480
105	584.18	178.06	51	303	371	3530	49	43	229	4	119	19	75	472

106	584.22	178.07	45	286	370	3592	49	44	233	4	118	15	77	470
107	584.25	178.08	45	253	308	2150	44	47	214	4	121	15	83	286
108	584.28	178.09	38	231	273	2522	40	40	202	4	121	13	77	261
109	584.31	178.10	44	222	262	2007	45	51	215	4	129	18	86	199
110	584.35	178.11	43	216	262	2293	46	49	221	5	132	17	85	212
111	584.38	178.12	39	34	47	1581	26	33	181	0	356	17	11	101
112	584.41	178.13	19	29	28	65	4	12	26	2	383	12	15	14
113	584.45	178.14	19	28	28	78	5	13	32	1	372	16	13	12
114	584.48	178.15	21	34	40	88	7	15	42	1	351	18	19	11
115	584.51	178.16	36	44	55	3279	44	48	284	0	365	29	14	211
116	584.54	178.17	54	45	42	2002	68	115	444	0	356	31	9	299
117	584.58	178.18	34	182	174	682	21	35	156	6	115	40	95	74
118	584.61	178.19	36	185	190	658	21	34	152	6	135	77	93	65
119	584.64	178.20	34	184	185	646	22	35	153	6	117	58	92	63
120	584.68	178.21	32	194	194	756	16	29	150	6	73	15	87	62
121	584.71	178.22	31	192	187	679	18	33	182	6	58	17	100	77
122	584.74	178.23	26	157	161	690	16	31	165	6	72	9	108	76
123	584.77	178.24	25	114	135	477	26	45	199	8	84	5	124	131
124	584.81	178.25	25	117	120	416	24	45	200	7	86	4	127	117
125	584.84	178.26	25	114	128	439	26	48	209	7	105	21	120	98
C7003														
1	462.99	141.12	9	16	21	24	4	10	7	2	619	11	12	4
2	463.02	141.13	13	20	20	26	6	10	2	2	604	12	15	6
3	463.06	141.14	4	14	18	16	3	10	5	1	781	11	3	7
4	463.09	141.15	5	14	18	24	4	10	6	0	815	12	3	3
5	463.12	141.16	5	12	21	20	4	10	6	1	766	14	6	3
6	463.16	141.17	6	13	20	39	4	11	4	1	741	11	8	4
7	463.19	141.18	6	13	13	22	4	10	6	0	762	17	6	3

8	463.22	141.19	11	15	16	25	4	10	5	1	671	20	9	6
9	463.25	141.20	22	24	23	35	6	11	4	3	417	12	38	7
10	463.29	141.21	24	38	30	70	13	16	8	5	337	29	107	15
11	463.32	141.22	15	43	39	97	14	16	9	9	176	20	180	14
12	463.35	141.23	16	54	55	116	17	18	10	9	177	21	178	18
13	463.38	141.24	18	60	47	106	27	25	15	9	158	18	174	17
14	463.42	141.25	36	167	179	644	16	21	70	7	131	52	103	15
15	463.45	141.26	14	55	44	114	24	24	19	8	167	19	164	21
16	463.48	141.27	17	51	56	110	19	19	15	8	152	25	189	18
17	463.52	141.28	20	72	73	190	22	22	18	9	139	25	183	20
18	463.55	141.29	20	74	68	239	26	23	22	9	128	25	174	18
19	463.58	141.30	17	56	38	116	22	21	14	8	170	19	169	21
20	463.61	141.31	21	92	89	154	21	22	29	9	108	15	153	20
21	463.65	141.32	23	94	81	119	17	20	29	9	110	15	153	22
22	463.68	141.33	21	88	93	133	16	18	23	10	108	16	148	18
23	463.71	141.34	20	84	92	153	20	21	29	10	113	16	149	24
24	463.75	141.35	21	86	89	118	13	17	26	10	104	14	153	25
25	463.78	141.36	21	89	97	153	14	19	31	9	98	11	149	29
26	463.81	141.37	24	102	88	174	15	19	30	9	100	11	152	25
27	463.84	141.38	6	67	81	194	26	29	59	8	111	5	153	54
28	463.88	141.39	24	104	106	258	16	21	48	9	98	11	139	46
29	463.91	141.40	25	109	118	206	15	21	52	10	96	6	137	39
30	463.94	141.41	28	132	187	435	15	19	50	7	89	4	113	40
31	463.98	141.42	30	163	201	689	21	21	43	6	208	70	89	36
32	464.01	141.43	31	171	191	584	18	20	46	6	242	75	82	36
33	464.04	141.44	27	175	192	694	13	16	47	6	268	85	77	30
34	464.07	141.45	27	176	203	868	12	15	55	5	310	108	75	23
35	464.11	141.46	25	164	178	987	14	17	62	5	438	153	70	19

36	464.14	141.47	34	186	196	868	16	20	76	6	177	62	97	29
37	464.17	141.48	37	195	209	1203	17	21	89	6	136	31	101	26
38	464.21	141.49	35	178	166	712	15	21	83	7	150	50	101	21
39	464.24	141.50	36	179	170	718	16	21	79	6	164	57	104	21
40	464.27	141.51	38	178	165	667	17	23	81	7	109	27	107	23
41	464.30	141.52	34	163	154	606	15	21	80	8	129	44	106	16
42	464.34	141.53	36	167	179	644	16	21	70	7	131	52	103	15
43	464.37	141.54	30	160	180	570	14	18	58	7	176	119	106	9
44	464.40	141.55	30	154	165	605	13	18	57	7	115	49	117	13
45	464.43	141.56	25	121	143	442	13	18	53	8	106	39	141	11
46	464.47	141.57	23	115	133	346	13	18	47	8	104	31	144	13
47	464.50	141.58	25	113	139	300	13	18	41	8	102	29	152	12
48	464.53	141.59	21	102	128	297	14	18	41	8	99	25	151	10
49	464.57	141.60	21	89	107	201	16	20	41	8	104	26	167	16
50	464.60	141.61	19	79	101	212	16	20	34	8	102	28	176	16
51	464.63	141.62	18	74	100	204	16	19	32	8	102	27	166	17
52	464.66	141.63	19	76	93	208	18	21	29	8	101	26	166	17
53	464.70	141.64	18	76	99	245	19	20	31	8	102	25	160	15
54	464.73	141.65	19	74	104	219	17	20	27	8	100	24	162	17
55	464.76	141.66	19	78	105	227	19	21	32	8	103	23	163	17
56	464.80	141.67	18	78	107	208	17	21	29	8	100	25	160	17
57	464.83	141.68	18	76	96	219	20	22	30	8	98	20	158	15
58	464.86	141.69	17	72	97	201	18	21	31	9	103	23	155	16
59	464.89	141.70	20	86	107	227	17	20	34	8	101	24	150	15
60	464.93	141.71	19	81	95	207	18	21	34	8	107	22	160	15
61	464.96	141.72	19	80	98	231	15	19	31	8	102	21	154	15
62	464.99	141.73	20	84	93	236	19	21	36	9	93	19	158	16
63	465.03	141.74	19	84	102	228	13	17	36	9	99	17	145	14

64	465.06	141.75	16	71	85	216	15	19	40	9	96	17	140	17
65	465.09	141.76	20	84	96	252	14	18	38	9	94	17	146	21
66	465.12	141.77	16	69	82	222	19	22	46	9	104	12	143	29
67	465.16	141.78	18	76	94	195	17	22	51	9	103	7	141	31
68	465.19	141.79	20	88	110	258	19	23	58	9	93	11	135	36
69	465.22	141.80	18	80	95	217	17	23	57	9	100	12	144	31
70	465.25	141.81	19	80	101	251	19	24	65	9	90	10	139	30
71	465.29	141.82	20	87	120	250	18	25	74	9	108	7	138	27
72	465.32	141.83	22	96	122	263	21	27	74	8	91	6	130	37
73	465.35	141.84	24	105	133	305	14	22	72	8	83	7	119	21
74	465.39	141.85	31	185	290	722	18	21	68	6	66	3	84	22
75	465.42	141.86	34	221	332	960	17	21	84	5	147	65	70	20
76	465.45	141.87	31	224	331	992	15	18	75	4	161	75	64	17
77	465.48	141.88	29	199	263	814	10	15	69	6	114	55	69	19
78	465.52	141.89	31	204	264	827	9	15	72	6	54	8	71	29
79	465.55	141.90	38	216	263	1015	15	22	111	5	93	35	79	42
80	465.58	141.91	41	207	199	998	21	27	122	5	79	4	91	55
81	465.62	141.92	44	199	167	760	21	30	124	5	175	111	86	41
82	465.65	141.93	35	166	146	818	18	26	114	6	153	79	96	29
83	465.68	141.94	35	156	139	598	18	26	106	7	109	16	106	31
84	465.71	141.95	34	159	138	607	15	24	100	7	112	23	108	29
85	465.75	141.96	29	140	135	727	21	24	84	7	232	200	101	13
86	465.78	141.97	33	144	143	513	19	27	99	7	109	15	108	30
87	465.81	141.98	36	222	233	965	14	21	109	4	57	17	55	194
88	465.85	141.99	28	187	194	988	15	19	89	4	85	74	55	146
89	465.88	142.00	18	143	195	2104	14	12	76	5	131	137	69	99
90	465.91	142.01	37	220	276	2527	40	32	156	4	144	7	65	252
91	465.94	142.02	36	248	342	3474	40	28	160	4	114	7	60	369

92	465.98	142.03	39	264	376	4072	43	28	171	4	117	9	62	407
93	466.01	142.04	35	254	319	3904	31	19	138	4	96	16	58	384
94	466.04	142.05	34	242	326	3708	29	18	134	5	82	14	60	383
95	466.08	142.06	36	224	278	2030	21	21	120	4	79	19	57	262
96	466.11	142.07	41	251	335	2163	24	24	140	4	77	17	66	284
97	466.14	142.08	37	203	259	1665	33	34	149	5	123	10	67	161
98	466.17	142.09	35	169	209	598	25	37	143	5	214	72	72	89
99	466.21	142.10	29	140	153	324	19	31	120	5	262	87	67	65
100	466.24	142.11	33	145	153	464	23	33	124	5	231	68	73	62
C7005														
1	500.25	152.48	52	27	28	39	12	17	26	5	462	23	78	36
2	500.28	152.49	45	31	28	37	11	17	30	3	640	31	52	42
3	500.32	152.50	44	21	23	30	10	16	27	1	864	24	28	30
4	500.35	152.51	53	22	23	34	14	20	33	1	831	21	31	36
5	500.38	152.52	37	58	45	58	22	26	44	5	456	24	97	38
6	500.41	152.53	46	57	47	62	23	29	57	5	435	18	87	32
7	500.45	152.54	51	82	60	78	26	31	59	4	503	42	63	41
8	500.48	152.55	25	123	101	151	12	20	51	3	516	138	51	52
9	500.51	152.56	42	187	147	239	20	27	79	6	109	14	92	136
10	500.55	152.57	24	103	91	307	23	30	84	9	89	7	142	180
11	500.58	152.58	21	89	96	309	22	30	90	9	88	6	140	133
12	500.61	152.59	24	112	139	309	15	25	90	7	83	1	124	98
13	500.64	152.60	51	263	242	693	16	27	131	4	74	8	65	240
14	500.68	152.61	47	271	322	2154	25	28	165	4	104	8	67	375
15	500.71	152.62	40	236	307	2392	33	33	178	5	156	11	74	337
16	500.74	152.63	46	213	259	970	28	41	188	5	179	11	88	191
17	500.77	152.64	40	178	195	659	22	38	179	5	210	56	88	107
18	500.81	152.65	38	183	185	430	12	28	163	6	82	20	91	79

19	500.84	152.66	37	196	218	634	16	34	195	5	152	60	80	60
20	500.87	152.67	28	136	143	314	15	32	158	7	97	23	116	74
21	500.91	152.68	27	115	119	245	20	37	163	7	173	47	122	88
22	500.94	152.69	30	168	191	619	13	28	166	6	150	49	101	63
23	500.97	152.70	36	204	237	688	13	29	179	5	116	41	85	72
24	501.00	152.71	42	254	280	797	11	28	195	4	74	30	64	90
25	501.04	152.72	59	288	286	650	15	39	245	4	64	7	63	128
26	501.07	152.73	51	264	254	859	17	36	232	4	94	28	66	113
27	501.10	152.74	52	263	254	746	16	39	256	4	81	32	68	97
28	501.14	152.75	44	227	246	743	15	36	234	4	120	67	71	66
29	501.17	152.76	45	238	240	607	14	37	244	4	57	7	69	67
30	501.20	152.77	44	232	234	630	13	36	238	4	113	71	67	65
31	501.23	152.78	49	250	260	641	14	36	245	5	67	13	70	69
32	501.27	152.79	46	262	278	706	13	34	233	4	57	5	66	70
33	501.30	152.80	46	270	310	696	10	30	225	4	60	12	69	64
34	501.33	152.81	52	293	363	824	10	30	231	4	61	15	67	62
35	501.37	152.82	43	251	288	852	11	28	206	4	67	18	72	51
36	501.40	152.83	36	200	228	611	11	25	158	5	124	77	79	31
37	501.43	152.84	20	148	117	589	8	19	120	4	114	76	101	21
38	501.46	152.85	38	191	202	275	13	29	161	5	89	15	86	27
39	501.50	152.86	34	171	169	612	13	28	160	5	88	8	89	27
40	501.53	152.87	31	133	132	218	16	33	153	6	113	11	108	26
41	501.56	152.88	31	132	141	290	14	30	148	6	106	10	103	25
42	501.60	152.89	31	139	148	235	17	32	148	6	95	10	103	23
43	501.63	152.90	38	157	158	294	17	33	157	5	108	19	96	23
44	501.66	152.91	26	115	124	626	15	24	106	6	109	13	105	16
45	501.69	152.92	23	88	96	237	15	25	95	6	137	20	108	16
46	501.73	152.93	30	102	115	228	16	27	102	5	171	57	106	14

47	501.76	152.94	28	90	108	167	15	24	86	6	183	46	105	14
48	501.79	152.95	26	78	92	149	18	27	92	6	150	20	110	17
49	501.82	152.96	26	79	97	162	15	24	78	6	172	40	109	14
50	501.86	152.97	22	63	69	153	18	25	64	6	157	23	119	15
51	501.89	152.98	27	72	88	131	16	24	69	6	171	23	111	13
52	501.92	152.99	25	58	73	117	20	24	49	7	176	25	127	18
53	501.96	153.00	23	65	75	342	18	22	54	6	168	23	123	13
54	501.99	153.01	22	51	70	106	18	22	47	7	169	28	130	16
55	502.02	153.02	22	52	69	115	17	22	45	7	171	34	125	14
56	502.05	153.03	22	51	63	105	16	21	41	7	168	27	121	11
57	502.09	153.04	23	53	64	112	16	21	40	6	195	31	124	16
58	502.12	153.05	26	58	69	96	16	21	37	7	197	26	129	17
59	502.15	153.06	24	55	51	105	15	20	33	6	196	32	127	13
60	502.19	153.07	23	49	52	85	13	18	31	7	202	31	124	13
61	502.22	153.08	23	44	56	62	16	20	27	7	216	34	127	16
62	502.25	153.09	22	43	48	57	15	19	25	7	201	31	133	11
63	502.28	153.10	26	53	65	66	15	19	28	7	198	33	133	20
64	502.32	153.11	22	45	55	54	15	19	22	7	201	33	139	14
65	502.35	153.12	24	46	51	52	13	18	20	7	208	31	131	16
66	502.38	153.13	25	48	53	52	18	20	21	7	208	33	139	17
67	502.42	153.14	23	45	57	60	14	17	18	7	213	37	132	11
68	502.45	153.15	24	44	49	76	14	17	19	7	217	33	136	10
69	502.48	153.16	26	41	41	48	18	20	22	7	224	32	132	14
70	502.51	153.17	23	42	36	79	17	19	20	6	219	32	132	9
71	502.55	153.18	22	42	55	51	15	18	18	7	217	33	136	11
72	502.58	153.19	23	37	45	50	13	16	17	7	204	29	141	9
73	502.61	153.20	22	35	44	54	13	17	16	7	219	35	138	12
74	502.65	153.21	25	36	38	50	15	18	17	7	236	36	135	9

75	502.68	153.22	24	36	40	66	15	16	13	7	202	33	146	15
76	502.71	153.23	23	36	39	67	18	19	13	7	194	34	144	15
77	502.74	153.24	20	35	34	53	16	18	12	7	183	31	146	12
78	502.78	153.25	23	39	39	50	17	19	12	6	192	29	142	16
79	502.81	153.26	17	36	36	49	18	20	15	6	160	28	140	21
80	502.84	153.27	18	37	40	54	22	22	12	7	151	26	149	18
81	502.87	153.28	21	38	37	47	23	22	15	6	144	25	140	17
82	502.91	153.29	23	39	44	60	23	22	16	7	124	25	145	21
83	502.94	153.30	18	36	38	156	21	20	14	7	118	23	139	15
84	502.97	153.31	19	40	42	48	17	20	15	7	118	24	149	15
85	503.01	153.32	19	38	44	49	20	21	15	7	125	24	142	15
86	503.04	153.33	21	39	45	64	19	20	15	7	110	25	134	14
87	503.07	153.34	17	38	46	60	23	22	14	6	114	22	137	19
88	503.10	153.35	13	33	43	49	21	21	14	7	114	22	136	12
89	503.14	153.36	17	46	45	48	21	21	16	7	110	24	138	18
90	503.17	153.37	14	36	42	64	18	18	12	7	99	19	139	16
91	503.20	153.38	12	37	39	51	19	20	16	7	97	17	136	16
92	503.24	153.39	11	37	37	54	24	23	16	7	99	22	131	33
93	503.27	153.40	13	35	38	49	18	20	13	7	94	20	139	18
94	503.30	153.41	15	35	38	50	20	20	10	7	95	19	132	13
95	503.33	153.42	11	33	37	61	19	20	12	7	94	21	129	21
96	503.37	153.43	10	30	43	51	28	25	13	7	105	18	133	26
97	503.40	153.44	6	33	40	46	31	27	14	7	98	20	134	18
98	503.43	153.45	13	37	41	57	26	24	12	7	93	20	129	13
99	503.47	153.46	15	32	42	49	23	21	10	7	94	21	139	15
100	503.50	153.47	16	32	43	49	19	19	8	7	96	18	138	10
101	503.53	153.48	21	35	47	50	24	22	9	8	98	20	135	18
102	503.56	153.49	21	36	49	50	20	20	9	8	97	22	141	9

103	503.60	153.50	22	37	54	52	17	18	9	8	101	22	137	11
104	503.63	153.51	19	34	49	47	18	19	11	8	96	20	140	5
105	503.66	153.52	22	41	53	53	15	17	9	8	94	24	137	6
106	503.69	153.53	20	33	47	48	21	20	9	8	97	22	136	10
107	503.73	153.54	20	33	49	53	16	18	10	8	96	24	141	8
108	503.76	153.55	21	35	57	48	17	19	9	8	94	22	140	4
109	503.79	153.56	20	34	54	58	16	18	11	8	103	30	141	7
110	503.83	153.57	21	34	47	62	15	16	6	8	106	27	137	6
111	503.86	153.58	24	34	52	48	15	17	7	8	98	23	139	10
112	503.89	153.59	21	30	63	57	16	18	7	8	106	29	145	3
113	503.92	153.60	95	15	21	29	7	13	6	1	415	28	17	10
114	503.96	153.61	44	10	21	21	3	9	4	1	460	28	17	6
115	503.99	153.62	41	13	21	24	5	10	5	2	463	29	19	2
116	504.02	153.63	44	14	25	24	4	10	7	1	495	29	15	3
117	504.06	153.64	27	12	22	22	3	9	3	1	459	25	18	3
118	504.09	153.65	29	11	21	23	2	8	2	2	436	26	21	2
119	504.12	153.66	36	13	22	27	3	9	6	2	434	26	17	4
120	504.15	153.67	35	14	26	53	2	9	6	1	498	33	18	3
121	504.19	153.68	35	12	18	23	4	10	5	2	491	28	17	1
122	504.22	153.69	89	13	25	29	8	13	8	1	455	40	18	12
123	504.25	153.70	85	15	29	29	7	12	10	1	525	41	17	14
124	504.29	153.71	21	22	45	57	14	16	8	6	233	41	81	0
125	504.32	153.72	14	32	60	53	11	16	12	7	113	27	105	4
126	504.35	153.73	15	31	69	51	14	17	15	7	104	29	104	5
127	504.38	153.74	15	35	65	48	13	16	13	8	104	35	106	3
128	504.42	153.75	12	36	79	67	14	17	19	7	96	30	104	4
129	504.45	153.76	11	36	76	50	13	17	18	7	88	32	101	5
130	504.48	153.77	10	34	76	46	14	17	18	8	91	30	100	9

131	504.52	153.78	14	41	89	53	11	16	20	7	85	31	96	9
132	504.55	153.79	10	37	90	43	13	17	20	7	87	30	94	8
133	504.58	153.80	7	32	83	46	12	16	18	7	79	28	94	6
134	504.61	153.81	7	35	86	50	11	16	19	7	90	30	95	8
135	504.65	153.82	8	43	89	47	12	16	21	6	77	26	90	7
136	504.68	153.83	12	33	87	50	12	15	14	7	87	35	94	5
137	504.71	153.84	7	34	83	48	14	17	16	7	87	38	99	6
138	504.74	153.85	12	38	88	46	14	18	15	7	88	37	100	6
139	504.78	153.86	14	39	91	54	17	18	11	8	93	39	107	6
140	504.81	153.87	14	36	97	56	13	16	12	7	88	28	97	8
141	504.84	153.88	15	32	103	48	13	17	11	7	91	29	108	13
142	504.88	153.89	9	28	99	50	21	21	9	7	102	31	106	17
143	504.91	153.90	0	30	86	47	31	28	17	6	109	59	84	11
144	504.94	153.91	19	35	127	50	20	20	12	8	104	34	127	9
145	504.97	153.92	17	37	132	54	15	16	8	9	111	41	132	12
146	505.01	153.93	16	33	144	55	15	16	6	8	105	41	137	13
147	505.04	153.94	15	35	128	56	15	17	5	9	110	32	136	12
148	505.07	153.95	15	35	117	49	14	17	5	8	104	36	129	9
149	505.11	153.96	14	36	117	55	18	18	7	9	109	38	134	13
150	505.14	153.97	13	35	118	53	18	18	4	8	104	35	133	11
151	505.17	153.98	11	34	121	59	16	18	6	8	105	34	130	11
152	505.20	153.99	14	37	122	54	16	17	6	9	106	38	135	11
153	505.24	154.00	14	34	141	56	14	16	6	9	108	35	136	13
154	505.27	154.01	14	36	131	56	15	16	3	9	107	34	137	11
155	505.30	154.02	14	35	121	56	17	18	6	9	108	32	137	12
156	505.34	154.03	16	38	120	57	17	18	3	9	105	30	138	14
157	505.37	154.04	15	33	127	60	14	16	4	9	107	29	138	14
158	505.40	154.05	14	29	126	58	16	17	3	9	113	32	141	13

159	505.43	154.06	15	35	114	58	18	19	6	9	112	30	135	17
160	505.47	154.07	15	36	125	61	23	20	4	8	111	25	133	17
161	505.50	154.08	13	36	129	59	18	19	6	9	110	29	134	19
162	505.53	154.09	13	32	153	54	13	15	4	9	110	30	137	16
163	505.56	154.10	6	27	128	59	17	17	6	9	109	33	140	21
164	505.60	154.11	12	30	141	57	16	17	4	9	119	29	138	15
165	505.63	154.12	13	34	148	54	16	16	5	9	114	30	138	13
166	505.66	154.13	12	37	150	59	18	18	4	9	113	30	136	18
167	505.70	154.14	12	35	151	58	17	17	4	9	115	30	138	15
168	505.73	154.15	12	30	143	59	15	16	3	9	106	32	141	15
169	505.76	154.16	11	29	139	59	16	16	3	9	109	29	135	11
170	505.79	154.17	0	24	133	50	16	17	4	8	106	31	126	29
171	505.83	154.18	13	35	158	62	15	17	3	9	108	33	141	17
172	505.86	154.19	10	29	126	64	17	17	4	9	109	31	144	19
173	505.89	154.20	7	27	131	60	15	17	5	9	107	33	143	24
174	505.93	154.21	13	31	139	59	18	18	4	9	112	30	137	13
175	505.96	154.22	7	26	95	51	20	19	4	9	108	30	137	13
176	505.99	154.23	8	29	128	62	18	18	4	9	114	37	144	21
177	506.02	154.24	7	28	143	64	19	19	4	9	106	35	140	20
178	506.06	154.25	11	29	109	65	18	18	3	9	114	30	137	21
179	506.09	154.26	10	28	109	58	22	20	4	9	109	32	142	19
180	506.12	154.27	10	28	121	63	18	18	2	9	111	29	138	17
181	506.16	154.28	0	24	95	58	18	18	5	9	106	30	131	22
182	506.19	154.29	9	31	159	59	17	18	5	9	116	28	139	20
183	506.22	154.30	6	23	94	44	15	17	6	7	107	28	115	16
184	506.25	154.31	5	27	116	56	16	18	5	9	117	27	133	20
185	506.29	154.32	8	29	98	56	16	17	4	9	115	29	140	14
C7009														

1	357.89	109.08	18	43	44	102	12	15	6	9	193	18	166	16
2	357.92	109.09	19	46	44	121	14	16	10	9	187	20	163	18
3	357.95	109.10	18	46	43	92	16	18	12	9	177	19	155	15
4	357.99	109.11	20	54	43	108	17	20	15	9	172	23	164	16
5	358.02	109.12	19	65	69	141	18	19	15	10	143	26	169	13
6	358.05	109.13	24	84	80	185	25	24	26	9	130	19	157	16
8	358.12	109.15	22	83	85	159	19	20	23	10	112	16	149	15
9	358.15	109.16	19	72	81	192	18	19	26	10	101	11	155	19
10	358.18	109.17	19	76	87	157	16	19	21	9	111	6	151	15
11	358.22	109.18	21	76	96	124	15	18	21	10	105	13	149	18
12	358.25	109.19	22	80	87	190	23	24	37	9	103	6	159	33
13	358.28	109.20	25	102	103	236	16	18	31	10	92	10	140	32
14	358.31	109.21	25	102	108	187	13	18	37	10	97	4	143	29
15	358.35	109.22	38	165	210	356	16	20	42	7	83	5	101	40
16	358.38	109.23	26	145	167	449	14	17	27	5	303	154	79	28
17	358.41	109.24	32	165	179	476	16	18	35	7	205	85	87	39
18	358.44	109.25	33	192	209	676	11	15	46	7	96	19	87	34
19	358.48	109.26	36	209	227	802	15	17	47	7	85	9	86	38
20	358.51	109.27	38	203	214	875	14	17	56	6	150	56	77	31
21	358.54	109.28	27	182	182	2221	23	13	53	5	257	105	79	27
22	358.58	109.29	36	177	156	637	20	21	55	7	143	32	102	29
23	358.61	109.30	36	178	167	630	17	20	55	8	106	10	108	32
24	358.64	109.31	34	160	157	479	16	20	53	8	112	14	111	24
25	358.67	109.32	23	105	124	257	16	19	36	8	115	33	143	17
26	358.71	109.33	26	113	127	234	17	19	36	9	112	27	139	14
27	358.74	109.34	25	95	124	190	16	21	44	8	106	27	154	21
28	358.77	109.35	21	77	112	187	19	22	35	8	107	19	155	24
29	358.81	109.36	26	90	114	202	21	23	40	8	105	21	153	22

30	358.84	109.37	23	84	114	223	22	23	39	8	104	22	151	25
31	358.87	109.38	19	77	112	204	28	29	53	8	107	20	149	26
32	358.90	109.39	21	80	100	217	24	26	43	8	105	20	149	19
33	358.94	109.40	23	88	115	253	23	22	35	9	99	22	152	19
34	358.97	109.41	23	92	112	224	19	22	38	8	102	17	142	21
35	359.00	109.42	23	88	116	233	20	22	44	8	102	20	147	19
36	359.04	109.43	23	91	114	335	17	20	43	8	102	13	143	16
37	359.07	109.44	22	90	106	220	14	19	41	9	109	14	141	17
38	359.10	109.45	23	88	105	259	16	19	37	9	94	15	137	15
39	359.13	109.46	18	72	87	214	20	23	46	9	105	11	141	19
40	359.17	109.47	19	75	89	177	19	24	49	9	104	6	139	30
41	359.20	109.48	20	81	106	225	19	24	53	9	104	7	136	37
42	359.23	109.49	21	83	101	238	17	22	53	9	103	8	139	33
43	359.26	109.50	21	79	97	208	15	21	52	9	101	12	142	26
44	359.30	109.51	21	90	114	257	19	25	65	9	96	9	135	34
45	359.33	109.52	23	93	121	240	16	22	60	9	95	7	135	26
46	359.36	109.53	25	104	146	324	17	22	62	8	87	6	123	17
47	359.40	109.54	29	152	223	691	16	19	59	7	74	3	99	19
48	359.43	109.55	34	224	323	1131	18	19	72	6	68	18	69	17
49	359.46	109.56	26	194	244	855	12	15	59	5	173	107	68	10
50	359.49	109.57	32	213	263	939	13	17	70	6	65	11	75	21
51	359.53	109.58	33	205	235	986	12	16	77	6	66	3	77	28
52	359.56	109.59	37	189	177	781	15	22	92	6	88	7	83	31
53	359.59	109.60	42	188	159	693	19	26	106	6	122	13	97	36
54	359.63	109.61	36	158	145	551	20	28	105	7	127	18	109	26
55	359.66	109.62	34	151	128	520	20	28	101	7	130	31	106	27
56	359.69	109.63	34	146	131	507	21	29	101	7	128	20	110	28
57	359.72	109.64	35	156	154	510	16	23	85	8	96	10	110	28

58	359.76	109.65	31	153	145	342	13	20	68	8	88	23	115	19
59	359.79	109.66	21	90	103	243	16	23	75	8	91	19	139	17
60	359.82	109.67	23	87	97	244	16	25	78	8	97	15	142	26
61	359.86	109.68	22	84	96	241	19	27	75	8	94	17	145	25
62	359.89	109.69	20	76	87	215	17	25	80	8	100	15	144	29
63	359.92	109.70	23	85	92	218	20	28	81	8	94	12	142	31
64	359.95	109.71	20	81	94	230	17	25	84	8	95	12	139	34
65	359.99	109.72	22	86	89	229	17	25	83	8	92	11	134	38
66	360.02	109.73	21	82	89	111	20	30	91	9	95	10	132	100
67	360.05	109.74	18	75	82	46	20	30	94	9	96	11	134	88
68	360.09	109.75	19	75	92	48	20	32	99	8	91	7	134	95
70	360.15	109.77	25	102	106	46	20	32	102	8	95	8	132	152
71	360.18	109.78	19	76	91	109	20	32	103	8	94	6	132	89
72	360.22	109.79	20	83	103	346	23	34	118	9	101	12	137	107
73	360.25	109.80	29	165	256	883	14	22	112	6	67	7	86	88
74	360.28	109.81	22	162	190	836	6	14	80	5	57	14	60	105
75	360.31	109.82	29	200	243	946	9	17	106	4	50	7	53	133
76	360.35	109.83	44	283	389	4200	37	27	196	3	98	22	64	320
77	360.38	109.84	39	259	330	2955	33	29	174	4	82	11	63	296
78	360.41	109.85	38	251	360	3672	40	33	200	4	104	9	64	325
79	360.45	109.86	38	201	285	1477	31	42	196	4	103	10	78	151
80	360.48	109.87	44	201	270	954	36	53	223	4	125	28	79	142
81	360.51	109.88	68	211	202	661	43	125	552	0	101	32	66	234
82	360.54	109.89	26	161	158	636	12	22	114	5	176	144	84	43
83	360.58	109.90	31	183	179	611	15	29	157	5	110	69	97	55
84	360.61	109.91	25	151	157	605	10	24	142	7	74	6	99	43
85	360.64	109.92	24	152	150	590	11	24	138	6	113	72	92	42
86	360.68	109.93	31	152	149	405	19	35	169	7	79	4	106	58

APPENDIX F

DUPLICATE XRF MEASUREMENTS TRACE ELEMENTS

Marks from top of core (cm)	Depth (m)	Mo Original (ppm)	Mo Rescan (ppm)	Mo Ratio O/R	Cu Original (ppm)	Cu Rescan (ppm)	Cu Ratio O/R	Ni Original (ppm)	Ni Rescan (ppm)	Ni Ratio O/R	Zn Original (ppm)	Zn Rescan (ppm)	Zn Ratio O/R	Co Original (ppm)	Co Rescan (ppm)	Co Ratio O/R
Core C7003																
60	141.71	15	13	1.15	95	109	0.87	81	83	0.98	207	271	0.76	19	20	0.95
61	141.72	15	14	1.07	98	102	0.96	80	89	0.90	231	216	1.07	19	21	0.90
62	141.73	16	14	1.14	93	94	0.99	84	78	1.08	236	194	1.22	20	19	1.05
63	141.74	14	17	0.82	102	98	1.04	84	86	0.98	228	240	0.95	19	20	0.95
64	141.75	17	13	1.31	85	99	0.86	71	83	0.86	216	222	0.97	16	19	0.84
65	141.76	21	16	1.31	96	100	0.96	84	73	1.15	252	211	1.19	20	17	1.18
90	142.01	252	95	2.65	276	231	1.19	220	137	1.61	2527	882	2.87	37	21	1.76
91	142.02	369	305	1.21	342	298	1.15	248	230	1.08	3474	3064	1.13	36	33	1.09
92	142.03	407	386	1.05	376	352	1.07	264	251	1.05	4072	3812	1.07	39	35	1.11
93	142.04	384	339	1.13	319	309	1.03	254	252	1.01	3904	3110	1.26	35	36	0.97
94	142.05	383	405	0.95	326	341	0.96	242	258	0.94	3708	3887	0.95	34	35	0.97
95	142.06	262	415	0.63	278	370	0.75	224	272	0.82	2030	3450	0.59	36	41	0.88
Core C7005																
25	152.72	74	120	0.62	143	281	0.51	136	277	0.49	314	583	0.54	28	56	0.50
26	152.73	88	116	0.76	119	271	0.44	115	263	0.44	245	894	0.27	27	51	0.53
27	152.74	63	93	0.68	191	260	0.73	168	263	0.64	619	1039	0.60	30	50	0.60
28	152.75	72	63	1.14	237	231	1.03	204	230	0.89	688	672	1.02	36	43	0.84
29	152.76	90	66	1.36	280	237	1.18	254	226	1.12	797	760	1.05	42	43	0.98
30	152.77	128	69	1.86	286	235	1.22	288	224	1.29	650	634	1.03	59	44	1.34
130	153.77	9	6	1.50	76	73	1.04	34	31	1.10	46	70	0.66	10	10	1.00
131	153.78	9	9	1.00	89	85	1.05	41	42	0.98	53	52	1.02	14	14	1.00

Marks from top of core (cm)	Depth (m)	Mo Original (ppm)	Mo Rescan (ppm)	Mo Ratio O/R	Cu Original (ppm)	Cu Rescan (ppm)	Cu Ratio O/R	Ni Original (ppm)	Ni Rescan (ppm)	Ni Ratio O/R	Zn Original (ppm)	Zn Rescan (ppm)	Zn Ratio O/R	Co Original (ppm)	Co Rescan (ppm)	Co Ratio O/R
132	153.79	8	9	0.89	90	87	1.03	37	38	0.97	43	48	0.90	10	10	1.00
133	153.80	6	12	0.50	83	97	0.86	32	32	1.00	46	49	0.94	7	3	2.33
134	153.81	8	8	1.00	86	100	0.86	35	35	1.00	50	51	0.98	7	7	1.00
135	153.82	7	10	0.70	89	97	0.92	43	28	1.54	47	44	1.07	8	3	2.67
Core C7009																
30	109.37	25	27	0.93	114	110	1.04	84	80	1.05	223	294	0.76	23	21	1.10
31	109.38	26	23	1.13	112	114	0.98	77	77	1.00	204	207	0.99	19	19	1.00
32	109.39	19	21	0.90	100	103	0.97	80	81	0.99	217	218	1.00	21	22	0.95
33	109.40	19	18	1.06	115	114	1.01	88	92	0.96	253	242	1.05	23	24	0.96
34	109.41	21	26	0.81	112	118	0.95	92	75	1.23	224	228	0.98	23	19	1.21
35	109.42	19	18	1.06	116	115	1.01	88	87	1.01	233	217	1.07	23	23	1.00
76	109.83	320	219	1.46	389	321	1.21	283	256	1.11	4200	1637	2.57	44	41	1.07
77	109.84	296	291	1.02	330	332	0.99	259	264	0.98	2955	2694	1.10	39	40	0.98
78	109.85	325	321	1.01	360	347	1.04	251	253	0.99	3672	3655	1.00	38	39	0.97
79	109.86	151	150	1.01	285	268	1.06	201	197	1.02	1477	1527	0.97	38	35	1.09
80	109.87	142	113	1.26	270	259	1.04	201	197	1.02	954	1057	0.90	44	40	1.10
Average Deviation from 1:1 Ratio				0.25			0.11			0.13			0.23			0.21

APPENDIX G

XRF DATA FOR ALL MAJOR ELEMENTS

Marks from top of core (cm)	Depth (m below KB)	Depth (ft below KB)	Na (wt %)	Mg (wt %)	Al (wt %)	Si (wt %)	P (wt %)	S (wt %)	K (wt %)	Ca (wt %)	Ti (wt %)	V (ppm)	Cr (ppm)	Mn (ppm)	Fe (wt %)
C6848															
1	177.02	580.77	0.14	0.96	0.42	1.57	0.02	0.46	0.28	36.78	0.01	0	0	250	0.26
2	177.03	580.80	0.15	0.56	0.26	1.28	0.00	0.46	0.25	37.20	0.01	0	0	251	0.26
3	177.04	580.84	0.15	0.42	0.29	1.36	0.01	0.44	0.25	37.08	0.01	0	0	251	0.26
4	177.05	580.87	0.20	1.65	1.01	6.60	0.08	0.55	0.46	28.66	0.05	63	1	364	0.82
5	177.06	580.90	0.17	0.82	0.57	3.40	0.03	0.45	0.34	33.20	0.03	4	0	278	0.46
6	177.07	580.93	0.16	0.80	0.44	2.34	0.03	0.45	0.30	35.64	0.01	8	0	262	0.29
7	177.08	580.97	0.22	0.95	1.47	8.74	0.07	0.65	0.51	25.73	0.07	81	4	361	0.91
8	177.09	581.00	0.20	1.29	0.91	7.00	0.08	0.57	0.41	29.39	0.04	61	2	335	0.63
9	177.10	581.03	0.22	3.01	1.95	10.73	0.10	0.83	0.70	22.14	0.11	86	0	634	1.67
10	177.11	581.07	0.16	1.37	0.41	2.29	0.01	0.50	0.28	35.52	0.01	8	0	289	0.38
11	177.12	581.10	0.14	0.68	0.26	1.10	0.01	0.57	0.24	37.64	0.01	0	0	252	0.48
12	177.13	581.13	0.16	0.52	0.20	1.20	0.00	0.55	0.24	36.65	0.01	0	0	245	0.50
13	177.14	581.16	0.16	0.00	0.04	0.58	0.00	0.47	0.21	36.71	0.00	0	0	237	0.39
14	177.15	581.20	0.15	0.27	0.15	0.44	0.00	0.48	0.21	37.91	0.00	0	0	242	0.34
15	177.16	581.23	0.18	0.71	0.69	4.14	0.03	0.54	0.42	31.19	0.05	28	0	373	0.81
16	177.17	581.26	0.24	2.69	2.82	13.15	0.14	1.15	0.98	19.41	0.20	97	10	568	2.04
17	177.18	581.30	0.17	0.76	0.61	3.23	0.03	0.60	0.28	34.73	0.02	5	0	311	0.52
18	177.19	581.33	0.15	0.81	0.48	2.12	0.02	0.72	0.27	36.42	0.02	8	0	286	0.67
19	177.20	581.36	0.16	0.72	0.39	2.13	0.02	0.75	0.26	35.97	0.01	8	0	279	0.78
20	177.21	581.39	0.26	1.71	1.45	14.53	0.15	0.53	0.47	20.81	0.06	111	3	459	0.81
21	177.22	581.43	0.28	1.05	1.34	16.21	0.16	0.59	0.43	19.16	0.06	129	5	436	0.92
22	177.23	581.46	0.23	0.47	1.22	10.46	0.11	0.56	0.34	25.60	0.03	87	0	408	0.72

23	177.24	581.49	0.26	0.54	1.63	14.40	0.10	0.80	0.57	19.59	0.10	129	11	426	1.51
24	177.25	581.53	0.29	0.00	4.01	19.09	0.12	2.02	1.30	10.42	0.28	89	72	215	2.84
25	177.26	581.56	0.26	0.00	4.09	15.65	0.01	1.43	1.47	7.23	0.31	55	81	190	2.69
27	177.28	581.62	0.31	0.01	7.13	21.50	0.00	2.61	2.86	1.18	0.46	161	170	200	3.88
28	177.29	581.66	0.31	0.00	7.29	21.49	0.02	2.02	2.98	0.89	0.49	188	173	189	3.61
29	177.30	581.69	0.30	0.18	6.90	21.04	0.00	2.62	2.95	1.20	0.48	170	165	203	4.22
30	177.31	581.72	0.26	0.03	5.09	15.47	1.12	2.12	2.27	4.97	0.32	299	335	162	3.16
31	177.32	581.76	0.26	0.10	4.62	14.96	1.62	2.15	2.07	5.63	0.32	358	373	156	2.69
32	177.33	581.79	0.26	0.14	4.55	14.83	1.38	2.45	2.03	5.52	0.30	332	311	213	3.11
33	177.34	581.82	0.26	0.00	4.27	14.75	0.65	2.53	2.05	4.62	0.32	366	398	169	2.91
34	177.35	581.85	0.23	1.06	4.02	13.11	5.49	2.06	1.63	10.48	0.28	111	256	128	3.07
35	177.36	581.89	0.26	0.09	4.94	15.80	0.84	2.26	2.10	6.55	0.32	212	296	115	3.30
36	177.37	581.92	0.28	0.15	5.73	17.25	0.40	2.45	2.42	4.18	0.38	259	317	166	3.60
37	177.38	581.95	0.28	0.00	5.53	16.82	0.05	2.45	2.45	3.48	0.36	251	293	159	3.86
38	177.39	581.98	0.27	0.00	5.46	16.73	0.25	2.46	2.46	3.05	0.34	246	297	157	3.80
39	177.40	582.02	0.30	0.00	6.02	19.47	0.03	2.12	2.59	1.60	0.38	194	279	172	3.32
40	177.41	582.05	0.30	0.00	6.44	20.62	0.06	1.89	2.63	1.47	0.41	222	262	177	3.09
41	177.42	582.08	0.30	0.00	6.49	20.45	0.15	1.84	2.62	1.76	0.40	147	244	173	3.10
42	177.43	582.12	0.31	0.00	6.58	20.90	0.05	1.89	2.64	1.17	0.41	185	233	179	3.29
43	177.44	582.15	0.31	0.00	6.49	21.72	0.08	2.43	2.63	1.06	0.43	136	208	244	3.35
44	177.45	582.18	0.31	0.00	6.67	22.08	0.09	2.47	2.64	1.01	0.46	164	200	237	3.44
45	177.46	582.21	0.31	0.00	6.85	22.21	0.08	2.44	2.70	0.92	0.44	156	194	243	3.58
46	177.47	582.25	0.31	0.21	6.59	21.93	0.07	2.90	2.63	0.92	0.44	131	183	252	3.88
47	177.48	582.28	0.31	0.00	6.44	21.58	0.04	2.69	2.58	0.86	0.43	149	180	230	3.74
48	177.49	582.31	0.31	0.00	6.82	22.32	0.07	2.86	2.67	0.82	0.44	157	176	257	3.88
49	177.50	582.35	0.31	0.00	6.69	22.19	0.06	2.54	2.68	0.79	0.45	124	184	235	3.70
50	177.51	582.38	0.31	0.00	6.98	22.41	0.06	2.60	2.72	0.80	0.44	114	181	240	3.57
51	177.52	582.41	0.31	0.02	6.83	21.88	0.03	2.69	2.75	0.75	0.46	145	185	247	3.75
52	177.53	582.44	0.30	0.22	6.67	21.52	0.04	2.94	2.63	0.74	0.44	137	170	278	3.93

53	177.54	582.48	0.31	0.00	6.92	21.92	0.03	2.62	2.71	0.62	0.44	127	180	238	3.75
54	177.55	582.51	0.31	0.15	7.00	22.28	0.02	2.54	2.77	0.59	0.46	175	181	266	3.57
55	177.56	582.54	0.31	0.00	7.12	22.18	0.01	2.58	2.76	0.55	0.45	149	178	237	3.70
56	177.57	582.58	0.31	0.13	7.07	22.40	0.02	2.76	2.78	0.58	0.43	134	177	241	3.82
57	177.58	582.61	0.31	0.00	6.99	22.10	0.00	2.44	2.81	0.48	0.45	174	178	221	3.53
58	177.59	582.64	0.31	0.05	6.86	21.77	0.00	2.53	2.80	0.53	0.43	175	172	218	3.61
59	177.60	582.67	0.31	0.00	6.84	21.32	0.00	2.82	2.74	0.49	0.42	191	167	212	4.01
60	177.61	582.71	0.31	0.00	6.98	21.65	0.00	2.69	2.87	0.53	0.44	256	162	237	3.78
61	177.62	582.74	0.31	0.00	6.76	21.42	0.00	2.73	2.80	0.39	0.42	277	152	206	3.96
62	177.63	582.77	0.30	0.00	6.73	21.31	0.00	3.24	2.80	0.41	0.42	394	159	216	4.53
63	177.64	582.81	0.30	0.14	6.85	21.59	0.00	3.19	2.74	0.48	0.42	375	166	199	4.28
64	177.65	582.84	0.31	0.00	6.56	20.81	0.00	2.60	2.73	0.47	0.41	344	178	217	3.71
65	177.66	582.87	0.31	0.00	6.96	21.67	0.00	2.87	2.83	0.54	0.44	413	195	194	3.85
66	177.67	582.90	0.31	0.00	6.80	21.48	0.00	2.81	2.74	0.37	0.44	499	215	189	4.05
67	177.68	582.94	0.30	0.00	7.05	21.02	0.00	3.20	2.74	0.37	0.41	458	225	200	4.48
68	177.69	582.97	0.28	0.00	5.05	17.45	0.33	2.75	2.05	2.40	0.33	554	323	160	3.43
69	177.70	583.00	0.25	0.06	4.00	13.47	2.49	2.13	1.48	7.63	0.26	572	322	111	2.77
70	177.71	583.03	0.27	0.00	4.97	15.86	0.00	3.34	1.85	0.64	0.30	1025	430	199	3.63
71	177.72	583.07	0.25	0.00	4.20	13.87	0.95	2.57	1.72	4.56	0.25	1096	436	102	2.76
72	177.73	583.10	0.26	0.00	4.50	14.55	0.06	2.91	1.91	2.50	0.26	1377	456	135	2.95
73	177.74	583.13	0.26	0.00	4.34	13.95	0.57	2.79	1.90	4.08	0.28	1387	415	128	3.12
74	177.75	583.17	0.27	0.00	4.79	15.20	0.00	3.42	2.12	1.72	0.30	1773	433	148	3.54
75	177.76	583.20	0.26	0.00	4.81	15.42	0.00	3.77	2.13	2.47	0.34	1530	352	167	4.23
76	177.77	583.23	0.26	0.00	5.09	15.75	0.40	3.08	2.13	3.96	0.36	967	305	142	4.36
77	177.78	583.26	0.28	0.23	6.04	17.79	0.00	2.82	2.42	2.33	0.39	778	316	151	4.26
78	177.79	583.30	0.28	0.00	6.05	18.18	0.00	2.60	2.51	2.29	0.40	669	284	168	4.14
79	177.80	583.33	0.28	0.14	5.85	17.61	0.10	2.76	2.46	3.31	0.39	543	243	178	4.15
80	177.81	583.36	0.28	0.06	5.89	18.40	0.00	3.29	2.50	1.89	0.41	673	247	177	4.73
81	177.82	583.40	0.29	0.00	6.10	19.48	0.00	2.48	2.65	1.17	0.41	641	258	225	3.82

82	177.83	583.43	0.32	0.00	6.79	22.74	0.04	2.03	2.74	0.69	0.45	416	241	222	3.09
83	177.84	583.46	0.31	0.00	6.52	22.04	0.02	2.12	2.63	0.68	0.43	349	211	239	3.20
84	177.85	583.49	0.31	0.00	7.03	22.67	0.00	2.28	2.78	0.45	0.44	369	205	249	3.49
85	177.86	583.53	0.31	0.00	6.63	22.18	0.00	2.35	2.64	0.61	0.44	338	184	269	3.31
86	177.87	583.56	0.31	0.00	6.95	22.70	0.03	2.27	2.76	0.67	0.45	336	192	212	3.48
87	177.88	583.59	0.31	0.00	6.70	22.19	0.01	2.44	2.71	0.57	0.45	391	184	240	3.41
88	177.89	583.63	0.32	0.00	7.19	22.50	0.00	2.39	2.79	0.40	0.46	429	190	186	3.51
89	177.90	583.66	0.31	0.00	6.62	21.82	0.00	2.44	2.72	0.39	0.45	467	186	200	3.44
90	177.91	583.69	0.31	0.00	6.72	21.78	0.00	2.44	2.73	0.39	0.46	480	187	203	3.47
91	177.92	583.72	0.31	0.00	6.89	21.84	0.00	2.42	2.74	0.36	0.44	515	184	184	3.60
92	177.93	583.76	0.30	0.08	6.60	21.75	0.00	3.20	2.74	0.32	0.45	801	172	171	4.21
93	177.94	583.79	0.31	0.00	6.94	22.01	0.00	2.89	2.83	0.31	0.45	818	159	183	4.36
94	177.95	583.82	0.31	0.00	6.62	21.67	0.00	2.81	2.76	0.28	0.45	892	160	172	4.15
95	177.96	583.85	0.30	0.15	6.62	21.47	0.00	2.85	2.76	0.33	0.45	967	163	167	4.29
96	177.97	583.89	0.31	0.00	7.13	22.37	0.00	2.79	2.81	0.30	0.46	938	164	157	4.07
97	177.98	583.92	0.30	0.03	6.84	21.91	0.00	3.37	2.76	0.32	0.46	1107	160	175	4.51
98	177.99	583.95	0.31	0.00	7.06	22.22	0.00	2.62	2.90	0.30	0.47	1313	192	146	3.89
99	178.00	583.99	0.31	0.00	6.70	21.56	0.00	2.57	2.85	0.34	0.47	1501	216	134	3.88
100	178.01	584.02	0.30	0.00	6.59	20.49	0.00	2.34	2.87	0.31	0.45	1722	289	122	3.76
101	178.02	584.05	0.29	0.00	5.19	18.01	0.00	2.90	2.15	0.55	0.39	1943	310	167	3.50
102	178.03	584.08	0.26	0.00	3.96	13.63	0.00	3.22	1.64	1.21	0.31	3044	413	122	3.52
103	178.04	584.12	0.24	0.00	3.40	12.30	0.09	4.14	1.88	2.42	0.31	3291	350	172	4.63
104	178.05	584.15	0.24	0.00	3.85	12.54	0.04	3.98	2.10	3.15	0.33	3483	350	140	4.70
105	178.06	584.18	0.24	0.00	3.86	12.78	0.07	3.90	2.10	4.16	0.33	3282	318	156	4.50
106	178.07	584.22	0.24	0.00	3.78	13.16	0.00	4.06	2.11	3.93	0.33	3201	338	94	4.50
107	178.08	584.25	0.25	0.00	4.02	13.37	0.00	4.21	2.12	4.34	0.35	2915	316	111	4.53
108	178.09	584.28	0.25	0.00	4.02	14.44	0.00	3.81	2.10	4.27	0.31	2887	308	126	4.25
109	178.10	584.31	0.26	0.00	4.18	14.84	0.00	3.55	2.11	4.05	0.34	2438	324	124	4.49
110	178.11	584.35	0.26	0.00	4.31	14.91	0.01	3.66	2.20	4.20	0.36	2305	308	160	4.66

111	178.12	584.38	0.15	0.80	0.46	2.67	0.02	2.02	0.31	32.61	0.03	149	0	759	2.00
112	178.13	584.41	0.19	0.38	0.81	5.33	0.05	0.84	0.38	30.59	0.04	198	0	824	0.68
113	178.14	584.45	0.18	0.72	0.79	5.09	0.05	0.93	0.38	31.08	0.03	185	0	833	0.73
114	178.15	584.48	0.19	0.37	0.79	4.96	0.06	1.10	0.38	29.97	0.04	170	0	740	0.86
115	178.16	584.51	0.16	0.66	0.57	3.15	0.10	1.03	0.32	32.67	0.02	123	0	715	0.96
116	178.17	584.54	0.15	0.82	0.62	3.08	0.09	2.03	0.30	31.63	0.03	123	0	695	2.10
117	178.18	584.58	0.27	0.18	5.20	16.17	0.08	2.39	2.59	3.63	0.39	1536	338	207	3.64
118	178.19	584.61	0.26	0.20	4.84	15.09	0.52	2.32	2.40	4.85	0.39	1405	328	186	3.53
119	178.20	584.64	0.27	0.00	5.19	16.11	0.00	2.78	2.58	2.30	0.39	1658	350	209	3.70
120	178.21	584.68	0.26	0.00	4.26	14.65	1.51	2.19	1.95	5.90	0.34	1257	307	143	2.92
121	178.22	584.71	0.28	0.00	5.13	17.09	0.01	2.90	2.33	1.18	0.40	1512	345	163	3.76
122	178.23	584.74	0.29	0.00	6.00	19.29	0.00	2.61	2.65	0.56	0.43	1558	349	150	3.62
123	178.24	584.77	0.30	0.07	6.75	20.80	0.00	2.74	2.90	0.48	0.44	1572	334	124	3.83
124	178.25	584.81	0.30	0.00	6.53	20.67	0.03	2.62	2.88	1.05	0.43	1492	322	144	3.64
125	178.26	584.84	0.30	0.00	6.44	20.27	0.12	2.66	2.90	1.25	0.44	1556	360	126	3.77
C7003															
1	141.12	462.99	0.18	1.56	1.03	5.33	0.07	0.59	0.41	31.04	0.04	49	0	309	0.74
2	141.13	463.02	0.18	1.84	0.99	5.59	0.06	0.76	0.40	29.96	0.04	77	0	402	1.15
3	141.14	463.06	0.16	0.82	0.48	2.14	0.02	0.56	0.28	35.87	0.02	0	0	234	0.44
4	141.15	463.09	0.15	0.95	0.46	1.70	0.02	0.60	0.26	36.68	0.02	0	0	243	0.48
5	141.16	463.12	0.15	0.85	0.59	2.05	0.03	0.68	0.29	36.25	0.02	0	0	241	0.56
6	141.17	463.16	0.16	0.83	0.67	2.29	0.02	0.72	0.29	35.58	0.01	11	0	246	0.69
7	141.18	463.19	0.16	0.98	0.57	2.56	0.02	0.70	0.28	35.59	0.02	12	0	269	0.70
8	141.19	463.22	0.18	1.02	0.86	4.65	0.04	0.81	0.32	32.08	0.03	35	0	321	1.04
9	141.20	463.25	0.24	3.23	2.98	13.48	0.10	0.98	1.03	18.22	0.19	93	0	753	2.25
10	141.21	463.29	0.27	1.63	4.11	16.67	0.13	1.66	1.33	13.80	0.29	64	42	348	2.97
11	141.22	463.32	0.32	0.39	7.27	23.50	0.02	1.71	2.51	3.29	0.47	83	116	228	3.00
12	141.23	463.35	0.31	0.08	7.04	22.09	0.01	1.77	2.45	3.53	0.48	75	115	239	3.39
13	141.24	463.38	0.31	0.41	7.29	22.83	0.02	2.29	2.65	2.52	0.46	92	122	244	4.24

14	141.25	463.42	0.31	0.34	7.32	22.57	0.04	2.26	2.66	2.64	0.48	97	130	217	4.17
15	141.26	463.45	0.31	0.48	7.53	22.77	0.02	1.93	2.73	2.18	0.48	87	132	229	3.87
16	141.27	463.48	0.31	0.54	7.45	22.61	0.03	1.86	2.80	2.17	0.49	115	142	236	3.69
17	141.28	463.52	0.30	0.21	7.40	21.66	0.06	2.71	2.73	1.83	0.46	138	141	250	4.23
18	141.29	463.55	0.31	0.73	8.22	22.91	0.03	2.21	2.82	1.39	0.47	115	152	256	4.11
19	141.30	463.58	0.30	0.31	7.45	21.24	0.02	2.71	2.80	0.95	0.46	153	159	194	4.41
20	141.31	463.61	0.32	0.52	7.03	22.89	0.03	2.11	2.54	3.25	0.48	102	121	243	3.65
21	141.32	463.65	0.30	0.27	7.10	20.75	0.00	3.05	2.88	1.27	0.49	201	168	249	4.24
22	141.33	463.68	0.30	0.53	7.58	21.82	0.00	2.73	2.97	0.84	0.48	204	166	286	4.19
23	141.34	463.71	0.30	0.00	7.29	21.18	0.00	2.49	2.95	0.81	0.46	161	169	235	3.99
24	141.35	463.75	0.32	0.15	7.74	23.03	0.00	2.12	2.90	0.58	0.47	156	168	259	3.39
25	141.36	463.78	0.31	0.16	7.43	22.32	0.00	2.20	2.96	0.60	0.47	198	190	248	3.71
26	141.37	463.81	0.31	0.42	7.76	22.11	0.00	2.38	2.98	0.48	0.45	220	178	240	3.63
27	141.38	463.84	0.28	0.52	6.83	19.65	0.00	4.54	2.64	0.44	0.44	284	164	263	6.65
28	141.39	463.88	0.31	0.23	7.53	21.63	0.00	2.44	2.96	0.48	0.47	332	207	240	3.84
29	141.40	463.91	0.30	0.07	7.45	21.35	0.00	2.19	3.03	0.33	0.45	302	240	211	3.73
30	141.41	463.94	0.29	0.00	6.38	19.36	0.00	2.68	2.61	0.46	0.41	313	239	234	4.07
31	141.42	463.98	0.23	1.64	3.90	13.50	5.68	2.29	1.68	10.51	0.31	120	194	139	3.27
32	141.43	464.01	0.25	0.79	4.62	14.79	2.12	2.21	2.03	6.77	0.33	206	259	181	3.38
33	141.44	464.04	0.23	1.00	3.76	12.98	4.67	2.10	1.75	10.13	0.29	158	261	159	2.98
34	141.45	464.07	0.22	1.30	3.71	12.52	6.59	1.83	1.47	11.77	0.26	116	265	128	2.65
35	141.46	464.11	0.22	1.53	3.49	12.79	5.86	2.06	1.62	10.84	0.29	141	282	138	2.93
36	141.47	464.14	0.25	0.62	4.59	14.91	1.47	2.29	2.03	6.43	0.32	150	282	163	3.47
37	141.48	464.17	0.26	0.37	4.76	15.72	1.60	2.43	2.16	5.52	0.36	206	291	181	3.92
38	141.49	464.21	0.27	0.26	5.75	17.28	0.60	2.32	2.43	3.81	0.38	193	307	193	3.89
39	141.50	464.24	0.27	0.61	5.25	16.52	1.18	2.25	2.20	5.17	0.33	133	274	165	3.72
40	141.51	464.27	0.28	0.29	6.05	18.50	0.08	2.56	2.53	2.59	0.39	220	292	192	4.07
41	141.52	464.30	0.28	0.47	6.05	18.27	0.48	2.27	2.47	3.73	0.37	199	263	194	3.83
42	141.53	464.34	0.27	0.57	5.67	17.50	0.56	2.33	2.48	3.73	0.39	191	258	206	4.12

43	141.54	464.37	0.28	0.08	5.59	17.71	0.46	2.20	2.41	3.92	0.36	193	241	194	3.59
44	141.55	464.40	0.29	0.00	5.99	18.86	0.21	2.45	2.40	2.84	0.37	213	242	190	3.45
45	141.56	464.43	0.31	0.00	6.57	21.40	0.10	1.88	2.61	1.51	0.42	146	236	210	3.30
46	141.57	464.47	0.31	0.00	6.65	21.52	0.06	1.99	2.66	1.29	0.42	131	236	204	3.35
47	141.58	464.50	0.31	0.00	6.85	22.07	0.09	1.75	2.60	1.42	0.44	147	223	203	3.14
48	141.59	464.53	0.31	0.04	7.04	21.95	0.07	2.01	2.65	1.19	0.41	107	211	240	3.36
49	141.60	464.57	0.31	0.29	6.80	21.99	0.05	2.29	2.60	0.99	0.43	127	207	229	3.58
50	141.61	464.60	0.32	0.10	6.96	23.39	0.08	2.35	2.62	0.81	0.49	140	188	291	3.60
51	141.62	464.63	0.32	0.43	7.05	23.72	0.07	2.28	2.63	0.75	0.49	150	189	248	3.72
52	141.63	464.66	0.32	0.37	7.08	23.49	0.06	2.22	2.66	0.84	0.46	114	187	237	3.47
53	141.64	464.70	0.32	0.35	6.90	23.58	0.06	2.50	2.62	0.75	0.46	126	176	233	3.91
54	141.65	464.73	0.32	0.07	6.93	23.21	0.06	2.48	2.57	0.84	0.46	117	170	231	3.81
55	141.66	464.76	0.32	0.31	6.93	23.17	0.05	2.57	2.56	0.81	0.46	114	164	247	3.86
56	141.67	464.80	0.32	0.33	7.23	23.58	0.05	2.65	2.63	0.81	0.45	104	174	236	3.92
57	141.68	464.83	0.32	0.28	7.17	23.27	0.04	2.55	2.68	0.76	0.48	126	172	270	3.79
58	141.69	464.86	0.31	0.21	6.77	22.65	0.04	2.94	2.64	0.91	0.46	115	173	226	4.07
59	141.70	464.89	0.32	0.14	7.15	23.01	0.02	2.19	2.66	0.69	0.46	146	177	233	3.67
60	141.71	464.93	0.31	0.37	7.19	22.86	0.02	2.44	2.63	0.66	0.46	112	170	262	3.97
61	141.72	464.96	0.32	0.04	7.13	23.13	0.01	2.30	2.71	0.64	0.47	114	175	246	3.69
62	141.73	464.99	0.31	0.07	7.19	22.74	0.00	2.18	2.74	0.66	0.47	145	177	229	3.59
63	141.74	465.03	0.32	0.29	7.35	23.27	0.01	2.33	2.72	0.58	0.46	144	168	245	3.69
64	141.75	465.06	0.31	0.10	7.12	22.01	0.00	2.24	2.76	0.60	0.46	162	174	230	3.64
65	141.76	465.09	0.31	0.00	7.39	22.26	0.00	2.28	2.78	0.55	0.45	152	177	207	3.78
66	141.77	465.12	0.31	0.55	7.51	22.84	0.00	2.72	2.83	0.57	0.47	209	169	240	3.80
67	141.78	465.16	0.31	0.07	7.43	22.44	0.00	2.33	2.82	0.45	0.47	240	169	207	3.93
68	141.79	465.19	0.31	0.32	7.19	22.39	0.00	2.75	2.85	0.45	0.46	285	163	238	4.00
69	141.80	465.22	0.31	0.22	7.30	22.52	0.00	2.77	2.84	0.42	0.46	320	167	197	4.25
70	141.81	465.25	0.30	0.53	6.83	21.97	0.00	3.09	2.76	0.50	0.45	323	161	267	4.19
71	141.82	465.29	0.31	0.06	7.16	22.44	0.00	2.75	2.83	0.37	0.44	326	188	203	4.11

72	141.83	465.32	0.31	0.00	7.26	22.30	0.00	2.59	2.86	0.40	0.44	437	229	199	4.11
73	141.84	465.35	0.30	0.27	6.93	20.99	0.00	2.91	2.68	0.36	0.41	380	229	195	4.50
74	141.85	465.39	0.29	0.00	5.99	19.29	0.00	3.11	2.21	0.41	0.36	451	289	201	4.13
75	141.86	465.42	0.25	0.02	4.44	15.55	0.67	3.34	1.56	4.03	0.29	575	336	162	3.99
76	141.87	465.45	0.24	0.13	3.77	13.26	2.19	2.85	1.41	6.12	0.25	573	365	149	3.48
77	141.88	465.48	0.25	0.06	4.05	13.92	0.71	2.87	1.70	4.88	0.27	712	379	142	3.30
78	141.89	465.52	0.26	0.00	4.57	14.99	0.12	3.15	2.01	2.19	0.30	785	411	186	3.60
79	141.90	465.55	0.25	0.00	4.25	13.72	0.00	3.47	1.96	1.89	0.33	938	389	211	4.22
80	141.91	465.58	0.26	0.00	5.32	15.56	0.00	3.72	2.09	2.16	0.35	838	341	202	4.59
81	141.92	465.62	0.26	0.29	5.28	15.86	0.00	3.76	2.15	2.22	0.36	843	332	212	4.62
82	141.93	465.65	0.26	0.51	5.24	16.18	1.04	2.70	2.08	5.87	0.35	402	264	150	4.31
83	141.94	465.68	0.28	0.24	5.96	17.90	0.08	2.88	2.42	2.82	0.38	446	284	193	4.59
84	141.95	465.71	0.28	0.00	6.24	18.35	0.00	2.54	2.47	2.38	0.42	385	275	179	4.28
85	141.96	465.75	0.28	0.20	6.15	18.48	0.00	2.62	2.52	2.38	0.42	366	243	222	4.33
86	141.97	465.78	0.24	1.15	4.89	14.87	3.83	2.03	1.86	8.89	0.33	216	189	178	3.56
87	141.98	465.81	0.29	0.47	6.55	19.61	0.02	2.69	2.64	2.56	0.42	366	226	222	4.50
88	141.99	465.85	0.24	0.14	3.61	13.62	0.00	4.71	1.72	1.67	0.33	2395	319	260	5.17
89	142.00	465.88	0.26	0.00	4.10	15.92	0.07	3.64	1.63	1.40	0.33	1818	287	235	4.00
90	142.01	465.91	0.28	0.00	4.83	18.08	0.02	3.36	1.94	0.71	0.38	1561	311	203	4.00
91	142.02	465.94	0.26	0.00	3.54	15.20	0.00	3.86	1.83	3.92	0.28	2443	295	171	3.93
92	142.03	465.98	0.25	0.00	3.44	14.35	0.00	4.22	1.82	3.95	0.29	2737	294	178	4.19
93	142.04	466.01	0.24	0.04	3.38	14.12	0.00	4.10	1.81	3.56	0.28	2920	290	185	4.22
94	142.05	466.04	0.24	0.00	3.21	13.36	0.00	4.19	1.76	3.42	0.27	3135	291	186	4.18
95	142.06	466.08	0.24	0.00	3.24	13.09	0.00	4.53	1.71	3.22	0.29	3284	280	202	4.56
96	142.07	466.11	0.24	0.00	3.29	12.77	0.00	4.58	1.80	2.72	0.30	3409	304	212	4.70
97	142.08	466.14	0.24	0.00	3.64	13.40	0.00	4.58	1.86	2.46	0.30	3105	324	213	4.82
98	142.09	466.17	0.27	0.07	3.95	17.26	0.03	3.55	1.84	3.95	0.30	1850	287	173	4.08
99	142.10	466.21	0.27	0.10	3.80	16.43	0.44	2.49	1.80	6.02	0.28	1411	265	202	3.55
100	142.11	466.24	0.25	0.02	3.25	14.02	1.12	1.84	1.60	8.84	0.25	1021	216	246	2.91

101	142.12	466.27	0.27	0.23	4.10	16.67	0.53	2.15	1.83	7.80	0.29	1070	232	280	3.10
C7005															
1	152.48	500.25	0.25	0.79	3.75	13.32	0.23	2.06	1.30	17.92	0.23	69	0	978	2.93
2	152.49	500.28	0.21	1.05	2.53	9.20	0.16	1.94	0.86	23.62	0.15	69	0	915	2.75
3	152.50	500.32	0.17	0.97	1.27	4.85	0.10	1.47	0.46	30.78	0.07	40	0	707	1.94
4	152.51	500.35	0.18	1.18	1.53	5.72	0.14	1.60	0.53	29.26	0.09	66	0	745	2.38
5	152.52	500.38	0.24	0.86	3.64	12.53	0.46	2.02	1.31	17.61	0.25	145	24	600	3.19
6	152.53	500.41	0.24	0.93	4.05	12.71	0.10	1.81	1.34	17.67	0.24	149	28	603	3.17
7	152.54	500.45	0.23	0.85	3.50	12.07	1.54	1.91	1.36	16.25	0.26	195	50	539	3.19
8	152.55	500.48	0.17	2.74	1.88	8.28	13.68	1.31	0.92	21.16	0.18	74	69	284	2.09
9	152.56	500.51	0.25	0.10	4.25	14.19	0.14	3.41	2.03	5.89	0.37	565	154	451	4.66
10	152.57	500.55	0.30	0.30	6.82	21.77	0.00	3.06	2.93	0.69	0.46	1131	205	227	4.32
11	152.58	500.58	0.30	0.00	6.64	20.95	0.00	2.61	2.87	0.61	0.43	1267	233	177	3.99
12	152.59	500.61	0.30	0.00	6.66	20.77	0.00	2.24	2.84	0.54	0.42	1401	305	211	3.74
13	152.60	500.64	0.23	0.00	3.26	12.01	0.00	4.33	1.76	2.35	0.33	1891	305	290	5.32
14	152.61	500.68	0.24	0.00	3.34	11.53	0.00	3.94	1.91	4.18	0.31	2134	274	267	4.48
15	152.62	500.71	0.24	0.00	3.84	12.67	0.00	3.69	2.05	5.22	0.30	1992	268	266	4.05
16	152.63	500.74	0.25	0.07	4.35	14.10	0.04	3.10	2.19	5.98	0.32	1590	271	259	3.90
17	152.64	500.77	0.26	0.21	4.94	15.33	0.50	2.34	2.33	5.75	0.36	1285	270	281	3.60
18	152.65	500.81	0.26	0.40	5.08	15.42	0.36	2.23	2.50	4.08	0.37	1197	285	286	3.57
19	152.66	500.84	0.26	0.18	4.85	15.44	0.47	2.40	2.37	3.89	0.35	1056	284	269	3.62
20	152.67	500.87	0.28	0.00	5.31	17.50	0.91	2.03	2.29	3.63	0.37	1035	306	165	3.27
21	152.68	500.91	0.29	0.71	6.37	19.88	0.72	2.10	2.72	2.96	0.40	1116	319	126	3.62
22	152.69	500.94	0.28	0.05	5.13	17.49	0.67	2.24	2.31	3.21	0.38	1019	367	151	3.49
23	152.70	500.97	0.26	0.03	4.12	15.54	0.59	2.98	1.97	2.95	0.37	1154	381	202	3.95
24	152.71	501.00	0.24	0.00	3.16	12.87	0.87	3.04	1.67	4.82	0.32	1113	355	264	3.87
25	152.72	501.04	0.24	0.00	3.90	13.53	0.00	3.88	2.19	2.23	0.32	1500	416	299	4.65
26	152.73	501.07	0.25	0.00	3.86	13.22	0.18	2.96	2.14	3.97	0.30	1388	403	260	4.04
27	152.74	501.10	0.26	0.00	4.62	14.63	0.01	3.21	2.33	3.20	0.33	1413	413	321	4.28

28	152.75	501.14	0.25	0.31	4.35	14.02	0.52	2.66	2.24	5.34	0.34	1148	401	249	3.65
29	152.76	501.17	0.26	0.00	4.27	14.15	0.02	2.86	2.36	2.74	0.32	1235	426	305	3.87
30	152.77	501.20	0.25	0.00	4.02	13.54	0.46	2.96	2.08	5.09	0.31	1078	383	271	4.03
31	152.78	501.23	0.26	0.00	4.82	15.29	0.00	3.12	2.42	2.30	0.33	1181	434	278	4.11
32	152.79	501.27	0.26	0.00	4.59	14.56	0.00	3.13	2.25	1.72	0.31	1309	455	225	4.03
33	152.80	501.30	0.25	0.00	4.39	14.43	0.00	3.47	2.05	1.76	0.37	1488	485	244	4.18
34	152.81	501.33	0.25	0.00	4.12	14.26	0.00	3.75	1.98	1.52	0.33	1321	459	260	4.37
35	152.82	501.37	0.25	0.00	3.86	13.23	0.01	3.63	1.80	1.94	0.41	2354	535	225	3.45
36	152.83	501.40	0.26	0.00	4.86	15.84	0.27	2.78	2.05	3.75	0.33	995	367	248	3.80
37	152.84	501.43	0.27	0.00	4.89	16.12	0.00	2.83	2.15	1.86	0.35	1150	390	258	3.68
38	152.85	501.46	0.28	0.00	5.31	16.88	0.00	2.99	2.22	1.79	0.36	913	351	238	4.06
39	152.86	501.50	0.28	0.00	5.50	17.17	0.00	2.71	2.34	1.48	0.39	775	351	216	3.86
40	152.87	501.53	0.29	0.00	6.54	19.11	0.00	2.65	2.50	1.10	0.47	723	346	209	3.76
41	152.88	501.56	0.29	0.00	6.47	19.50	0.00	2.54	2.53	1.33	0.41	576	301	224	3.92
42	152.89	501.60	0.29	0.00	5.89	18.36	0.00	2.68	2.43	1.23	0.39	559	285	234	4.06
43	152.90	501.63	0.27	0.00	4.83	16.48	0.00	3.54	1.95	2.06	0.53	822	289	310	3.99
44	152.91	501.66	0.29	0.00	5.85	18.91	0.00	2.55	2.27	2.28	0.42	544	237	338	3.61
45	152.92	501.69	0.29	0.00	6.07	19.06	0.00	2.31	2.24	3.15	0.42	422	210	347	3.29
46	152.93	501.73	0.27	0.01	5.29	17.54	0.18	2.59	2.00	5.29	0.35	397	169	356	3.78
47	152.94	501.76	0.28	0.00	5.13	17.22	0.04	2.60	1.89	5.38	0.42	465	173	379	3.32
48	152.95	501.79	0.28	0.00	5.27	17.71	0.00	2.78	1.99	4.52	0.41	356	157	392	3.71
49	152.96	501.82	0.28	0.00	5.38	17.84	0.03	2.85	2.00	4.70	0.42	320	155	383	3.68
50	152.97	501.86	0.28	0.00	5.44	18.23	0.00	2.81	1.94	4.77	0.45	282	148	386	3.41
51	152.98	501.89	0.28	0.00	5.67	18.54	0.00	2.59	2.08	4.69	0.37	220	129	370	3.91
52	152.99	501.92	0.29	0.00	5.74	18.79	0.00	2.34	2.06	5.13	0.40	172	111	398	3.57
53	153.00	501.96	0.29	0.14	5.97	19.28	0.01	2.61	2.09	4.95	0.43	191	117	380	3.69
54	153.01	501.99	0.29	0.15	5.91	19.52	0.00	2.69	2.15	4.32	0.45	132	121	418	3.61
55	153.02	502.02	0.30	0.12	6.37	20.20	0.02	2.51	2.25	4.40	0.42	111	113	418	3.74
56	153.03	502.05	0.30	0.00	5.93	19.54	0.02	2.28	2.10	4.88	0.41	145	103	412	3.61

57	153.04	502.09	0.29	0.48	5.79	19.30	0.03	2.65	1.98	5.93	0.41	95	103	407	3.80
58	153.05	502.12	0.29	0.24	6.11	19.64	0.02	2.43	2.15	5.36	0.39	124	100	384	3.75
59	153.06	502.15	0.29	0.22	5.71	19.09	0.03	2.69	2.04	5.85	0.42	108	98	400	3.83
60	153.07	502.19	0.29	0.00	5.72	18.72	0.01	2.32	2.01	5.55	0.39	85	95	398	3.61
61	153.08	502.22	0.30	0.00	5.92	19.80	0.02	2.47	2.11	5.52	0.41	109	93	409	3.58
62	153.09	502.25	0.30	0.18	6.16	19.95	0.02	2.49	2.12	5.51	0.41	70	95	406	3.69
63	153.10	502.28	0.30	0.04	6.11	20.28	0.02	2.70	2.10	5.25	0.42	95	90	412	3.79
64	153.11	502.32	0.30	0.37	6.19	20.11	0.02	2.34	2.06	5.47	0.39	61	85	406	3.52
65	153.12	502.35	0.29	0.27	5.74	19.20	0.03	2.83	1.96	6.33	0.43	122	81	438	3.80
66	153.13	502.38	0.30	0.34	6.09	20.14	0.03	2.53	2.06	5.62	0.43	83	88	424	3.81
67	153.14	502.42	0.29	0.19	6.05	19.80	0.04	2.33	2.02	6.73	0.41	105	84	414	3.52
68	153.15	502.45	0.29	0.10	5.93	19.59	0.03	2.58	2.01	6.36	0.41	72	79	442	3.58
69	153.16	502.48	0.28	0.48	5.55	18.61	0.03	2.72	1.89	7.17	0.36	42	79	429	3.94
70	153.17	502.51	0.28	0.15	5.46	18.45	0.03	2.81	1.81	7.08	0.47	111	81	459	3.92
71	153.18	502.55	0.28	0.29	5.64	18.99	0.04	2.97	1.90	7.15	0.39	74	73	434	4.02
72	153.19	502.58	0.30	0.24	6.08	20.29	0.03	2.44	2.11	5.37	0.41	54	88	410	3.50
73	153.20	502.61	0.29	0.43	6.06	20.35	0.06	2.75	2.00	6.47	0.43	71	82	433	3.75
74	153.21	502.65	0.29	0.28	5.78	19.33	0.04	2.50	1.84	7.53	0.41	74	68	434	3.63
75	153.22	502.68	0.29	0.61	5.85	20.18	0.04	2.83	1.93	6.16	0.44	46	77	448	3.80
76	153.23	502.71	0.29	0.15	5.82	19.66	0.03	2.71	1.93	6.29	0.42	65	78	410	3.88
77	153.24	502.74	0.30	0.29	5.92	20.37	0.01	2.92	1.97	5.05	0.42	52	81	419	3.94
78	153.25	502.78	0.29	0.18	5.61	19.90	0.02	3.31	1.89	4.84	0.42	75	79	414	4.30
79	153.26	502.81	0.29	0.35	5.44	19.45	0.01	3.60	1.89	4.37	0.45	69	85	431	4.71
80	153.27	502.84	0.28	0.11	5.56	19.37	0.01	4.11	1.90	3.77	0.43	74	89	403	4.85
81	153.28	502.87	0.28	0.28	5.52	19.45	0.02	4.31	1.92	3.61	0.45	99	86	456	5.47
82	153.29	502.91	0.27	0.02	5.24	18.36	0.00	4.15	1.89	3.10	0.43	86	88	450	5.13
83	153.30	502.94	0.28	0.36	5.54	19.24	0.00	4.36	2.02	2.48	0.45	89	84	525	5.46
84	153.31	502.97	0.29	0.13	5.82	19.77	0.00	3.86	2.08	1.99	0.47	120	88	522	4.88
85	153.32	503.01	0.28	0.09	5.72	19.37	0.00	3.96	2.04	1.98	0.45	56	84	555	4.65

86	153.33	503.04	0.29	0.00	5.89	20.00	0.00	4.27	2.10	1.71	0.46	101	89	504	4.88
87	153.34	503.07	0.28	0.05	5.50	19.28	0.00	4.67	1.98	1.96	0.44	101	89	491	5.49
88	153.35	503.10	0.27	0.17	5.28	18.51	0.00	5.11	1.97	2.05	0.44	110	86	527	5.32
89	153.36	503.14	0.28	0.18	5.52	19.60	0.00	4.69	2.04	1.59	0.45	123	102	384	5.41
90	153.37	503.17	0.28	0.15	5.58	19.69	0.00	5.05	2.09	1.57	0.47	137	103	445	5.22
91	153.38	503.20	0.27	0.30	5.23	18.48	0.00	5.16	1.99	1.52	0.47	144	107	428	5.27
92	153.39	503.24	0.28	0.05	5.48	19.09	0.00	5.28	2.01	1.51	0.44	114	98	443	5.76
93	153.40	503.27	0.28	0.08	5.62	19.29	0.00	4.79	2.14	1.08	0.46	120	105	421	5.25
94	153.41	503.30	0.28	0.14	5.69	19.48	0.00	5.33	2.13	1.22	0.44	103	104	384	5.67
95	153.42	503.33	0.28	0.05	5.58	19.08	0.00	5.00	2.12	1.08	0.46	138	97	435	5.59
96	153.43	503.37	0.28	0.23	5.65	19.56	0.00	5.33	2.17	1.09	0.46	91	96	434	5.77
97	153.44	503.40	0.28	0.70	5.84	19.73	0.00	5.34	2.17	1.03	0.45	75	95	453	5.80
98	153.45	503.43	0.28	0.28	6.00	20.24	0.00	5.50	2.22	0.95	0.49	76	100	478	5.90
99	153.46	503.47	0.28	0.34	5.77	19.10	0.00	4.74	2.21	1.02	0.45	99	86	506	5.14
100	153.47	503.50	0.28	0.13	5.78	19.58	0.00	5.11	2.23	1.18	0.47	113	88	511	5.17
101	153.48	503.53	0.29	0.15	6.46	20.77	0.00	4.39	2.39	0.91	0.44	110	79	552	4.86
102	153.49	503.56	0.28	0.21	6.18	19.53	0.00	4.44	2.38	0.97	0.43	31	73	665	4.65
103	153.50	503.60	0.28	0.45	6.30	20.23	0.00	5.03	2.37	0.82	0.46	57	79	639	4.98
104	153.51	503.63	0.28	0.08	6.20	19.45	0.00	4.43	2.38	0.92	0.45	40	87	552	4.48
105	153.52	503.66	0.28	0.17	6.37	19.82	0.00	4.83	2.29	0.96	0.46	109	82	560	4.82
106	153.53	503.69	0.29	0.00	6.16	20.04	0.00	4.54	2.37	1.10	0.44	67	80	590	4.53
107	153.54	503.73	0.29	0.22	6.16	20.10	0.00	4.56	2.33	0.93	0.44	87	79	561	4.80
108	153.55	503.76	0.29	0.09	6.49	20.73	0.00	4.22	2.48	0.88	0.45	35	81	602	4.26
109	153.56	503.79	0.29	0.00	6.40	20.40	0.00	3.88	2.46	0.91	0.46	69	76	582	4.18
110	153.57	503.83	0.29	0.00	6.59	20.16	0.00	3.96	2.49	0.86	0.46	71	76	599	4.29
111	153.58	503.86	0.29	0.00	6.36	20.16	0.00	4.08	2.44	0.89	0.43	29	72	639	4.25
112	153.59	503.89	0.29	0.00	6.39	19.81	0.00	3.85	2.45	1.22	0.45	47	81	556	4.11
113	153.60	503.92	0.12	1.91	1.17	3.86	0.02	5.11	0.38	26.78	0.09	89	0	1043	8.27
114	153.61	503.96	0.16	1.12	1.00	3.54	0.03	1.48	0.42	31.73	0.06	36	0	953	2.65

115	153.62	503.99	0.16	1.31	0.91	3.21	0.04	1.11	0.41	32.87	0.05	13	0	874	1.82
116	153.63	504.02	0.15	1.14	0.79	2.71	0.03	1.26	0.37	33.38	0.04	11	0	772	1.79
117	153.64	504.06	0.16	0.68	0.93	2.98	0.04	0.83	0.42	34.18	0.04	0	0	982	0.86
118	153.65	504.09	0.16	0.72	1.06	3.41	0.04	0.86	0.49	33.29	0.05	0	0	1151	0.89
119	153.66	504.12	0.17	0.71	0.88	3.20	0.04	1.06	0.42	33.32	0.04	0	0	1020	1.26
120	153.67	504.15	0.16	0.91	0.89	3.19	0.06	1.14	0.42	33.06	0.05	0	0	1010	1.40
121	153.68	504.19	0.16	0.84	0.87	2.93	0.04	1.23	0.40	33.52	0.04	0	0	1135	1.55
122	153.69	504.22	0.14	1.08	0.86	2.89	0.02	2.86	0.38	31.41	0.05	39	0	1041	3.78
123	153.70	504.25	0.14	1.00	1.02	2.97	0.02	3.24	0.39	30.94	0.06	44	0	854	4.33
124	153.71	504.29	0.23	0.29	3.15	10.85	0.07	2.08	1.20	19.30	0.22	60	17	472	2.57
125	153.72	504.32	0.27	0.00	4.97	16.39	0.00	3.91	2.05	2.17	0.43	114	87	434	4.28
126	153.73	504.35	0.27	0.08	5.56	17.70	0.00	5.00	2.16	1.76	0.42	112	93	456	4.81
127	153.74	504.38	0.27	0.00	5.50	17.66	0.00	4.80	2.08	1.59	0.39	116	92	442	4.87
128	153.75	504.42	0.27	0.07	5.56	18.25	0.00	4.87	2.20	0.98	0.41	144	98	411	4.71
129	153.76	504.45	0.27	0.00	5.30	17.27	0.00	5.09	2.09	0.97	0.40	126	95	441	4.76
130	153.77	504.48	0.27	0.00	5.47	17.94	0.00	5.17	2.13	0.86	0.41	140	101	380	5.19
131	153.78	504.52	0.27	0.04	5.34	17.72	0.00	5.28	2.09	0.76	0.41	138	96	427	5.28
132	153.79	504.55	0.26	0.01	5.21	16.87	0.00	5.32	2.03	0.79	0.40	146	101	387	5.56
133	153.80	504.58	0.26	0.00	4.98	16.26	0.00	5.49	1.99	0.67	0.39	152	101	388	5.69
134	153.81	504.61	0.25	0.61	4.82	16.57	0.00	6.50	1.94	0.77	0.40	158	87	508	5.93
135	153.82	504.65	0.25	0.14	4.67	15.88	0.00	6.02	1.87	0.59	0.40	154	99	430	6.19
136	153.83	504.68	0.26	0.00	4.87	16.32	0.00	5.39	2.01	0.76	0.39	134	84	505	5.27
137	153.84	504.71	0.27	0.00	5.47	18.03	0.00	5.33	2.11	0.77	0.38	123	101	361	5.46
138	153.85	504.74	0.27	0.00	5.71	18.19	0.00	5.08	2.14	0.75	0.38	117	96	376	5.45
139	153.86	504.78	0.28	0.20	6.07	19.28	0.00	4.65	2.31	0.68	0.38	135	88	415	4.92
140	153.87	504.81	0.25	0.55	4.80	15.85	0.01	6.29	1.80	2.51	0.36	120	56	677	5.37
141	153.88	504.84	0.28	0.15	5.98	19.39	0.00	5.36	2.16	0.71	0.39	115	86	534	5.29
142	153.89	504.88	0.27	0.47	5.79	19.01	0.02	6.04	2.11	0.56	0.38	113	77	514	6.02
143	153.90	504.91	0.22	0.77	4.08	15.23	0.14	8.69	1.64	1.73	0.34	150	62	572	9.33

144	153.91	504.94	0.29	0.24	6.36	20.03	0.00	4.45	2.39	0.52	0.40	90	80	533	4.63
145	153.92	504.97	0.30	0.00	7.00	21.36	0.00	3.45	2.53	0.52	0.40	80	89	439	3.98
146	153.93	505.01	0.31	0.00	7.34	21.41	0.00	3.22	2.61	0.53	0.39	68	98	398	3.81
147	153.94	505.04	0.31	0.19	7.37	22.13	0.00	3.61	2.62	0.42	0.40	78	94	376	4.20
148	153.95	505.07	0.30	0.20	7.26	22.13	0.00	3.73	2.60	0.43	0.39	47	95	441	4.46
149	153.96	505.11	0.30	0.49	7.25	22.28	0.01	4.16	2.59	0.40	0.39	69	96	386	4.91
150	153.97	505.14	0.30	0.21	7.26	21.77	0.00	3.83	2.57	0.44	0.37	64	101	363	4.64
151	153.98	505.17	0.30	0.23	6.99	21.50	0.00	4.06	2.47	0.41	0.37	46	96	322	5.00
152	153.99	505.20	0.30	0.00	6.60	20.15	0.00	3.19	2.48	0.48	0.39	52	100	345	4.21
153	154.00	505.24	0.31	0.19	7.59	22.19	0.00	3.09	2.64	0.43	0.40	87	101	346	3.98
154	154.01	505.27	0.31	0.35	7.46	22.16	0.00	3.55	2.62	0.45	0.42	120	95	364	4.20
155	154.02	505.30	0.31	0.00	7.39	22.04	0.00	3.40	2.60	0.39	0.38	61	95	383	4.23
156	154.03	505.34	0.31	0.31	8.01	22.88	0.00	2.96	2.73	0.41	0.39	68	97	398	3.90
157	154.04	505.37	0.31	0.00	7.33	21.64	0.00	2.74	2.64	0.47	0.40	95	102	338	3.85
158	154.05	505.40	0.31	0.26	8.13	23.06	0.00	3.00	2.79	0.44	0.40	86	96	360	3.94
159	154.06	505.43	0.31	0.62	7.79	22.60	0.00	3.57	2.68	0.36	0.41	82	94	411	4.82
160	154.07	505.47	0.30	0.06	7.07	21.72	0.00	3.61	2.54	0.35	0.40	81	92	366	4.94
161	154.08	505.50	0.31	0.36	7.44	22.28	0.00	3.63	2.57	0.34	0.38	55	95	360	4.93
162	154.09	505.53	0.30	0.00	7.09	21.24	0.00	2.63	2.58	0.39	0.38	71	101	315	3.88
163	154.10	505.56	0.29	0.68	6.92	21.01	0.00	4.37	2.48	0.40	0.43	91	99	326	5.72
164	154.11	505.60	0.30	0.00	6.31	19.30	0.00	2.50	2.39	0.50	0.36	69	99	325	3.76
165	154.12	505.63	0.31	0.12	7.63	22.48	0.00	2.88	2.66	0.36	0.39	72	97	315	3.79
166	154.13	505.66	0.31	0.33	7.30	22.43	0.00	3.83	2.59	0.35	0.38	81	101	302	4.80
167	154.14	505.70	0.31	0.10	7.41	21.96	0.00	3.25	2.62	0.40	0.38	113	98	328	4.51
168	154.15	505.73	0.31	0.22	7.79	22.68	0.00	2.84	2.70	0.38	0.39	55	98	328	3.94
169	154.16	505.76	0.30	0.17	7.29	21.00	0.00	2.99	2.63	0.48	0.40	109	102	320	4.13
170	154.17	505.79	0.28	0.23	5.89	19.67	0.00	5.16	2.31	0.43	0.38	122	99	274	6.39
171	154.18	505.83	0.31	0.22	7.46	22.16	0.00	3.12	2.65	0.38	0.39	82	100	312	4.17
172	154.19	505.86	0.30	0.44	7.27	21.44	0.00	3.81	2.58	0.35	0.41	72	97	375	5.24

173	154.20	505.89	0.30	0.58	7.25	22.03	0.00	4.37	2.53	0.34	0.41	54	97	348	5.47
174	154.21	505.93	0.31	0.20	7.73	22.99	0.00	3.55	2.68	0.36	0.40	86	95	349	4.33
175	154.22	505.96	0.30	0.28	7.02	21.35	0.00	3.28	2.53	0.33	0.40	72	96	316	5.04
176	154.23	505.99	0.30	0.32	7.29	22.14	0.00	3.82	2.60	0.36	0.39	62	96	340	5.11
177	154.24	506.02	0.30	1.14	7.41	22.37	0.01	4.75	2.59	0.37	0.42	98	90	393	5.52
178	154.25	506.06	0.30	0.35	7.48	22.10	0.00	3.82	2.66	0.36	0.39	74	90	375	5.05
179	154.26	506.09	0.30	0.52	7.55	22.33	0.00	3.87	2.64	0.33	0.39	73	94	341	5.26
180	154.27	506.12	0.31	0.66	7.75	22.68	0.01	4.01	2.65	0.35	0.41	123	94	336	5.11
181	154.28	506.16	0.30	0.51	7.27	22.04	0.01	4.52	2.57	0.38	0.38	83	104	252	5.47
182	154.29	506.19	0.30	0.66	7.37	22.33	0.00	3.60	2.58	0.36	0.38	76	94	327	4.82
183	154.30	506.22	0.30	0.47	7.43	21.96	0.00	4.02	2.55	0.40	0.41	102	102	293	5.10
184	154.31	506.25	0.29	0.00	6.38	19.74	0.00	3.32	2.38	0.37	0.39	94	93	325	5.25
185	154.32	506.29	0.31	0.34	7.64	22.86	0.00	3.64	2.61	0.35	0.39	55	95	333	4.89
C7009															
1	109.08	357.89	0.32	0.83	7.52	23.27	0.04	1.53	2.81	3.83	0.48	88	108	344	3.15
2	109.09	357.92	0.32	0.41	7.25	22.73	0.04	1.62	2.70	3.59	0.46	77	107	326	3.42
3	109.10	357.95	0.32	0.26	7.42	22.75	0.04	1.67	2.66	3.52	0.45	87	110	315	3.47
4	109.11	357.99	0.31	0.58	7.27	22.31	0.06	1.81	2.70	3.26	0.46	107	115	304	3.47
5	109.12	358.02	0.31	0.16	7.14	21.68	0.03	2.00	2.82	2.41	0.45	92	129	279	3.65
6	109.13	358.05	0.31	0.00	7.40	21.38	0.03	1.76	2.87	1.88	0.45	80	141	284	3.54
8	109.15	358.12	0.31	0.29	7.74	22.44	0.00	2.04	3.01	0.66	0.47	130	166	238	3.99
9	109.16	358.15	0.32	0.68	8.44	24.00	0.00	2.36	3.30	0.55	0.52	226	179	287	4.11
10	109.17	358.18	0.29	0.00	6.40	19.18	0.00	2.05	2.70	0.76	0.40	96	162	230	3.78
11	109.18	358.22	0.31	0.30	7.47	22.17	0.00	2.26	3.02	0.56	0.47	158	169	285	3.93
12	109.19	358.25	0.30	0.50	7.22	21.23	0.00	3.36	2.91	0.52	0.48	233	152	319	5.41
13	109.20	358.28	0.30	0.17	7.27	21.36	0.00	2.67	2.92	0.54	0.45	242	168	304	4.03
14	109.21	358.31	0.31	0.04	7.44	21.63	0.00	2.27	3.10	0.37	0.46	271	216	245	3.90
15	109.22	358.35	0.31	0.00	7.15	21.02	0.00	2.15	2.91	0.34	0.42	214	218	276	3.68
16	109.23	358.38	0.21	1.52	3.91	11.75	5.79	2.49	1.35	13.57	0.23	88	142	159	2.97

17	109.24	358.41	0.27	0.00	5.34	16.36	0.05	3.03	2.37	1.95	0.48	351	284	272	4.43
18	109.25	358.44	0.27	0.00	5.22	16.60	0.05	3.05	2.43	2.58	0.32	280	318	242	3.46
19	109.26	358.48	0.26	0.42	5.18	16.82	0.22	3.38	2.39	3.67	0.34	243	329	267	3.56
20	109.27	358.51	0.25	0.68	4.58	14.87	1.95	2.83	1.99	6.54	0.32	151	270	242	3.84
21	109.28	358.54	0.20	1.94	3.38	11.37	8.88	2.30	1.32	14.20	0.25	10	170	163	2.85
22	109.29	358.58	0.27	0.69	5.34	18.03	0.86	2.47	2.38	4.79	0.40	150	255	246	3.74
23	109.30	358.61	0.29	0.39	6.01	19.64	0.06	2.48	2.62	2.77	0.41	148	269	274	3.74
24	109.31	358.64	0.29	0.38	6.44	20.16	0.06	2.31	2.71	2.55	0.42	135	253	259	3.76
25	109.32	358.67	0.31	0.38	6.98	22.51	0.09	2.30	2.82	1.64	0.45	156	213	284	3.28
26	109.33	358.71	0.30	0.00	6.66	20.81	0.04	1.95	2.67	1.11	0.44	145	202	246	3.56
27	109.34	358.74	0.31	0.00	6.74	21.90	0.05	2.45	2.63	0.97	0.46	105	184	291	3.74
28	109.35	358.77	0.31	0.17	6.73	21.70	0.06	2.64	2.60	1.05	0.46	115	162	351	3.69
29	109.36	358.81	0.30	0.22	6.64	21.47	0.03	2.85	2.57	1.00	0.44	99	162	318	4.14
30	109.37	358.84	0.30	0.49	6.82	21.71	0.04	2.83	2.62	0.99	0.43	60	168	297	4.09
31	109.38	358.87	0.30	0.32	6.67	21.60	0.05	3.47	2.66	0.83	0.46	149	163	269	5.08
32	109.39	358.90	0.30	0.25	6.73	21.84	0.04	3.17	2.69	0.83	0.46	133	161	285	4.80
33	109.40	358.94	0.31	0.18	6.97	22.14	0.04	2.94	2.72	0.82	0.49	167	164	303	4.07
34	109.41	358.97	0.30	0.18	6.67	21.28	0.02	3.25	2.72	0.83	0.46	127	167	279	4.75
35	109.42	359.00	0.30	0.50	6.83	21.44	0.01	2.94	2.72	0.70	0.47	137	169	296	4.21
36	109.43	359.04	0.30	0.15	6.88	21.26	0.00	2.94	2.75	0.68	0.46	148	167	292	4.28
37	109.44	359.07	0.30	0.24	6.94	21.13	0.00	2.58	2.79	0.71	0.46	138	159	310	3.88
38	109.45	359.10	0.30	0.00	7.02	21.25	0.00	2.73	2.83	0.68	0.45	141	160	291	3.92
39	109.46	359.13	0.30	0.21	7.12	21.46	0.00	2.75	2.92	0.62	0.47	202	156	276	4.03
40	109.47	359.17	0.30	0.07	6.96	21.21	0.00	2.76	2.92	0.45	0.46	240	154	273	4.42
41	109.48	359.20	0.30	0.30	6.98	21.39	0.00	2.93	2.90	0.49	0.47	304	154	255	4.43
42	109.49	359.23	0.31	0.00	7.11	21.53	0.00	2.51	2.90	0.42	0.48	275	161	274	4.10
43	109.50	359.26	0.31	0.00	7.28	21.67	0.00	2.43	2.96	0.55	0.45	247	174	259	3.93
44	109.51	359.30	0.30	0.00	6.95	21.28	0.00	2.74	2.81	0.38	0.45	325	191	239	4.39
45	109.52	359.33	0.30	0.17	7.18	21.46	0.00	2.34	2.85	0.41	0.44	301	203	238	4.06

46	109.53	359.36	0.30	0.00	6.86	20.60	0.00	2.72	2.77	0.36	0.42	305	212	260	4.57
47	109.54	359.40	0.30	0.00	6.29	19.86	0.00	2.61	2.48	0.32	0.37	300	241	260	3.90
48	109.55	359.43	0.27	0.00	5.13	17.41	0.00	3.55	1.96	0.51	0.33	467	332	253	4.29
49	109.56	359.46	0.25	0.28	3.88	13.65	1.63	2.65	1.69	5.60	0.26	483	360	162	3.16
50	109.57	359.49	0.26	0.00	4.36	14.73	0.03	3.15	2.05	2.57	0.31	610	357	217	3.72
51	109.58	359.53	0.26	0.00	4.47	14.85	0.00	3.49	2.06	1.96	0.31	638	340	258	3.86
52	109.59	359.56	0.27	0.00	5.08	16.14	0.00	3.15	2.22	2.44	0.35	419	283	237	4.17
53	109.60	359.59	0.27	0.08	5.85	17.54	0.00	2.85	2.40	2.82	0.41	337	276	219	4.39
54	109.61	359.63	0.29	0.29	6.31	19.07	0.00	2.46	2.58	2.62	0.40	242	255	249	4.12
55	109.62	359.66	0.29	0.48	6.42	19.61	0.06	2.45	2.56	2.88	0.39	241	233	241	4.09
56	109.63	359.69	0.29	0.39	6.43	19.28	0.03	2.42	2.61	2.47	0.39	231	224	245	4.10
57	109.64	359.72	0.29	0.06	6.53	19.50	0.00	2.40	2.74	1.61	0.41	300	216	272	4.07
58	109.65	359.76	0.30	0.02	6.35	20.22	0.00	2.19	2.71	0.78	0.42	277	207	335	3.62
59	109.66	359.79	0.31	0.00	6.78	21.89	0.00	2.05	2.71	0.56	0.44	255	212	249	3.36
60	109.67	359.82	0.31	0.00	6.93	22.71	0.00	2.24	2.75	0.50	0.46	233	191	295	3.53
61	109.68	359.86	0.31	0.11	6.97	22.67	0.00	2.29	2.74	0.48	0.46	221	180	304	3.59
62	109.69	359.89	0.32	0.00	7.26	23.22	0.00	2.29	2.85	0.43	0.49	292	183	302	3.67
63	109.70	359.92	0.31	0.21	7.05	22.23	0.00	2.24	2.80	0.41	0.48	332	175	282	3.74
64	109.71	359.95	0.31	0.05	7.18	22.55	0.00	2.24	2.84	0.41	0.46	351	173	278	3.71
65	109.72	359.99	0.31	0.02	7.21	22.47	0.00	2.44	2.81	0.41	0.46	366	178	290	3.79
66	109.73	360.02	0.31	0.00	6.75	21.60	0.00	2.69	2.82	0.38	0.45	572	171	222	4.28
67	109.74	360.05	0.31	0.02	6.93	22.31	0.00	2.82	2.86	0.39	0.46	650	164	226	4.36
68	109.75	360.09	0.31	0.06	7.00	22.17	0.00	2.70	2.79	0.40	0.47	713	167	228	4.22
70	109.77	360.15	0.30	0.00	6.51	21.17	0.00	3.19	2.65	0.42	0.41	882	166	196	4.11
71	109.78	360.18	0.31	0.05	6.90	22.09	0.00	2.72	2.85	0.33	0.45	1018	191	206	4.11
72	109.79	360.22	0.31	0.00	6.48	20.92	0.00	2.21	2.85	0.33	0.44	1376	277	156	3.91
73	109.80	360.25	0.29	0.00	5.28	19.83	0.00	3.32	2.18	0.44	0.39	1610	319	246	3.96
74	109.81	360.28	0.27	0.00	3.80	16.06	0.00	3.42	1.58	0.83	0.31	2389	412	190	3.54
75	109.82	360.31	0.25	0.00	3.31	13.46	0.00	4.00	1.53	1.14	0.29	2973	423	195	4.13

76	109.83	360.35	0.24	0.00	3.02	12.83	0.00	4.43	1.77	2.35	0.28	3223	365	230	4.59
77	109.84	360.38	0.23	0.00	3.18	12.52	0.00	4.44	1.75	3.35	0.27	2913	344	202	4.15
78	109.85	360.41	0.24	0.15	3.89	14.22	0.00	4.26	1.96	3.68	0.29	2651	351	219	4.34
79	109.86	360.45	0.27	0.27	4.40	17.16	0.00	3.43	2.13	3.18	0.32	1679	365	217	4.34
80	109.87	360.48	0.27	0.00	3.67	14.64	0.04	2.47	1.96	3.89	0.34	1390	336	208	3.82
81	109.88	360.51	0.28	0.55	3.65	19.88	0.12	3.90	1.47	3.70	0.26	752	149	658	5.50
82	109.89	360.54	0.27	0.21	4.21	17.07	1.09	2.21	1.92	5.02	0.33	915	305	177	3.09
83	109.90	360.58	0.28	0.00	4.62	17.22	0.29	2.73	2.10	2.47	0.38	1051	328	256	3.65
84	109.91	360.61	0.30	0.00	5.68	20.81	0.00	2.52	2.48	0.57	0.41	981	383	218	3.27
85	109.92	360.64	0.30	0.02	5.50	20.25	0.37	2.22	2.31	2.73	0.37	815	336	195	3.02
86	109.93	360.68	0.31	0.00	6.22	21.69	0.00	2.57	2.65	0.33	0.42	937	384	226	3.56

APPENDIX H

DUPLICATE XRF MEASUREMENTS MAJOR ELEMENTS

Marks from top of core (cm)	Depth (m below KB)	Fe Original (wt %)	Fe Rescan (wt %)	Fe Ratio O/R	Si Original (wt %)	Si Rescan (wt %)	Si Ratio O/R	Al Original (wt %)	Al Rescan (wt %)	Al Ratio O/R	S Original (wt %)	S Rescan (wt %)	S Ratio O/R
Core C7003													
94	142.05	4.47	4.18	1.07	12.69	13.36	0.95	3.25	3.21	1.01	4.37	4.19	1.04
95	142.06	4.71	4.56	1.03	12.18	13.09	0.93	3.08	3.24	0.95	4.58	4.53	1.01
96	142.07	4.79	4.70	1.02	13.05	12.77	1.02	3.55	3.29	1.08	4.57	4.58	1.00
Core C7005													
13	152.60	4.48	5.32	0.84	12.86	12.01	1.07	3.40	3.26	1.04	3.44	4.33	0.79
14	152.61	4.67	4.48	1.04	12.07	11.53	1.05	3.54	3.34	1.06	3.99	3.94	1.01
15	152.62	3.91	4.05	0.96	13.91	12.67	1.10	4.26	3.84	1.11	3.25	3.69	0.88
Core C7009													
75	109.82	3.77	4.13	0.91	13.40	13.46	1.00	3.28	3.31	0.99	3.61	4.00	0.90
76	109.83	4.70	4.59	1.03	12.83	12.83	1.00	3.10	3.02	1.02	4.40	4.43	0.99
77	109.84	4.22	4.15	1.02	14.31	12.52	1.14	3.54	3.18	1.11	3.95	4.44	0.89
Average Deviation from 1:1 Ratio				0.05			0.06			0.06			0.07

Marks from top of core (cm)	Depth (m below KB)	Ti Original (wt %)	Ti Rescan (wt %)	Ti Ratio O/R	K Original (wt %)	K Rescan (wt %)	K Ratio O/R	V Original (ppm)	V Rescan (ppm)	V Ratio O/R	Cr Original (ppm)	Cr Rescan (ppm)	Cr Ratio O/R
Core C7003													
94	142.05	0.28	0.27	1.04	1.83	1.76	1.04	3352	3135	1.07	312	291	1.07
95	142.06	0.29	0.29	1.00	1.75	1.71	1.03	3482	3284	1.06	321	280	1.15
96	142.07	0.30	0.30	1.01	1.85	1.80	1.02	3111	3409	0.91	324	304	1.07
Core C7005													
13	152.60	0.33	0.33	0.99	1.75	1.76	0.99	1530	1891	0.81	303	305	0.99
14	152.61	0.32	0.31	1.00	1.99	1.91	1.04	2107	2134	0.99	277	274	1.01
15	152.62	0.31	0.30	1.03	2.16	2.05	1.05	1872	1992	0.94	279	268	1.04
Core C7009													
75	109.82	0.27	0.29	0.91	1.47	1.53	0.96	2669	2973	0.90	421	423	1.00
76	109.83	0.27	0.28	0.97	1.76	1.77	1.00	3165	3223	0.98	390	365	1.07
77	109.84	0.28	0.27	1.04	1.79	1.75	1.02	2583	2913	0.89	332	344	0.97
Average Deviation from 1:1 Ratio				0.03			0.03			0.08			0.05

VITA

Graduate School
Southern Illinois University

Jacob Dyson

xjacques94@gmail.com

Southern Illinois University Carbondale
Bachelor of Science, Geology, May 2016

Special Honors and Awards:

Medlin Research Scholar Geological Society of America 2018

Thesis Paper Title:

Geochemistry and organic petrology of the Anna Shale (Pennsylvanian) and the occurrence of pyrite "suns" in southwestern Illinois

Major Professor: Dr. Susan Rimmer

Publications:

Dyson, J. R., Rimmer, S. M., Elrick, S. D., 2018. Geochemistry and organic petrology of the Anna Shale (Pennsylvanian) and pyrite suns in Southwestern Illinois. Geological Society of America Abstracts with Programs 50, Geological Society of America Annual Meeting, Indianapolis, IN, 6 November 2018.

Dyson, J. R., 2018. Chemostratigraphy, geochemistry, and petrography of the Anna Shale and pyrite suns of the Illinois Basin. Search and Discovery Article #51486, AAPG Southwest Section Annual Convention, El Paso, TX, 7-10 April 2018.